CHAPTER

1 INTRODUCTION

CONTENTS

1.1 BACKGROUND

With increasing deterioration of the infrastructure and the need for upgrading in order to satisfy new design requirements, the issue of retrofitting has been one of great importance over the past years. One form of retrofitting, whereby plates made from materials such as steel or fibre reinforced polymer (FRP) are adhesively bonded to the surface of reinforced concrete beams, has become a very popular method in strengthening and stiffening existing structures in recent years. This plating technique is simple and rapid to apply, inexpensive, unobtrusive, and can be applied while the structure is in use.

1.1.1 FORMS OF ADHESIVE PLATING

There are various forms of adhesively bonding plates to RC members. For example the plates can be made from different materials, they can take any shape, can be positioned on any surface as desired, and can be adhesively bonded using different techniques.

The plates used in retrofitting are mostly made from steel or fibre reinforced polymer (FRP). In recent years there has been extensive research on the use of FRP plates to replace steel plates in plate bonding (Teng et al. 2002). FRP is impregnated with fibres such as carbon or glass, and as opposed to steel, it is a flexible, anisotropic material. The fracture stress of FRP is much greater than steel, exhibiting linear elastic properties prior to fracture of the material as illustrated in Figure 1.1. As FRP does not have a large ductile plateau like steel, the use of this form of plate poses an even greater concern in regards to the ductility of structures.

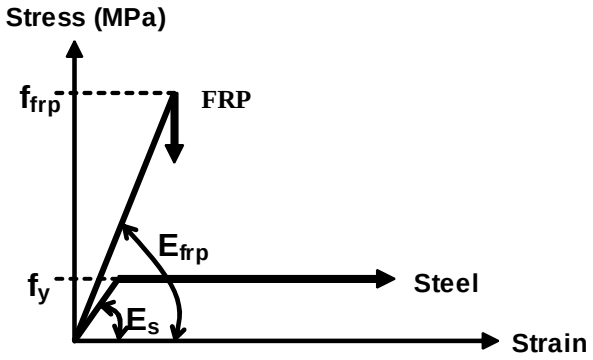

Figure 1.1 Material properties

Plates can be adhesively bonded to the side, tension or compression face of the beam as illustrated in Figure 1.2. The most common positions are tension faces. Positioning the plates on the tension face of the beam will most effectively increase the flexural strength of the member, however as the cross-sectional area of the plate is increased, the beam ductility will decrease. Adhesively bonded tension face plates are also prone to premature debonding due to stress concentrations induced by the plate being adjacent to those induced by the tension reinforcing bars. Plating to the side of the beam will increase both the flexural and vertical shear capacity of the member. Although this form of plating is less effective compared to tension face plates, it allows increase in strength without largely reducing the ductility of the member. Side plates are also less susceptible to debonding, as it is not adjacent to tension reinforcing bars. Plates can be bonded to the compression face of the beam to increase the ductility of the member, as well as to inhibit premature debonding. As tension face plates are most commonly used and also most susceptible to debonding, the research presented in this thesis is dealing primarily with tension face plates.

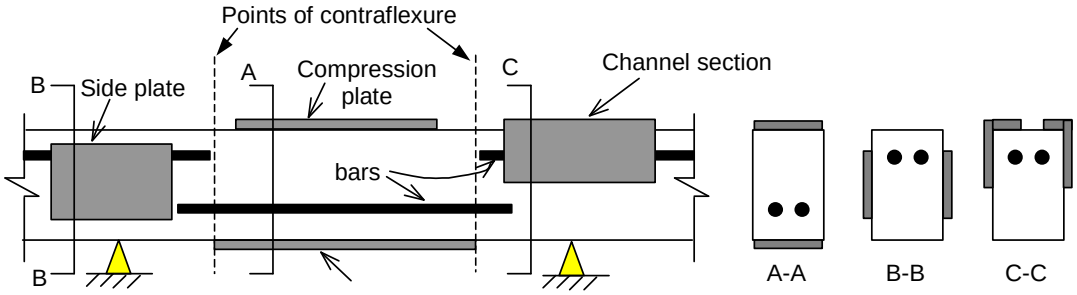

Figure 1.2 Plating shapes and positions

Plates can be adhesively bonded to the reinforced concrete beams using various techniques such as: wrapping, where the plate is adhesively bonded and vertically wrapped around a corner, as illustrated by section B-B in Figure 1.3 for a partially wrapped section; externally bonded (EB), where the plate is glued to the external surface of the beam such as at section A-A in Figure 1.2; and near surface mounted (NSM), where strips are imbedded into the beam by gluing FRP or steel strips into grooves which are cut into the concrete specimen perpendicular to its surface, as illustrated by section C-C in Figure 1.3.

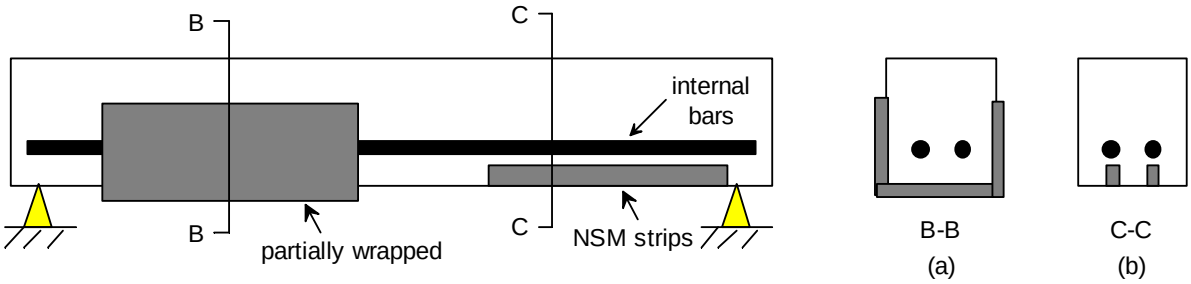

Figure 1.3 (a) Wrapped plates; (b) near surface mounted strips

1.1.2 DEBONDING MECHANISMS

The major concern in adhesively bonding plates to the external surface of reinforced concrete beams is the premature debonding of the plates, which are unique forms of failure of plated beams. Previous researchers (i.e. Oehlers & Seracino 2004; *fib* 2001; Teng et al. 2002) have identified different forms of debonding mechanisms and these can be classified into 3 main categories: (1) *plate end debonding*; (2) *critical diagonal crack debonding*; (3) *intermediate crack debonding*. It is worth noting that debonding almost always occurs at the concrete layer adjacent to the adhesive, due to the strength of the adhesive being much greater than the tensile strength of the adjacent concrete.

1.1.2.1 PLATE END (PE) DEBONDING

Plate end debonding is caused by the existence of high interfacial shear and normal stresses at the plate end due to abrupt termination of the plate. When the beam is bent, the plate will want to stay straight, therefore causing cracks to form at the plate ends and propagate inwards as shown in Figure 1.4. These debonding cracks may occur at the level of the tension reinforcement (also known as cover separation), or at the concrete/adhesive interface (also known as plate end interfacial debonding), and they usually propagate gradually at first, then rapidly at PE debonding failure (Oehlers & Seracino 2004; *fib* 2001; Teng et al. 2002). This form of debonding is associated with the curvature in the beam near the plate end and hence can be prevented by terminating the plate near the point of contra-flexure.

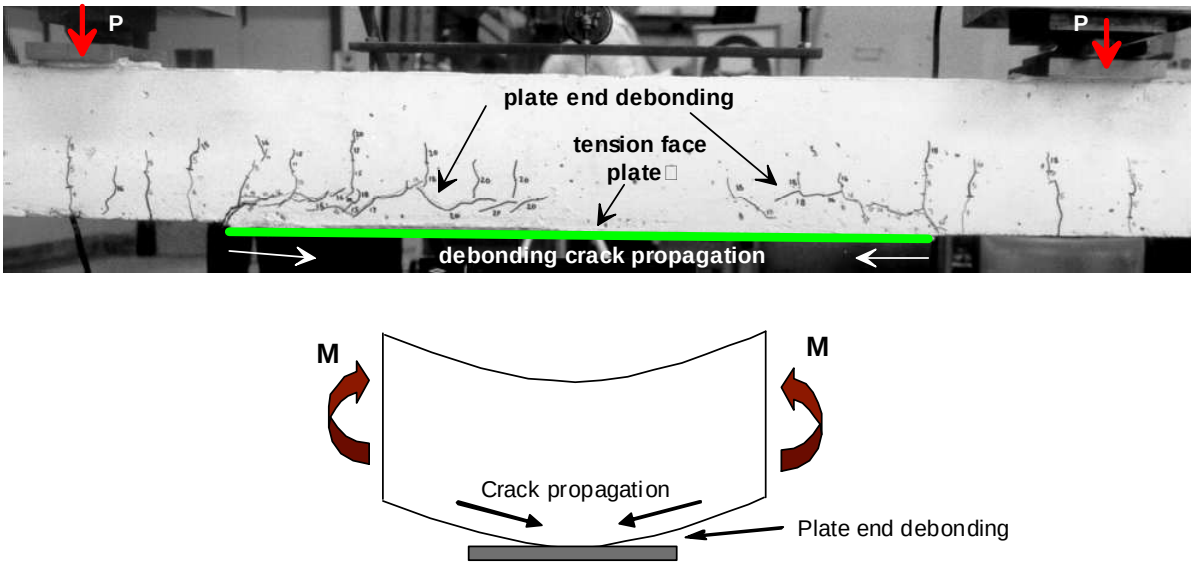

Figure 1.4 Plate end debonding of tension face plate

1.1.2.2 Critical Diagonal Crack (CDC) Debonding

This form of debonding, also known as vertical shear debonding, is associated with vertical shear deformations of the beam. When the critical diagonal crack forms, sliding and rotation action occurs across the crack causing the plate to separate from the beam by a debonding crack propagating from the root of the diagonal crack to the plate end as illustrated in Figure 1.5 (Mohamed Ali et al. 2001). As the critical diagonal crack intercepts the plate, the debonding crack propagation at the plate/concrete interface is dependent on the IC debonding strength P_{IC}. CDC debonding is a sudden failure with no visual warning and the presence of stirrups has little or no effect on CDC debonding. Therefore beams are prone to CDC debonding failure when the shear load exceeds the concrete shear capacity of the beam. Limited amounts of research have been carried out in this area of study, nevertheless several models have been developed to analyse the problem such as Mohamed Ali's critical diagonal crack debonding model (Mohamed Ali 2000), and Chen and Teng's Shear Strength Model (Teng et al. 2002). Like PE debonding, CDC debonding can be prevented by altering the plate geometries and the cross-section of the beam in the design process (Oehlers & Seracino 2004).

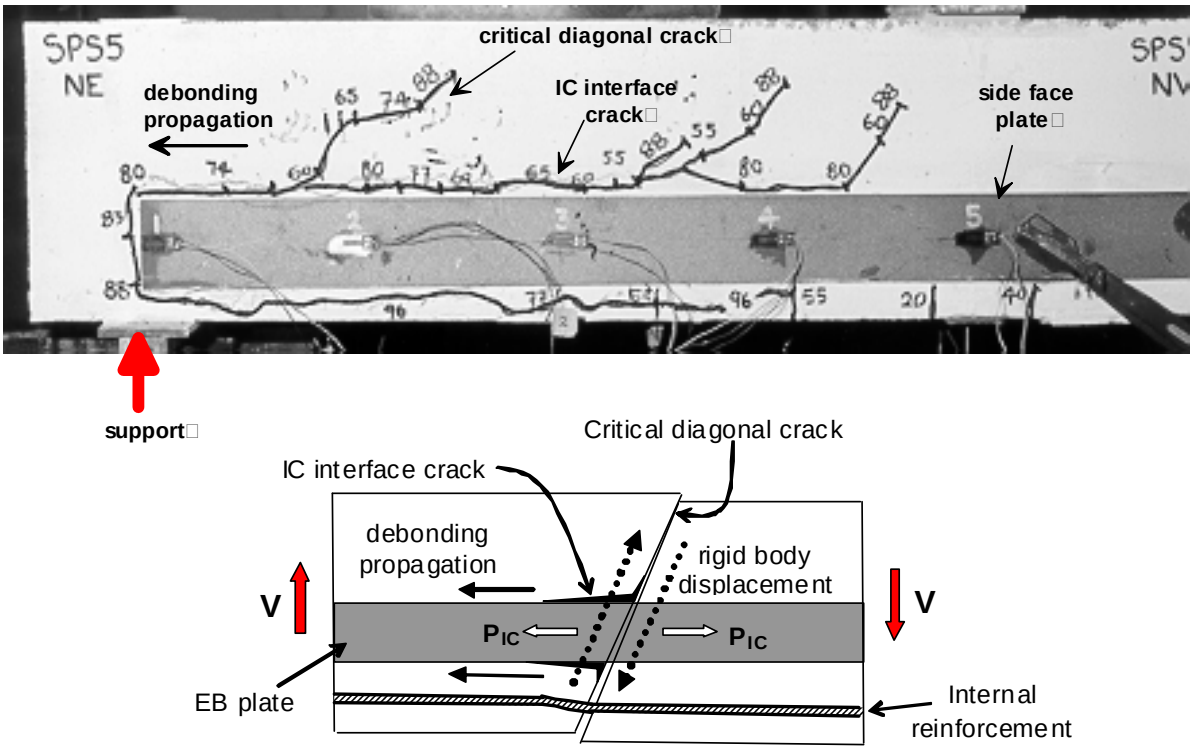

Figure 1.5 Critical diagonal crack debonding of side face plated beam

1.1.2.3 Intermediate Crack (IC) Debonding

Intermediate crack (IC) debonding is associated with the formation of flexural or flexural-shear cracks in the vicinity of the plate. Theoretically the plate requires infinite strains across the intercepting cracks. As this is impossible, horizontal or intermediate crack (IC) interface cracks occur at the interface in order to accommodate the intercepting cracks. IC interface cracks usually first occurs at position of maximum moment, where strains in the plate are largest (Oehlers & Seracino 2004), and propagate gradually from the roots of the intersecting cracks towards the plate ends as shown in Figure 1.6. These IC interface cracks usually have little impact on the overall strength of the beam until they propagate further along the beam causing plate strains to reduce, that is the plate is debonding and this is referred to as IC debonding, and eventually cause a decrease in strength of the beam as IC debonding failure takes place. Because concrete has a much lower strength than the adhesive, these debonding cracks generally occur in the concrete adjacent to the adhesive to concrete interface. For IC debonding induced by flexural crack, crack widening causes debonding propagation. For IC debonding induced by flexural shear crack, the relative vertical displacement between the two faces of the crack also produces peeling stresses at the interface, however this effect is less significant hence it is considered that the propagation of debonding is predominately caused by widening of crack (Teng et al. 2002).

Intermediate crack debonding is the most common failure mode, especially for side plated beams (Teng et al. 2002). Unlike PE debonding and CDC debonding, IC debonding is difficult to prevent, and since it is a much more ductile failure compared to PE and CDC debonding, it should be the failure mode that engineers design for when retrofitting beams using this technique. Most of the research to date has been concentrating on the bond-slip behaviour at the plate-concrete interface by looking at plated specimens subjected to axial loads only. Very little research has been carried out on IC debonding of flexural members where multiple cracks form along the beam.

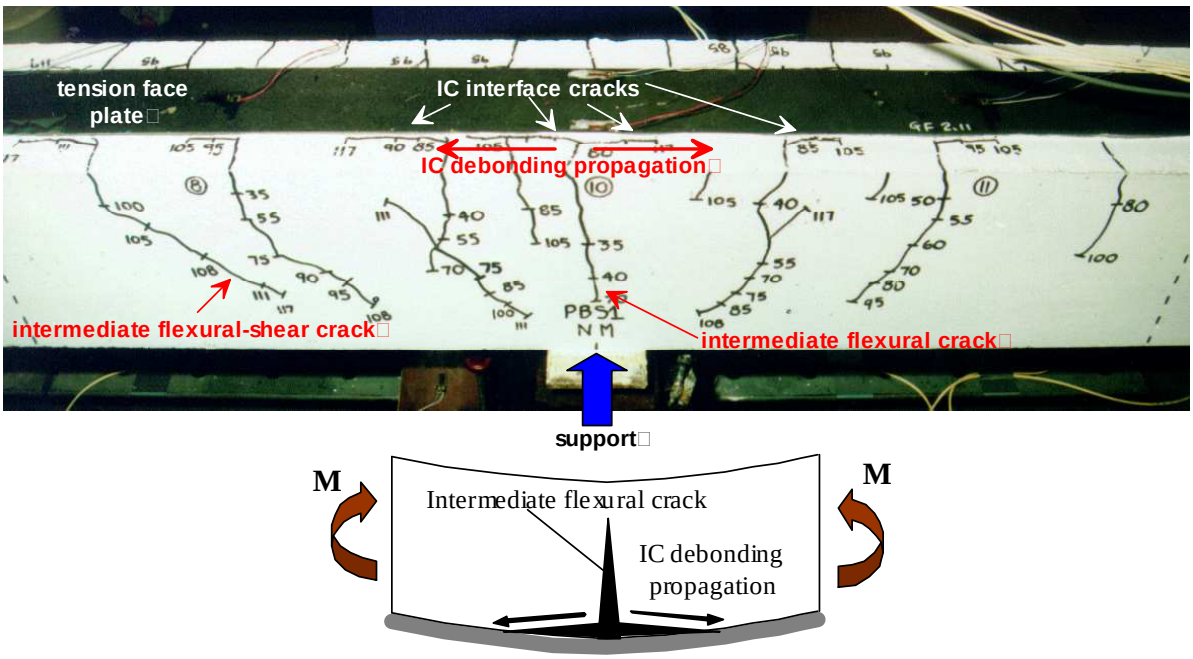

Figure 1.6 Intermediate crack debonding of tension face plate

1.1.3 Ductility and Moment Redistribution

Ductility is the ability of structures to sustain plastic deformation prior to collapse without substantial loss of resistance. It is desirable to have sufficient ductility as it gives warning before failure by allowing large deflections to occur, also many design approaches, such as the linear elastic analysis with and without moment redistribution, require plastic deformation (or rotation) capacity in plastic areas (CEB-FIP 1998). Ductile structures can provide the amount of rotation capacity required to achieve the desired moment redistribution. Ductility can be a major concern in plated structures as premature debonding of the adhesively bonded plates can lead to reduction in beam ductility, and hence affect the ability of the beam to redistribute moment. Even if premature debonding failure is prevented such that concrete crushing failure occurs, IC debonding will still occur which will affect the rotation capacity of the beam. Furthermore, as the beam is continually loaded after the maximum

flexural capacity is reached, i.e. after concrete crushing occurs, eventually the plate will completely debond due to the widening of the flexural cracks as the beam deflection increases. Therefore debonding must be accounted for when determining the ductility and moment redistribution of plated members.

Despite its importance, very little research has been carried out on the cross-sectional ductility of plated beams and their ability to redistribute moment or absorb energy in indeterminate structures. At the moment, there are only rules of thumb such as ensuring that the steel reinforcing bars yield before the FRP plates debond or fracture (*fib* 2001), and according to the existing design codes (*fib* 2001; Concrete Society 2000), no moment redistribution is allowed for beams with externally bonded FRP plates. The simple ductility rules in reinforced concrete codes that place limits on the neutral axis depth rely on the steel reinforcing bars yielding and hence cannot be applied to brittle FRP plates. It is therefore crucial that research is to be carried out in such an area so that proper design rules can be determined for use in practice.

1.2 SCOPE AND OBJECTIVES

Premature debonding can significantly affects the behaviour of reinforced concrete beams with adhesively bonded plates. Therefore to allow safe and effective use of this retrofitting technique, thorough understanding of each debonding mechanism is essential. As discussed in Section 1.1, much good research has been carried out looking at the plate end (PE) debonding of plated beams. Several models are also available for analysing critical diagonal crack (CDC) debonding. There is, however, a lack of research on intermediate crack (IC) debonding of flexural members, despite it being the most important debonding mechanism. The main objective of this research is to study the IC debonding behaviour of plated members, so that together with the existing models for PE and CDC debonding, all debonding mechanisms can be analysed. Another major aim in this research is to develop methods for analysing the moment redistribution behaviour of continuous plated beams, hence allowing more effective and economic use, and wider application of this retrofitting technique.

This research focuses on the IC debonding behaviour of reinforced concrete beams adhesively bonded with FRP or steel plates on the external surfaces, while beams with near surface mounted plates will also be considered when studying the moment redistribution of plated members. As IC debonding is most likely to occur with beams plated on the tension face, analytical studies were

carried out on the tension face plated members. In the scope of this research, a numerical model based on partial interaction analysis was developed, from which the IC debonding behaviour of flexural beams was analysed. This analysis enables the modeling of the local stress and strain behaviour between flexural cracks of plated RC beams at which IC debonding occurs, and hence, can predict the strength at which failure occurs. Based on the study of IC debonding, further development was made in the modelling of CDC debonding, which is dependent on the IC debonding resistance at the plate/concrete interface.

Another major area of study in this research is the moment redistribution of the plated beams. Models based on variation in flexural rigidity along the continuous beams were developed to analyse the statically indeterminate plated beams, such that the degree of moment redistribution at the plastic hinges can be evaluated. An experimental program was carried out on continuous beams with externally bonded plates and near surface mounted strips to verify the accuracy of the models.

1.3 THESIS OUTLINE

This thesis presents a collection of ten journal papers published, or submitted for publication, by the author. The papers can be categorized into three main areas: intermediate crack (IC) debonding; critical diagonal crack (CDC) debonding; and moment redistribution. Each area consists of chapters which first introduce the purpose and description of the studies carried out, followed by a review of the existing literature. The journal papers are then presented beginning with a brief introduction of the contents of the papers. The papers are further discussed and any additional studies carried out that are not presented in the papers are provided. Finally the chapters are summarized and individual references and notations included at the end of each chapter.

The thesis begins with an introduction in Chapter 1 which includes a general background on reinforced concrete beams with adhesively bonded plates, and a discussion on the scope and the objectives of this research.

The development of the numerical model for analysing the intermediate crack debonding behaviour of plated beams is presented in Chapter 2. Through the review of literature on both unplated and plated reinforced concrete beams, it was found that the two structural systems behave similarly to that of composite beams. By modifying the partial interaction theory for composite beams, a numerical model for analysing IC debonding of plated members was developed. The proposed model allows for beams

with multiple reinforcing layers, for example it accounts for the slip at the plate/concrete interface as well as the slip at the bar/concrete interface. Therefore this model is applicable to both plated and unplated reinforced concrete beams. Included in this chapter are two papers: Oehlers et al. (2005); and Liu et al. (2005a), describing the development and the application of the partial interaction model to an unplated and an externally bonded plated reinforced concrete beam. It is worth noting that although the model was developed based on externally bonded (EB) tension face plated beams, it is also applicable to beams with side and angle plates and those with near surface mounted strips.

Parametric study was carried out in Chapter 3, where the effects of crack spacing and the rate of change of moment on the IC debonding behaviour of beams with externally bonded FRP plates are examined in the paper presented (Liu et al. 2005b).

Based on the study of IC debonding, further development was made in the modelling of CDC debonding, which is dependent on the IC debonding strength. Through this study, covered in Chapter 4, it was found that in the case of CDC debonding, the externally bonded plates can be idealized as prestressing tendons. The existing prestress model developed by Zhang (1994, 1997) and the design codes for prestress concrete beams were modified to analyse the CDC debonding of plated RC beams. The accuracy of the proposed model and design methods were verified using test results obtained from existing literature. The results are shown in the papers Oehlers et al. (2004a) and Oehlers et al. (2004b) included in the chapter.

Existing design guidelines neglect moment redistribution in FRP plated structures, but from the few tests carried out by various researchers (Mukhopadhyaya et al. 1998; El-Refaie et al. 2003; Ashour et al. 2004), moment redistribution was observed. Experimental programs, presented in Chapter 5, were carried out to determine the amount of moment redistribution achievable in continuous beams with adhesively bonded plates. Seven continuous RC beams with externally bonded CFRP or steel plates over the interior support were tested with results summarised in the paper Oehlers et al. (2004c) in Chapter 5. Also included in this chapter is the paper Liu et al. (2005c), which describes the results of tests carried out on nine continuous RC beams with near surface mounted CFRP or steel strips over the interior support.

Through the experimental work performed, it was found that a significant amount of moment redistribution can be obtained from beams with EB and NSM plates, therefore theoretical studies were carried out in Chapter 6 to develop models to determine the moment redistribution of plated continuous members. The models proposed in Oehlers et al. (2004d) and Liu et al. (2005d), included

in Chapter 6, are based on variation in flexural rigidity along the continuous beams which allows the degree of moment redistribution to be evaluated at the plastic hinges of continuous beams with and without EB or NSM plates. Parametric studies were carried out in Liu et al. (2006) presented in Chapter 6, which looks at the amount of moment redistribution achievable for different plating materials and at various locations along the continuous beam.

Finally, the thesis is concluded in Chapter 7 with a summary of all the findings in this research and any future work to be carried out.

1.4 REFERENCES

Ashour, A.F., El-Refaie, S.A. and Garrity, S.W. (2004). "Flexural strengthening of RC continuous beams using CFRP laminates". *Cement & Concrete Composites*, 26, 765-775

CEB-FIP (1998). *Ductility of Reinforced Concrete Structures-synthesis report and individual contributions*. Comité Euro-International du Béton, Switzerland.

Concrete Society Committee (2000). *Design guidance for strengthening concrete structures using fibre composite materials*. Concrete Society Technical Report no. 55, The Concrete Society, UK

El-Refaie, S. A., Ashour, A.F., Garrity, S.W. (2003). "Sagging and Hogging Strengthening of Continuous Reinforced Concrete Beams Using Carbon Fiber-Reinforced Polymer Sheets." *ACI Structural Journal*, 100(4), 446-453.

fib Task Group 9.3 (2001). *Externally bonded FRP reinforcement for RC structures.* Technical report, International Federation for Structural Concrete, Lausanne

Jansze, W. (1997). *Strengthening of RC members in bending by externally bonded steel plates*. PhD Thesis, Delft university of Technology

Liu, I.S.T., Oehlers, D.J., and Seracino, R. (2005a). "Partial interaction numerical simulation of hinges in FRP plated reinforced concrete beams." *Computers and Structures*, submitted

Liu, I.S.T., Oehlers, D.J., Seracino, R., and Teng, J.G. (2005b). "Study of intermediate crack (IC) debonding on adhesively plated beams." *ASCE Special Journal of Composites for Constructions*, in press

Liu, I.S.T., Oehlers, D.J., and Seracino, R. (2005c). "Tests on the ductility of reinforced concrete beams retrofitted with FRP and steel near surface mounted plates." *ASCE Journal of Composites for Constructions*, submitted

Liu, I.S.T., Oehlers, D.J., and Seracino, R. (2005d). "Moment redistribution in FRP and steel plated reinforced concrete beams." *ASCE Journal of composites for constructions*, submitted

Liu, I.S.T., Oehlers, D.J., Seracino, R., Ju, G. (2006). "Moment redistribution parametric study of CFRP, GFRP and steel surface plated RC beams and slabs." *International Journal of Construction and Building Materials*, 20, 59-70

Mohamed Ali, M. S. (2000). *Peeling of plates adhesively bonded to reinforced concrete beams*. PhD thesis, School of Civil and Environmental Engineering, University of Adelaide

Mohamed Ali, M. S., Oehlers D.J. and Bradford M.A. (2001). "Shear peeling of steel plates bonded to the tension faces of RC beams." *ASCE Journal of Structural Engineering*, 127(12), 1453-1460

Oehlers, D.J. (1990) "Premature failure of externally plated reinforced concrete beams." *Journal of the Structural Division of the American Society of Civil Engineers*, 116(4), 978-995

Oehlers, D.J. and Seracino, R. (2004). *Design of FRP and Steel Plated RC Structures: retrofitting beams and slabs for strength, stiffness and ductility.* Oxford, Elsevier

Oehlers, D.J., Liu, I., and Seracino, R. (2004a). "Passive prestress approach for CDC debonding of adhesively bonded steel and FRP plates." *Magazine of Concrete Research*, 56(8), 475-486

Oehlers, D.J., Liu, I., and Seracino, R. (2004b). "Prestress code approach for shear deformation debonding of adhesively bonded plates." *Proceedings of the Institution of Civil Engineers*, Structures & Buildings, 160(SB1), 1–7

Oehlers, D.J., Ju, G., Liu, I., and R. Seracino. (2004c). "Moment redistribution in continuous plated RC flexural members. Part 1: neutral axis depth approach and tests." *Engineering structures*, 26, 2197-2207

Oehlers, D.J., Liu, I., Ju, G., and R. Seracino. (2004d). "Moment redistribution in continuous plated RC flexural members. Part 2: Flexural rigidity approach." *Engineering structures*, 26, 2209-2218

Oehlers, D.J., Liu, I.S.T., and Seracino, R. (2005). "The gradual formation of hinges throughout reinforced concrete beams." *Mechanics Based Design of Structures and Machines*, submitted

Raoof, M., Hassanen, M.H. (2000). "Peeling failure of reinforced concrete beams with fibre reinforced plastic or steel plates glued to their soffits", *Proceedings of the Institution of Civil Engineers: Structures and buildings,* 140(8), 291-305

Teng, J.G., Chen, J.F., Smith, S.T., Lam, L. (2002). *FRP Strengthened RC Structures*. John Wiley & Sons, England

Zhang, J. P. (1994). *Strength of cracked concrete Part 1 Series-R*. Technical University of Denmark, Lyngby, Denmark, 106

Zhang, J. P. (1997). "Diagonal cracking and shear strength of reinforced concrete beams." *Magazine of Concrete Research*, 49(178), 55-65.

Zhang, S., Raoof, M., Wood, L.A. (1995) "Prediction of peeling failure of reinforced concrete beams with externally bonded steel plates", *Proceedings of Institution of Civil Engineers: Structures and Buildings,* 110(8), 257-268

Ziraba, Y.N., Baluch, M.H., Basunbul, I.A., Sharif, A.M., Axad, A.K., Al-Sulaimani, G.J. (1994) "Guidelines towards the design of reinforced concrete beams with external plates", *ACI Structural Journal*, 91(6), 639-646

1.5 NOTATIONS

The following symbols are used in this chapter:

E_{frp}	young's modulus of FRP
E_s	young's modulus of steel
f_{frp}	fracture stress of FRP
f_y	yield stress of steel
M	moment
P_{IC}	IC debonding strength
V	vertical shear force

The following acronyms are used in this chapter:

CDC	critical diagonal crack
EB	externally bonded

FRP	fibre reinforced polymer
IC	Intermediate crack
NSM	near surface mounted
PE	plate end
RC	reinforced concrete

CHAPTER

2 NUMERICAL MODELLING OF INTERMEIDATE CRACK DEBONDING

CONTENTS

2.1 INTRODUCTION

Intermediate crack (IC) debonding has been briefly described in Chapter 1 and it has been shown that more research is required in the area of study. When a flexural or flexural-shear crack forms intercepting a plate, theoretically an infinite plate strain is required across the crack to accommodate it. As this is impossible in reality, horizontal cracks, which are defined as interface cracks, form from the root of the cracks. These interface cracks indicate that there is slip between the plate and the adjacent concrete. For beams with reinforcing bars, as the flexural cracks intercept the bars, slip is also induced at the bar/concrete interface, and hence, the behaviour at the bar/concrete interface is similar to that at the plate/concrete interface, the only difference being the bond that is provided. In order to model the IC debonding behaviour, the local deformation along the beam needs to be analysed, and to accurately model IC debonding, the slip behaviour at the bar/concrete interface after flexural cracking will also need to be accounted for in the analyses.

In this chapter, a literature review has been carried out on some of the existing local deformation models for unplated RC beams, which takes into account the slip at the bar/concrete interface. It was found that each of the models has their shortfalls and none of them can be modified to account for an additional plate at the external surface. A lot of research has been carried out by different researchers on studying the IC debonding behaviour of plated tensile members, which is equivalent to the bond behaviour at the plate concrete interface. A review is performed in Section 2.2.2 on some of the bond-slip models developed where one of the models was chosen to be incorporated into the partial interaction model proposed later in this chapter. Very limited research can be found on IC debonding of plated flexural beams, nevertheless the few available models and design guidelines for IC debonding of flexural members are discussed in Section 2.2.3. From reviewing the literature on IC debonding of plated beams and the sliding behaviour at the bar/concrete interface of unplated RC beams, it was realised that the two structures behave similarly to that of a composite beam. The partial interaction theory developed for composite beams (Johnson 1994) is hence revised in Section 2.2.4, leading to the development of the partial interaction model for plated and unplated RC beams.

The concept of the partial interaction model proposed for plated and unplated RC beams is first presented in Section 2.3. In the preliminary stages of developing the numerical model, tension specimens were considered (Section 2.4) as it is the easiest case which has similar behaviour to that of a pull test. An initial attempt was then made in Section 2.5 to apply partial interaction theory to externally plated flexural members with and without reinforcing bars. The shortcoming of this initial partial interaction model is that the disturbed region around a flexural crack is neglected. Better

simulation of the problem was made by modifying the partial interaction model to account for the disturbed regions in the beam in Section 2.6. The development and the application of this modified partial interaction model to unplated and externally plated RC beams are presented in the journal papers Oehlers et al. (2005) and Liu et al. (2005) in Sections 2.6.1 and 2.6.2 respectively. These papers also cover the studies performed on the sliding and IC debonding behaviour of beams based on the partial interaction model proposed. Further discussions on the development of the modified PI beam model are given in the subsequent section, where the fundamental behaviour of plated beams with multiple reinforcing layers, and the derivation of the governing equations used in the model are presented.

2.2 LITERATURE REVIEW

The two major factors that influence the behaviour of intermediate crack debonding are: the local deformation of the unplated reinforced concrete beam; and the bond-slip relation at the plate/concrete interface. In this literature review, the existing models for analysing the local deformation (or rotation) capacities of unplated RC beams where slip has occurred at the bar/concrete interface due to flexural cracks have been reviewed and the possibility of modifying the models to allow for external plates is discussed in Section 2.2.1. The bond-slip relationship at the plate/concrete interface is studied in Section 2.2.2, where one of the bond-slip models was chosen to be incorporated into the partial interaction model proposed in Sections 2.3 to 2.5. In Section 2.2.3, the available IC debonding models and design guidelines are reviewed. Partial interaction theory for composite beams is then described and the applicability of the theory to plated and unplated RC beams is discussed in Section 2.2.4.

2.2.1 UNPLATED REINFORCED CONCRETE BEAMS

Since the mid 90s, much research has been focusing on modelling the local deformation of unplated reinforced concrete beams. These models are used to determine the available rotation capacity of continuous members, which is a major influence in the capability of members to redistribute moment. Early approaches for determining the plastic rotation at a highly stressed region, also defined as a plastic hinge, assume that the curvature is constant over a hinge length (Baker 1961), where the curvature is governed by the maximum moment section. The obvious weakness of this method is the assumption that the rotation capacity of the plastic hinge is dependent on the curvature of a single

section only, neglecting the influence of the uncracked concrete between cracks. In addition, the assumption of Bernoulli's law of plane sections remaining plane may be invalid at high loads (CEB-fib 1998).

Further development in the rotation capacity analyses lead to smeared crack modelling, which divides the beam into equally sized blocks with the curvature and stress distributions inside each block assumed to be constant. The average curvature at each block is determined from the section with the highest moment in the block (Kodur 1992, Wong & Warner 1998, 1999). The problem with smeared crack modelling includes (Rebentrost 2003):

- Local strain variations between cracks are neglected;
- The rotation capacity is evaluated from the equivalent curvature at each block rather than the local behaviour along the beam;
- Effects of the shear and the tension in concrete is neglected or simplified in the analyses;
- Assumption of Bernoulli's law may not be valid at high loads.

Both plastic hinge and smeared crack models are based on taking average deformations such that the local strain distributions between cracks are ignored in the analyses. Therefore these methods do not allow for the tension stiffening effects in beams, that is the additional stiffness provided by the tensile stress in the concrete cracks. Tension stiffening effect can have significant influence on the beam behaviour when the deformations are sensitive to the local behaviour along the beams, such as for plated RC beams where the local variation in concrete and plate strains largely affects the IC debonding behaviour at the plate/concrete interface. Also, there is a potential problem with applying average strains for the elements in highly stressed areas where large variations in local deformation occur.

Recognizing the fact that deformations along the plasticized part of the beam are discontinuous and that curvature is concentrated in flexural cracks, while the contribution of the concrete between cracks is very small, Bachmann (1967) proposed the discretization of a flexural hinge, where vertical cracks occur, and a shear hinge with inclined cracks as illustrated in Figure 2.1. This led to the development of discrete crack models (i.e. Langer 1987), which considers the local variation in strains along the member and evaluates the local curvatures from these strains. This type of modelling is much more suitable for evaluating the deformation capacity of plastic hinge regions where the local deformations such as bar strains have large variations along the beam.

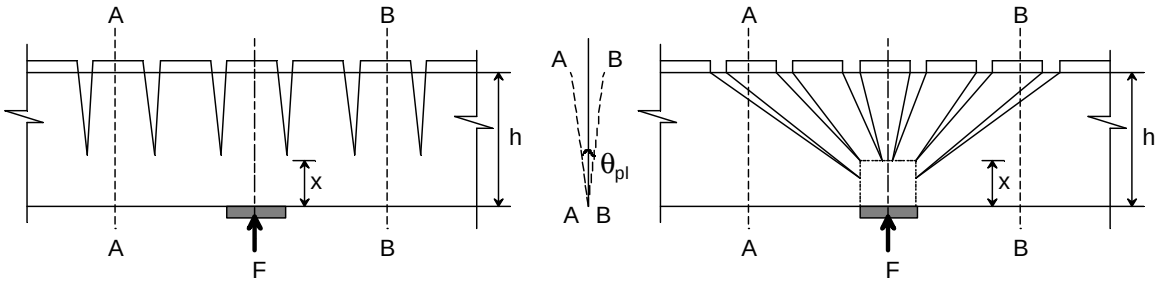

Figure 2.1 Flexural and shear crack hinge (Bachmann 1967)

The recent discrete crack models (i.e. Langer 1987, Graubner 1987, Cosenza et al. 1991, Fantelli et al. 1998, Manfredi & Pecce 1998, Gravina 2002, Kwak & Song 2002, Rebentrost & Warner 2002) acknowledge the importance of bond at the reinforcement concrete interface, and hence incorporate the bond-slip law, as well as realistic material relations for steel and concrete in simulating local deformations and rotation capacities of RC beams. Langer (1987) developed a discrete crack model whereby the moment-curvature is evaluated based on known dimensions of the cross-section of the beam as illustrated in Figure 2.2. The model assumes a linear strain profile at the cracked section where the curvature is determined from the moment-curvature or tensile force-curvature relationship. Cracks are equally spaced at predefined crack spacings, and the contribution of the concrete in tension between cracks is determined using an iterative solution of the differential equation of bond (Kreller 1989, Eligehausen et al. 1983). Researchers such as Graubner (1987, 1997), Cosenza et al. (1991) and Manfredi & Pecce (1998) have developed models based on Langer's model, all of which suffer similar shortfalls including the assumptions of: linear varying strain at cracked sections which is invalid at high loads and which also restricts the application of the models to a single reinforcing layer only; a predefined crack spacing; and the deformation of concrete in tension is neglected. Fantelli et al. (1998) and Gravina (2002) modified Langer's model such that the crack positions could be determined from the models.

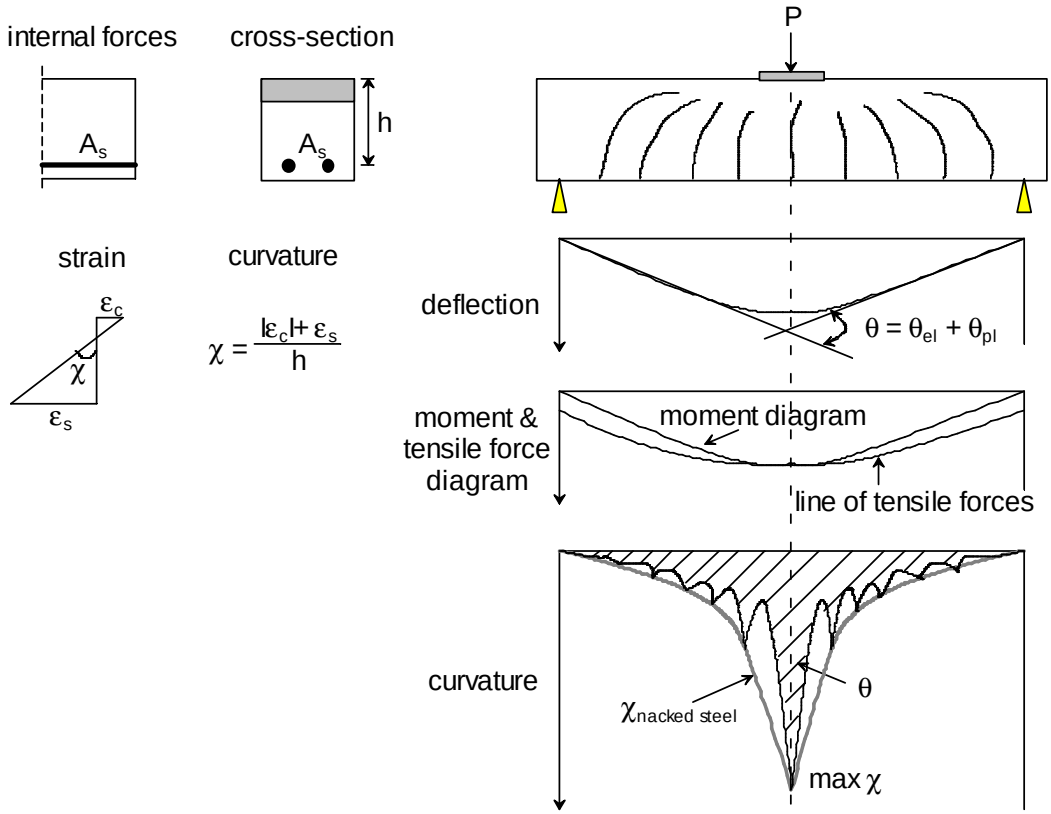

Figure 2.2 Rotational capacity model (Langer 1987)

Kwak & Song (2002) proposed a polynomial function to determine the local bar strain distribution between cracks, hence neglecting the local bond-stress behaviour in the analyses. This model is, however, unsuitable for plated RC beams as the different bond-slip behaviours at various interfaces need to be considered in modelling, and also the assumption that the point of zero slip occurs at the midpoint between two adjacent cracks is invalid for beams under varying moments.

All the models mentioned above can only allow for uncracked or fully cracked beams with a single reinforcing layer. Rebentrost's model (Rebentrost 2003, Rebentrost & Warner 2002) has the advantage of being able to analyse progressive cracking of multiple layered reinforced beams, however the model neglects the tensile strength in concrete, and it assumes that the there is always a point of zero slip in between adjacent cracks which is not true when sliding, or debonding, occurs at the reinforcement/concrete interface. It is also assumed in the model that the local concrete strain varies linearly between adjacent cracks.

It is worth noting that all of the existing rotation capacity models can only account for gradual rising moment-curvature branches in the post yielding region. Therefore these models can only predict

rotations up to the peak moment, however it is found experimentally that there is a significant increase in hinge deformation after the peak load has been reached (Pecce 1997; Alca et al. 1997).

Through the review of the various rotation capacity models for unplated RC beams, it was found that models based on discrete cracking are more suitable for analysing the local deformation of cracked RC beams. As intermediate crack debonding of plated beams is initiated by cracks intercepting the plate, to accurately model this debonding mechanism, which is largely dependent on the local deformation between cracks, beams should be analysed based on discrete cracking, as suggested by Sebastian (2001). This form of modelling allows the local deformation behaviour between cracks, and hence the local variation in strains, to be evaluated, such that any premature failures such as fracture of the plate or bar, or debonding failure can be accounted for in the analyses. However, most of the discrete crack models for unplated beams (except the model by Rebentrost 2003) are limited to a single layer of reinforcement only due to the assumption of linear variation in strains at the cracked sections, prohibiting the application of these models to plated RC structures. The predefined crack spacings required for most of these existing models also make them unsuitable for plated beams, as IC debonding behaviour is sensitive to the position of the intercepting flexural cracks which cause it.

2.2.2 Intermediate Crack Debonding of Tensile Specimens

2.2.2.1 Bond Strength at Plate/Concrete Interface

The bond that is necessary to transfer forces from the concrete into the plate governs the intermediate crack (IC) debonding resistance of plated members as it controls the propagation of the IC interface cracks and ultimately the IC debonding mechanisms and resistance (Oehlers & Seracino 2004). This bond behaviour can be analysed in simple shear or pull tests (Täljsten 1994; Chajes et al. 1995, 1996; Bizindavyi & Neale 1999) as illustrated in Figure 2.3 where an external plate of width b_p is adhesively bonded to a concrete block of width b_c. As the axial load T is applied, the concrete block is restrained resulting in debonding cracks that initiate from the loaded end and propagate towards the plate end causing IC debonding failure. The behaviour of pull tests is similar to that of a plated beam with a single flexural crack, where the flexural crack represents the loaded end of the concrete prism (Oehlers & Seracino 2004).

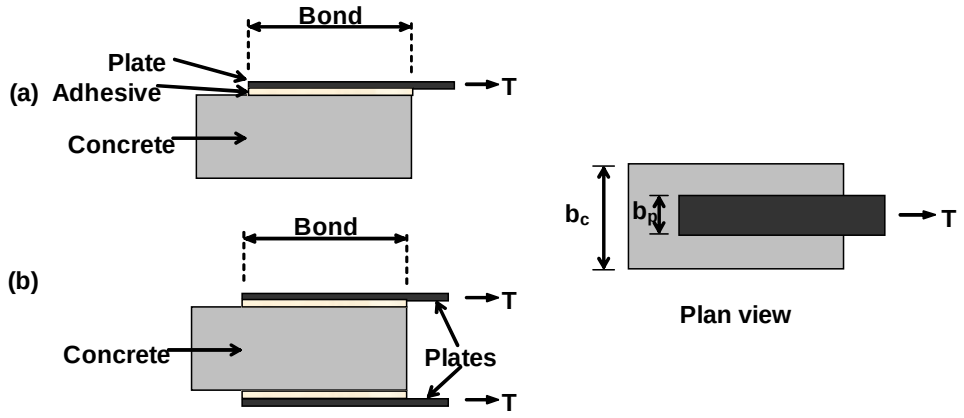

Figure 2.3 (a) Single; and (b) double shear tests of a plate-to-concrete-bonded joint

It is important to note that for plated specimens, there is an effective bond length beyond which further increase in bond length will not result in an increase in the bond strength at the interface (Täljsten 1994; Chajes et al. 1995, 1996). However, a longer bond length will improve the ductility of the failure process (Teng et al. 2002). This is distinctly different from the bond of an internal reinforcing bar in which the bond strength can always be increased with an increase in bond length. The variation of the bondstress (that is the shear stress along the plate/concrete interface) over the plate length is shown in Figure 2.4 with a crack occurring at distance zero. It can be seen that in the initial stage of loading, the bondstress is highest near the crack, however as the load increases, the location of maximum bondstress moves away from the crack. The bond behaviour is often shown in terms of bondstress τ_b verses slip, where slip is the displacement between the plate and the concrete. This τ_b-slip relationship can be treated as a material property, like the stress-strain relationship of concrete, such that it can be inputted into the numerical model presented later in this chapter to simulate the IC debonding behaviour of plated members.

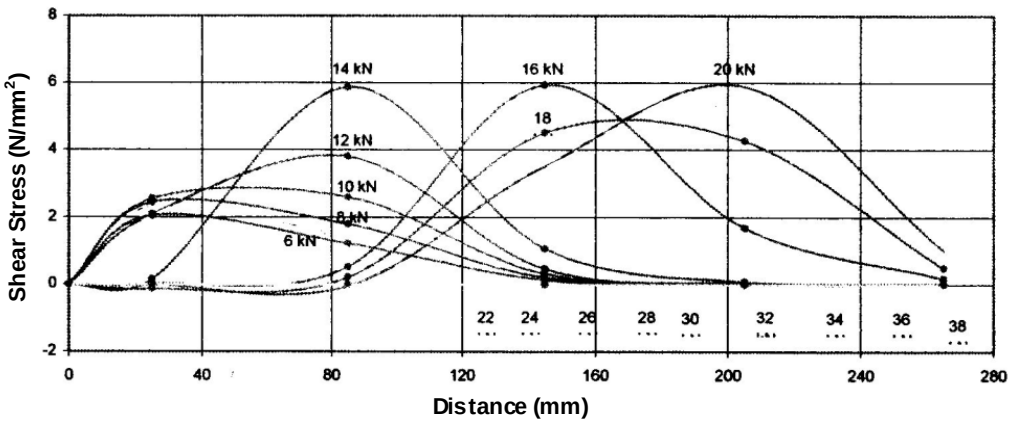

Figure 2.4 Distribution of shear stresses over plate length (Zilch et al. 1998)

The bond behaviour at the interface can also be represented by the variation of plate stress at the intermediate crack σ_{IC} with slip at the same position s_{IC} (Yuan et al. 2003). This local variation of σ_{IC}/ s_{IC} at a crack as illustrated at A in Figure 2.5, which is dependent on the material characteristics τ_b/slip (B in Figure 2.5), models the behaviour between two adjacent cracks, and hence, is equivalent to the bond-slip relationship of shear connectors in composite beams (Oehlers & Seracino 2004).

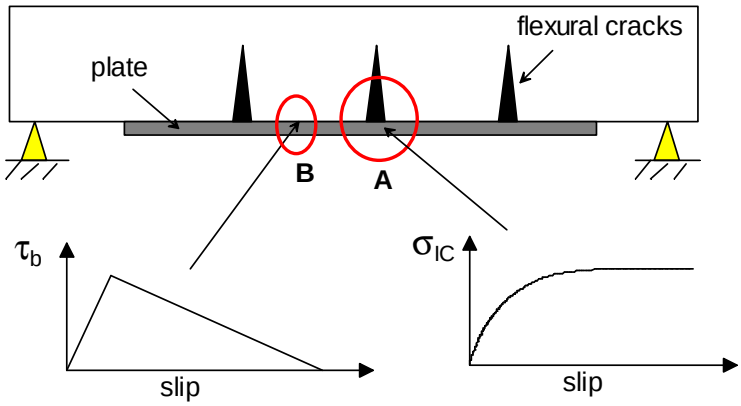

Figure 2.5 Bond behaviour at plate/concrete interface

Much research has been carried out by different researchers to model the bond-slip behaviour at the concrete-to-plate interface and these models can be classified into three categories:

- Empirical models
- Fracture mechanics models
- Design approaches

It is worth noting that from experimental observations, most interface cracks propagate in the concrete adjacent to the adhesive irrespective of the plating material (Chen & Teng 2001). This indicates that the bond models developed can be applied to both steel and FRP plated joints. A brief review of some of the existing bond models under the three categories above are presented in the following sections.

2.2.2.2 EMPIRICAL MODELS

These models were developed from regression analysis of data from shear tests. Hiroyuki and Wu (1997) and Tanaka (1996; cited Teng 2002) developed simple expressions for the average bondstress at failure τ_u (Equation 2.1& Equation 2.2 respectively) considering only the bond length *L*.

$$\tau_u = 5.88L^{-0.669} \quad \text{MPa} \qquad \textbf{Equation 2.1}$$

$$\tau_u = 6.13 - \ln L \quad \text{MPa}$$ **Equation 2.2**

Where *L* is in cm for Equation 2.1 and in mm for Equation 2.2.

Maeda (Maeda et al. 1997) developed a slightly better model taking into account the effective bond length L_e (mm), the modulus of elasticity E_p (MPa), the plate width b_p (mm) and the thickness of the plate t_p (mm). The ultimate bond strength P_u is given by Equation 2.3 below.

$$P_u = 110.2x10^{-6} E_p t_p b_p L_e$$ **Equation 2.3**

Clearly the accuracy of these empirical models is limited as they are overly simplified, and neglect the influence of the concrete properties on the performance of the bond.

2.2.2.3 FRACTURE MECHANICS MODELS

There are several fracture mechanics based models that have been developed. Although much more complicated, these models generally give better prediction of the behaviour of the bondstress than the empirical models mentioned above (Teng et al. 2002).

Holzenkämpfer (1994) used nonlinear fracture mechanics (NLFM) to develop a model for bond strength between steel and concrete (Equation 2.4), which was later modified by Niedermeier (1996; cited in Teng et al. 2002). This model takes into account the modulus of elasticity E_p, and the thickness of the plate t_p, fracture energy G_f, the tensile strength of the concrete f_{ct}, and width of plate b_p and beam b_c. To determine the fracture energy, a constant c_f need to be determined experimentally.

$$P_u = \begin{cases} 0.78 b_p \sqrt{2 G_f E_p t_p} & if \quad L \geq L_e \\ 0.78 b_p \sqrt{2 G_f E_p t_p}\, \dfrac{L}{L_e}\left(2 - \dfrac{L}{L_e}\right) & if \quad L < L_e \end{cases}$$ **Equation 2.4**

where $L_e = \sqrt{\dfrac{E_p t_p}{4 f_{ct}}}$ **Equation 2.5**

From conducting a series of double shear tests on CFRP plated concrete joints, Neubauer and Rostásy (1997) modified Holzenkämpfer's model by changing the factor of 0.78 to 0.64 in Equation 2.4, and increased the effective bond length by replacing $4f_{ct}$ with $2f_{ct}$ in Equation 2.5. Through these

modifications, the model can now apply to both steel and FRP plated beams. From the tests they carried out, Neubauer and Rostásy concluded that the bond-slip behaviour can be represented by a triangular model as shown in Figure 2.6 for both concrete fracture (i.e. failed by crack propagation in the concrete adjacent to the adhesive) and FRP delamination failures (i.e. bond failure in the adhesive layer), where the bond behaves linear elastically until the peak bondstress $\tau_{b.max}$ is reached at a relative slip of s_{max}. Further increase in slip beyond s_{max} causes micro-debonding, that is softening occurs and the bondstress reduces linearly until zero bond is obtained at an ultimate slip of s_f, after which macro-debonding occurs and all bond is lost at the plate/concrete interface. The area under the bond-slip graph is defined as the fracture energy G_f.

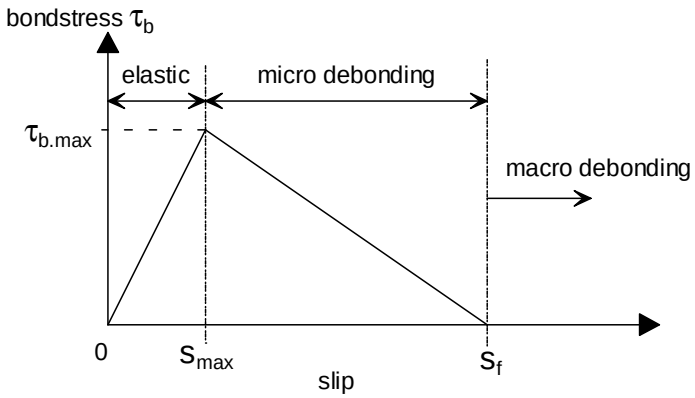

Figure 2.6 Triangular bond-slip model (Holzenkämpfer 1994)

Täljsten (1994) developed a model similar to Holzenkämpfer's, with the difference in that this model takes into account the elastic modulus E_c and the thickness t_c of the concrete (Equation 2.6 & Equation 2.7). This model indicates that as the thickness of the concrete tends to infinity i.e. for deep beams, the properties of the concrete has no influence on the bond strength at the concrete/plate interface.

$$P_u = \sqrt{\frac{2E_p t_p G_f}{1+\alpha}} b_p \qquad \textbf{Equation 2.6}$$

where $\alpha = \frac{E_p t_p}{E_c t_c}$ **Equation 2.7**

Yuan (1999, 2001) developed practically the same model as Täljsten (Equation 2.6), the only difference in that they have included the effect of the ratio of plate width b_p to concrete width b_c through multiplying α (Equation 2.7) by b_p/b_c.

Chen and Teng (2001) proposed a bond strength model (Equation 2.8 & Equation 2.9) based on combining fracture mechanics analysis with experimental results, assuming a triangular shear-slip relationship (Figure 2.6). They demonstrated the importance of b_p/b_c (width ratio of plate to concrete) on the ultimate bond strength. If b_p is smaller than b_c the force transfer from the plate to the concrete leads to a non-uniform stress distribution across the width of the concrete member, possibly resulting in a higher shear stress at the interface at failure due to the contribution from the concrete outside the bond area. Chen and Teng related the ultimate bondstress τ_f to the tensile strength, and hence the compressive strength, of concrete, making the model easier to apply compared to other fracture mechanics based models. An expression for effective bond length L_e is also approximated (Equation 2.10).

$$P_u = \alpha \beta_p \beta_L \sqrt{f_c'} b_p L_e \qquad \text{Equation 2.8}$$

where $\beta_p = \sqrt{\frac{2 - b_p / b_c}{1 + b_p / b_c}}$, $\beta_L = \begin{cases} 1 & if \quad L \geq L_e \\ \sin\left[\frac{\pi L}{2 L_e}\right] & if \quad L < L_e \end{cases}$ Equation 2.9

and $L_e = \sqrt{\frac{E_p t_p}{\sqrt{f_c'}}}$ Equation 2.10

The α coefficient was calibrated using a large number of pull tests with steel and FRP plates and a mean of 0.427 was obtained with a 95% characteristic value of 0.315. A possible limitation of all the fracture mechanics based models discussed is the exclusion of the properties of the adhesive which was proven by Leung (2001) to have an influence on the bond strength at the interface.

2.2.2.4 Design Approaches

Different design rules have been made by various researchers for estimating the bond strength of a plate-to-concrete joint. Van Gemert (1980) presented a rather conservative design proposal (Equation 2.11), however this proposal failed to recognize the importance of the effective bond length of plated members.

$$P_u = 0.5 b_p L f_{ct} \qquad \text{Equation 2.11}$$

Chaallal (Chaallal et al. 1998) developed a design model that is based on the assumption that the bond behaves as a Mohr Coulomb material (Equation 2.12). This model again lacks accuracy as it neglects the influence of the effective bond length. Also the model was developed based on limited experimental data and doesn't include the effect of the strength of the concrete on debonding failure. This model does however account for the elastic modulus E_a, width b_a, and thickness t_a of the adhesive (Equation 2.13).

$$\tau_u = \frac{2.7}{1 + k_1 \tan 33} \qquad \text{Equation 2.12}$$

where $k_1 = t_p \sqrt[4]{\frac{K_n}{4E_p I_p}}$ and $K_n = E_a \frac{b_a}{t_a}$ Equation 2.13

In which τ_u is the average bondstress at failure, and I_p is the second moment of area of the plate.

Khalifa (Khalifa et al. 1998) also developed a design rule by modifying Maeda (Maeda et al. 1997) empirical model. They related the bond strength at the concrete/plate interface with the strength of the concrete by multiplying Equation 2.3 by $(f'_c/42)^{2/3}$. Unlike the previous two design proposals, Khalifa's model accounts for the effective bond length.

2.2.2.5 ACCURACY OF EXISTING BOND MODELS

The accuracy of some of the existing bond models discussed above is assessed by comparing predicted bond strengths with experimental results of both FRP and steel plated joints (Chen & Teng 2001). From Figure 2.7 it can be seen that the empirical models by Hiroyuki and Wu (1997) and Tanaka (1996), and the design rules by van Gemert (1980) and Chaallal (Chaallal et al. 1998) all gave poor predictions of the bond strengths. This is possibly due to the fact that none of these models takes into account the influence of effective bond length on the bond strength of the joints. Khalifa's design proposal (Khalifa et al.1998), which is based on Maeda's (Maeda et al. 1997) empirical model, gives a reasonable estimation of the bond strength, however it tends to overestimate the bond strength (Figure 2.7) and underestimate the effective bond length (Table 2.1), making it unsafe to use in design. Neubauer's (Neubauer & Rostasy 1997) fracture mechanics model gives even better correlations between the experimental and predicted bond strengths (Figure 2.7). It can also predict rather accurately the effective bond lengths of joints (Table 2.1). However like Khalifa's model, this model overestimates the bond strength. Comparing all the existing models, Chen and Teng's model (Chen & Teng 2001) generally performs the best in predicting both the bond strength and the bond

length of FRP and steel plated joints. A problem with their model is that the influence of the adhesive on the bond strength is neglected.

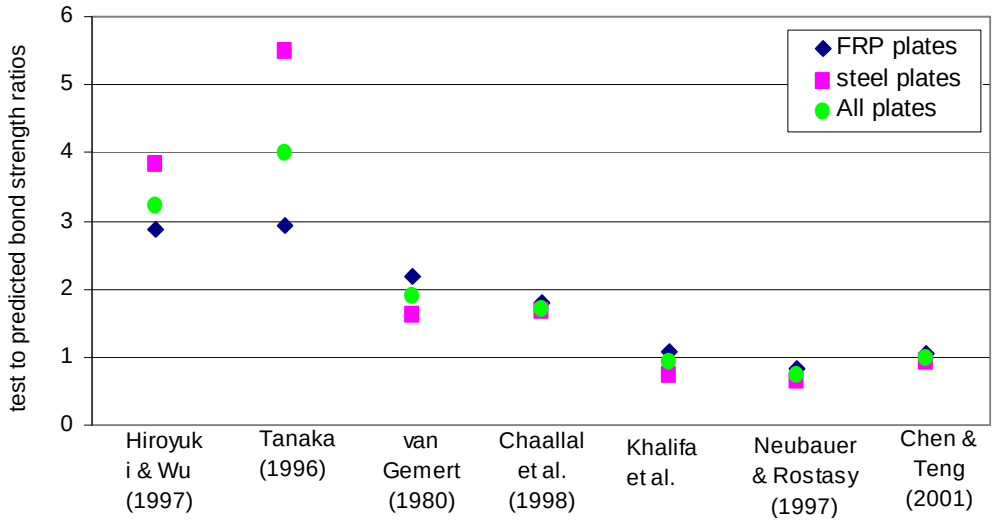

Figure 2.7 Test to predicted bond strengths ratios (Teng et al. 2002)

Table 2.1 Test and predicted effective bond length (Teng et al. 2002)

Researchers	Test specimen	Test L_e (mm)	Estimated L_e (mm)					
			Khalifa et al. (1998)		Neubauer & Rostasy (1997)		Chen & Teng (2001)	
			L_e	Est/test	L_e	Est/test	L_e	Est/test
Bizindavyi & Neale (1999)	BN1 (GFRP)	75	65.1	0.87	64.6	0.86	66.9	0.89
	BN2(GFRP)	100	43.6	0.44	91.3	0.91	94.6	0.895
	BN3 (CFRP)	55	71.3	1.3	59.7	1.09	61.9	1.13
	BN4 (CFRP)	70	47.7	0.68	84.5	1.21	87.5	1.25
Täljsten (1997)	(Steel)	~300	11.3	0.04	260-280	0.9	275-293	0.94

Est = estimated

From the literature review, it was found that the τ_b-slip behaviour is best represented by a triangular relationship with an initial ascending branch up to the peak bondstress followed by a linear descending branch until all bond is lost. Therefore based on the comparison of the various models in Figure 2.7, the bilinear model by Chen and Teng (2001) was used in the numerical simulations of plated members covered later in this chapter.

2.2.3 INTERMEDIATE CRACK DEBONDING OF FLEXURAL MEMBERS

Although it is possible to prevent premature intermediate crack debonding failure from occurring, IC interface cracking is inevitable whenever cracks form in the vicinity of the plate. As these interface cracks propagate, they will affect the local deformation along the beam, and hence, it is crucial that IC interface cracking or IC debonding is accounted for in analysing plated members.

Due to similar mechanisms behind the failure of a plated concrete joint subjected to pure tension and intermediate crack debonding failure of a flexural member, much research has been carried out in studying the bond strength at the concrete/plate interface alone, and very little has been carried out on IC debonding. Nevertheless a few attempts have been made by codes of practice (Concrete society 2000; fib 2001) and different researchers (Matthys 2000; Niedermeier 2000; Chen & Teng 2001; Leung 2001; Niu & Wu 2001a,b; Aiello & Ombres 2004) to give some guidance in dealing with the problem.

2.2.3.1 CONCRETE SOCIETY APPROACH

In the technical report prepared by the Concrete Society (2000), they suggested to limit the strain in the FRP plate in order to prevent IC debonding failure. It is proposed that the strain in the FRP should not exceed 0.008 under uniformly distribution loading, and 0.006 for point loading in regions where both vertical shear and moment are high. This approach provides simple rules of thumb that are based on experiment data on specific CFRP plated beams rather than a model to simulate the behaviour of IC debonding. Therefore these strain limits are not applicable for beams with different arrangements and plating materials to those tested. They also suggested that the longitudinal shear stress τ should be checked at positions where internal reinforcement first yields using Equation 2.14. An inherent problem with this is that for simply supported beams under uniformly distributed loading, reinforcement first yields at location where there is zero vertical shear force *V*, hence the resultant longitudinal shear stress is also zero. This contradicts previous experimental evidence (Teng et al. 2002; Oehlers 2000) that IC debonding always initiates at positions of maximum plating strain.

$$\tau = \frac{V\alpha_f A_f (h - d_n)}{I_{cs} b_a} \qquad \textbf{Equation 2.14}$$

Where in Equation 2.14 *V* is the ultimate shear force; α_f is the short-term modular ratio of FRP to concrete; A_f is the area of FRP plate; *x* is the depth of neutral axis of strengthened section; I_{cs} is the

second moment of area of strengthened concrete equivalent cracked section; and b_a is the width of adhesive layer.

2.2.3.2 *fib* APPROACH 1- BASED ON PULL TESTS

This approach idealizes the mechanism of intermediate crack debonding into that of a plate-to-concrete bonded joint under tension, by assuming that the debonding strength of a plated beam is affected by the bond strength at the plate/concrete interface only. The approach involves: (1) verification of the end anchorage using bond strength models (refer to Section 2.2.2) and bondstress-slip; (2) imposing a strain limitation on the plate to avoid debonding between plate ends. (*fib* 2001)

As the plate strength is assumed to depend on the bond strength only which in turn is dependent on the length between the axial load and the plate end, to prevent IC debonding failure, this approach requires that the plate to be terminated at the point of contraflexure i.e. in the uncracked region. Although this will allow as much anchorage strength to develop as possible, it is often difficult to determine the location of the uncracked regions.

The use of a strain limitation, which is also adopted in the Concrete Society Approach (Section 2.2.3.1), is a much simplified way of dealing with the problem of IC debonding, as the FRP strain corresponding to bond failure is not a fixed value. It is dependent on many different parameters such as loading arrangements, behaviour of internal reinforcement, and crack distributions (*fib* 2001).

2.2.3.3 *fib* APPROACH 2- NIEDERMEIER'S (2000) MODEL

This model developed by Niedermeier (2000; cited in *fib* 2001) is based on the bondstress-slip relationship and the envelope line of tensile stresses in FRP as shown in Figure 2.8, where N_s and N_f represents the tensile forces of reinforcing bars and external plate respectively. It involves comparing the maximum possible increases in tensile stress within the plate σ_{fd} (transferred by bondstress τ_f) between 2 subsequent flexural cracks (LHS of inequality equation in Figure 2.9), with the increase calculated assuming full interaction given by RHS of inequality equation in Figure 2.9. Debonding was found to occur when the increase in the plate's tensile stress exceeds that transferred by bond stresses. As analysis is required between cracks, therefore crack spacing need to be determined and the assumption of constant crack spacing is assumed. It is worth noting that Niedermeier assumed that the bond stress between two adjacent cracks occurs in one direction as shown in Figure 2.9, however in order to maintain equilibrium of forces, shear stress reversal is required between cracks such that the plate strains will be highest at the cracks, and decrease further away from cracks. Niedermeier has illustrated in his model that the force in the plate is dependent on the anchorage

force in the uncracked region, and the sum of the bond forces between subsequent flexural cracks that are caused by the beam action. A potential problem with this model is that if debonding occurs in the central region due to excessive slip before the anchorage force in the uncracked region can fully develop, then some limitation has to be placed in summing the overall strengths. Unfortunately, there are insufficient details given in the *fib* report to enable a deeper understanding in the theory behind this model.

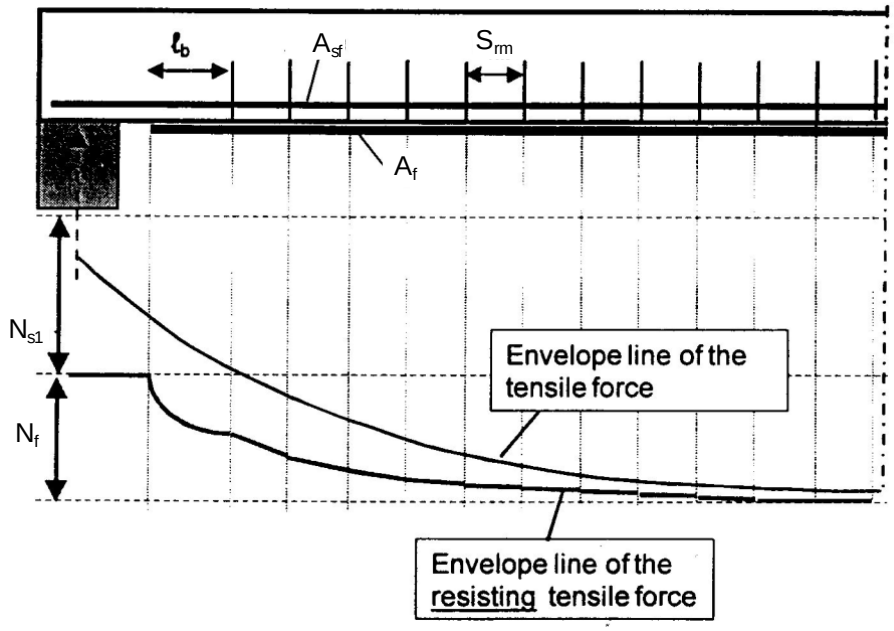

Figure 2.8 Envelope line of the resisting tensile forces (Niedermeier 2000)

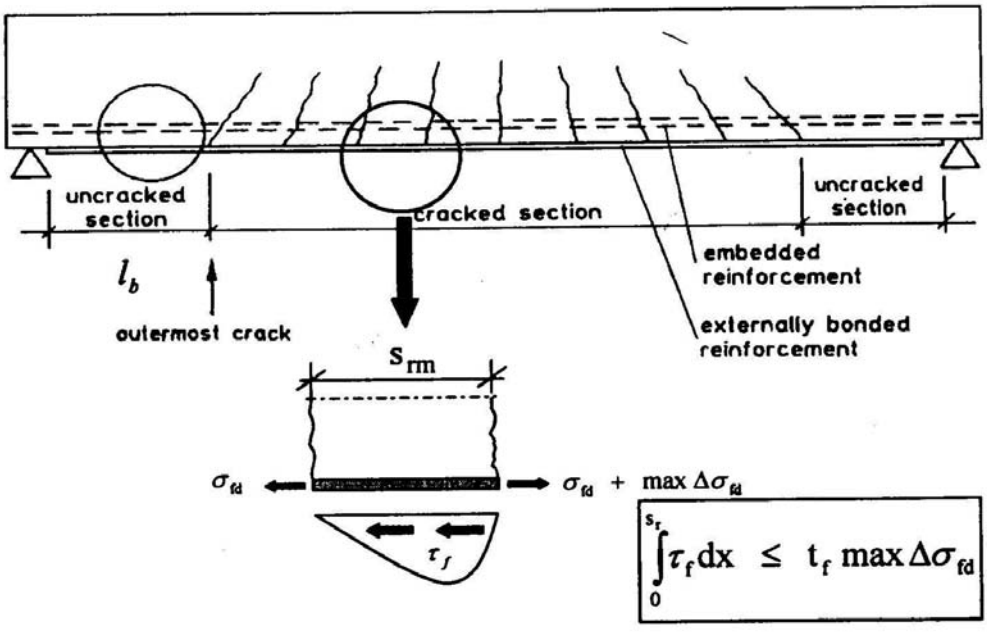

Figure 2.9 Element between 2 subsequent cracks (Niedermeier 2000)

2.2.3.4 *fib* APPROACH 3- MATTHYS'(2000) MODEL

This model proposed by Matthys (2000; cited in *fib* 2001) is similar to Approach 1 of *fib* report, whereby the end anchorage and the shear stress along the interface needs to be verified. A major set back in this approach is that it is based on the stress distribution for a homogeneous, uncracked beam. It also assumes that bondstress is constant along the beam, which contradicts experimental findings (Teng et al. 2001, Oehlers & Seracino 2004). This model is largely dependent on the vertical shear force in the member, indicating that IC debonding will not occur in regions of zero vertical shear such as in constant moment regions. This again opposes the results found experimentally (Oehlers & Seracino 2004).

2.2.3.5 CHEN AND TENG'S MODEL

Chen and Teng (Teng et al. 2002) recognized the similarities between IC debonding and simple shear tests (Figure 2.3), and hence proposed a model based on the bond strength model (refer to Section 2.2.2) that they developed (Chen & Teng 2001). Through finite element study (Chen et al. 2001), they realised that the stress distribution in debonded beams is different from those in bonded joints, particularly the peak values in the adhesive near an intermediate flexural crack. They made modifications to the bond strength model (Equation 2.15) by recalibrating it with a collection of test data of beams and slabs and proposed the following equation for determining the IC debonding stress σ_{IC}:

$$\sigma_{IC} = \alpha\beta_p\beta_L\sqrt{\frac{E_{frp}\sqrt{f_c}}{t_{frp}}} \qquad \textbf{Equation 2.15}$$

Where α is the coefficient that was calibrated. It is suggested that for design a value of 0.4 should be used. Although the equation works well for pull tests, it can be seen from Table 2.2 that the average and the characteristic (95%) values for α vary significantly for both beams and slabs, which indicates there is large scatter in results. There is also a variation in the values of α for beams and for slabs. This suggests that Chen and Teng's model does not sufficiently identify all the parameters that influences the IC debonding of beams. The fact that the α value for beams (0.887) is greater than that for pull tests (α=0.427) indicates that the distributed flexural cracks in beams allows greater plate forces to be achieved, and hence, the IC debonding of flexural members cannot be directly idealised into a simple pull test.

Table 2.2 IC debonding α coefficient (Teng et al. 2002)

α	Pull tests	Beams	Slabs	Beams & slabs
mean	0.427	1.100	0.720	0.887
95% characteristic	0.315	0.544	0.478	0.379

It is worth noting that the assumption of plane sections remaining plane was made in determining the coefficient α. This assumption is obviously invalid in debonded sections because the relative displacement between the plate and the adjacent concrete, will cause the strains in the plate and the adjacent concrete to be different. This model was developed for FRP plated beams and only applies to linearly elastic plating materials, hence it cannot be used for steel plated beams where yielding of the plate may occur.

2.2.3.6 LEUNG'S MODEL (2001)

Leung (2001) developed a model, based on fracture mechanics, for determining the interfacial stress at the plate to concrete interface, taking into account the effects of applied moment, vertical shear force, crack length and crack width. The use of this model is however very limited as it predicts only the likelihood of IC debonding and does not give a failure criterion i.e. it does not identify when IC debonding failure will occur. This model was verified by finite element analyses only, therefore lacks experimental support. An extensive parametric study was also carried out to assess the influence of different parameters on the interfacial stress. It was found that variations in plate geometry and stiffness, adhesive thickness, member size and reinforcement ratio will all affect the behaviour of the interfacial stress.

2.2.3.7 NIU AND WU'S APPROACH

Recognizing that IC debonding is the most dominant debonding failure mode especially for beams strengthened with thin plates, Niu and Wu performed studies to predict IC debonding initiation and failure based on fracture energy. By adopting a linear bond model and assuming that a single crack occurs in the beam, mathematical equations were proposed to evaluate the shear stress distribution along the plate/concrete interface (Wu and Niu 2000) based on linear elastic beam theory. Niu and Wu believed that the bond strength is responsible for the initiation of debonding while the propagation is governed by the interfacial energy, and hence, quantified the interfacial fracture energy for debonding based on test results and proposed equations to predict the debonding failure load for plated members where a single flexural crack has formed (Wu and Niu 2000).

Acknowledging the deficiency in adopting a linear bond model and that the debonding behaviour is very different for beams with multiple cracks, further studies were carried out by the researchers (Niu & Wu 2001a,b). They proposed a closed-form analytical solution for predicting interfacial shear stresses induced by flexural cracks, whereby a bilinear bond-slip model was considered (Niu & Wu 2001a). These mathematical derivations, however, have their limitations as they considered that all the materials were linear elastic, the bending moment in the plate was ignored, and it was assumed that plane sections remain plane. Therefore the accuracy of this proposed solution is questionable when analysing beams subjected to large loads where plasticity occurs and the strain profiles do not vary linearly.

Niu and Wu (2001b) noted that the shear stress transferred near flexural cracks in plated beams with a single crack is similar to that in simple shear tests. From mathematical solutions based on the fracture energy method, the maximum transferable load P_{max} in a simple shear test can be determined from Equation 2.16, provided that the bonding length is larger than the effective bond length L_e.

$$P_{\max} = b_2\sqrt{2G_f E_2 t_2} \qquad \textbf{Equation 2.16}$$

Where E_2, t_2, b_2 and G_f are elastic modulus, thickness, width of FRP and fracture energy respectively.

Niu and Wu also proposed an analytical method to predict the response of the plated beams (Niu & Wi 2001b). This method, however, neglects premature debonding failure of beams, with the assumptions that plane sections remain plane; slip does not take place at both the bar/concrete and plate/concrete interfaces; and the tensile strength of the adhesive is ignored.

Through their studies, Niu and Wu (2001a,b) found that for beams with distributed flexural cracks, the ultimate load at which debonding occurs can be significantly higher than that obtained from simple shear tests. Hence, they modified Equation 2.16 by assuming that the flexural cracks are smeared in the beam as illustrated in Figure 2.10 and the debonding failure load is predicted when complete debonding occurs between two flexural cracks with a spacing of an effective transfer length given by Equation 2.17.

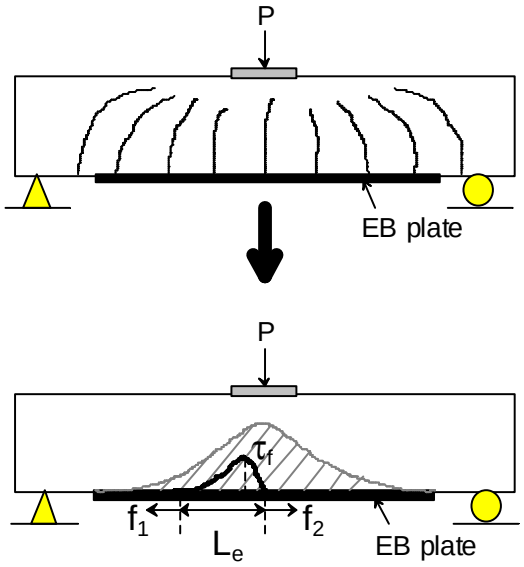

$$L_e = k\sqrt{E_2 t_2}$$

$$f_2 - f_1 = b_2\sqrt{2G_f E_2 t_2}$$

$$(f_2 - f_1) \Rightarrow P$$

Figure 2.10 Niu & Wu's model for predicting IC debonding failure (Niu & Wu 2001b)

$$L_e \approx \frac{2P_{\max}}{\tau_f b_2} = \frac{2\sqrt{2G_f E_2 t_2}}{\tau_f} \propto \sqrt{E_2 t_2} \Rightarrow L_e(mm) = k\sqrt{E_2 t_2 (MPa.mm)}$$

Equation 2.17

Where *k* is a coefficient determined from experiment.

For analysing intermediate crack debonding of plated flexural members, Niu and Wu (2001b) proposed that in cases where debonding does not occur, full interaction analysis is appropriate, where the moment capacity evaluated from full interaction analysis is reduced by a factor of 0.9 to account for local debonding. However, when debonding is observed, the simple smeared model (Figure 2.10) and equivalent bond length equation (Equation 2.17) should be applied to determine the ultimate capacity of the member. This proposed model overly simplifies the problem of IC debonding and does not model the true local debonding behaviour along the beam, and there seems to be a lack of experimental verification. Despite the ease of application of this proposed method, as stated in Section 2.2.1 and by Sebastian (2001), discrete crack modelling is needed in order to accurately analyse the IC debonding behaviour of plated members.

2.2.3.8 AIELLO AND OMBRES' MODEL (2004)

A model has been proposed by Aiello and Ombres (2004) to analyse the cracking and deformability of plated members based on the use of moment-curvature relationships evaluated using analysis of a cracked beam element between 2 contiguous cracks subjected to constant bending moment. This discrete crack model assumes that all cracks have spacings varying between a minimum value given by the development length L_b and a maximum value of $2L_b$. Through the model, the cracks width,

cracks spacing, curvature and the deflections of the beams are evaluated, with the bond-slip at the plate/concrete interface being accounted for in the analysis. This model, however, is only applicable to beams under constant moment, as it is assumed that slip is zero halfway between cracks, which is only true for constant moment regions. Equally spaced cracks are assumed in the analysis where the range of crack spacing is calculated, but the actual crack spacing is unknown. This may affect the accuracy of the model as it has been found by Wu & Niu (2003) that crack spacing can have a large influence on local debonding, and hence the local deformation behaviour of plated members.

2.2.3.9 REMARKS

Through reviewing the existing literature on intermediate crack debonding, it was found that there is a lack of understanding in the IC debonding behaviour of plated members and none of the methods considered can satisfactorily model this debonding mechanism. As mentioned in Section 2.2.1, since intermediate crack debonding is largely dependent on the local deformation between cracks, discrete cracking should be considered when analysing this debonding mechanism.

Due to the complexity of the problem, it is found that researchers commonly idealises the IC debonding mechanisms of flexural members into that of a simple pull test, however this assumption is only valid for beams with a single crack. Pull tests do not allow for the curvature in the beam, which may affect the interface normal stress distribution, nor do they allow for the interaction of interface stress distributions between closely spaced intermediate cracks. Experimentally, the bondstress in a cracked plated beam has been found to be a lot higher than that in a pull test (Teng et al. 2002). This is because in a beam with multiple cracks, the local stress and deformation of one uncracked concrete segment will affect the next. Each segment or 'tooth' between adjacent cracks contributes to the bond at the interface, and the total bond force, and hence the force in the plate, is given by the sum of resultant bond forces at each segment as shown in Figure 2.11b. This is the same as what happens in a composite beam, where each shear connector contributes to the total bond force in the beam as illustrated in Figure 2.11a. Therefore each segment between two adjacent cracks is equivalent to a shear stud, where the σ_{IC}/slip behaviour for each concrete tooth is different.

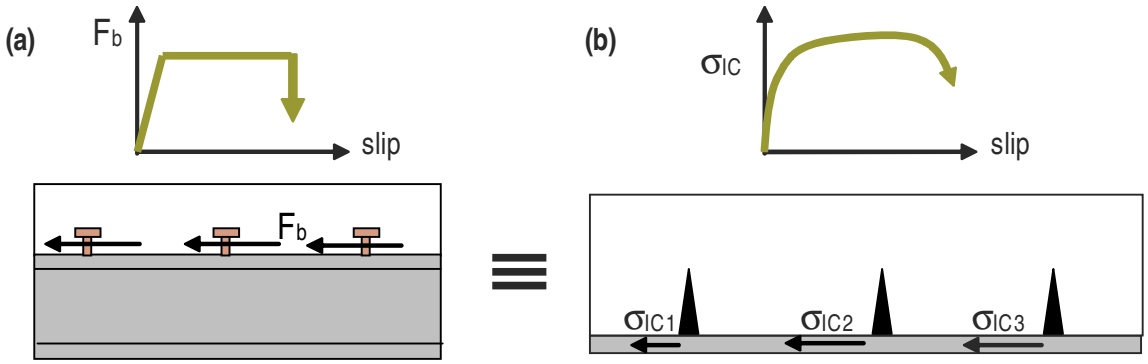

Figure 2.11 Behaviour of (a) composite beam and (b) plated beam

2.2.4 Partial Interaction Theory for Composite Beams

It has been shown in Section 2.2.3.9 that the IC debonding behaviour of plated beams is analogous to the behaviour of composite beams. Therefore a literature review was carried out on composite beams in this following section where the partial interaction (PI) theory, first developed by Newmark (1951), is considered. This theory analyses the local deformation of composite beams, taking into account the effects of slip at the concrete/steel interface, and since similarities arise between plated, unplated and composite beams, it is felt that partial interaction theory is also applicable to plated RC structures.

2.2.4.1 Fundamental Behaviour

A typical composite beam comprises of steel and concrete elements connected together by shear studs as illustrated in Figure 2.12. These shear studs/connectors allow longitudinal shear to be transferred from the concrete to the steel, similar to plated and unplated RC beams in which the shear transfer is provided by the adhesive and ribs of reinforcing bars respectively. The behaviour of composite beams is directly affected by the displacement at the steel and concrete interface, known as slip (Johnson 1994).

Consider the section of a composite beam illustrated in Figure 2.12. Before loading or when the composite beam is unloaded, the concrete and the steel elements at the interface, represented by points B and C in Figure 2.12a respectively, are in line with each other. That is there is no relative movement between the two elements. Upon loading in Figure 2.12b, flexural forces will cause the top fibre of the concrete, shown as point A, and the steel (point C) to contract, and the bottom fibres, points B and D, to expand. This will result in a sliding action across the interface, and the relative displacement between the concrete u_c and the steel u_s is referred to as slip *s* in Figure 2.12b. As a

result of the movement at the interface, the strains in the concrete and steel at the interface differ as illustrated by points B and C in Figure 2.12c respectively, and this is referred to as partial interaction (Oehlers & Bradford 1995).

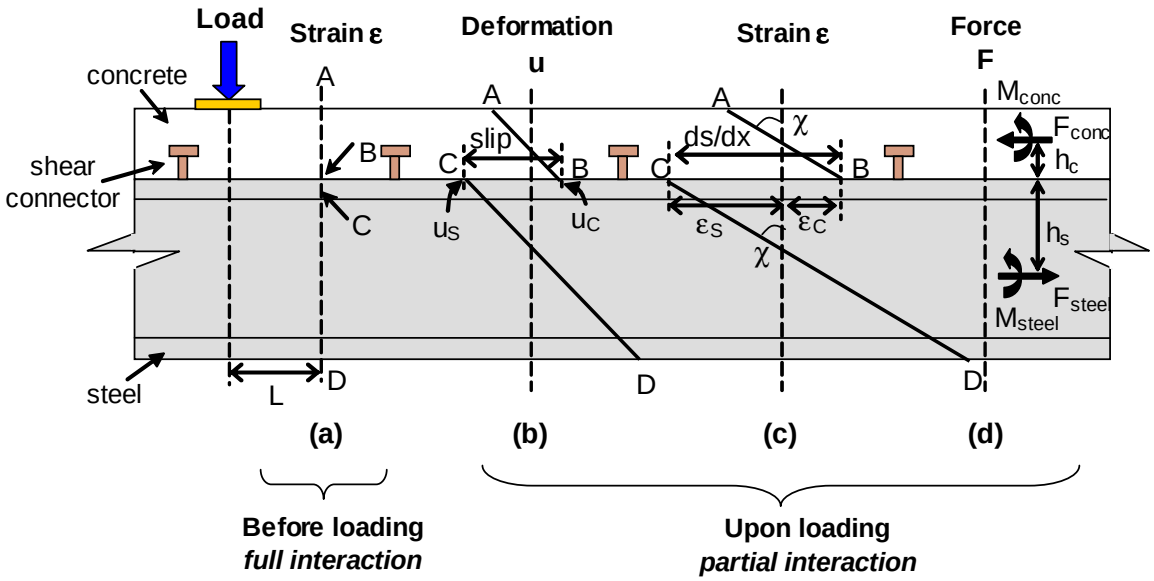

Figure 2.12 Slip and slip-strain of composite beam

Based on compatibility, the slip *s* can be calculated using Equation 2.18, where u_c and u_s is obtained by integrating the strains in the concrete ε_c and the steel ε_s over the length *L* using Equation 2.19 and Equation 2.20.

$$s = u_s - u_c \qquad \text{Equation 2.18}$$

$$u_c = \int_L \varepsilon_c dx \qquad \text{Equation 2.19}$$

$$u_s = \int_L \varepsilon_s dx \qquad \text{Equation 2.20}$$

The difference between the strain of concrete and steel at the interface is known as the slip-strain ds/dx as shown in Figure 2.12b and is evaluated by differentiating Equation 2.18:

$$\frac{ds}{dx} = \frac{du_s}{dx} - \frac{du_c}{dx} = \varepsilon_s - \varepsilon_c \qquad \text{Equation 2.21}$$

The internal forces within a composite beam is illustrated in Figure 2.12d, which consist of a resultant force F_{conc} and moment M_{conc} in the concrete acting at the centroid of the element at a distance h_c from the concrete/steel interface, and a resultant force F_{steel} and moment M_{steel} in the steel acting at a distance h_s from the concrete/steel interface (Oehlers & Bradford 1995). From horizontal and rotational equilibrium,

$$F_{steel} = F_{conc} \quad \text{Equation 2.22}$$

$$M = M_{conc} + M_{steel} + F_{conc}(h_c + h_s) \quad \text{Equation 2.23}$$

Where *M* is the resultant or applied moment of the section. Also from equilibrium of forces within the concrete element, F_{conc} is equal to the total force in the shear connectors over the shear span F_{shear}. Therefore the last component of Equation 2.23 is dependent on the shear strength at the steel/concrete interface due to composite action.

The problem of partial interaction of composite beams can be solved either by the simplified mixed analysis approach or using an iterative non-linear analysis procedure (Oehlers & Bradford 1995) described in Sections 2.2.4.2 and 2.2.4.3 respectively.

2.2.4.2 Mixed Analysis

For composite beams under partial interaction, the slip as well as the slip-strain varies along the beam and the variation is unknown, hence making it very difficult to analyse the problem. Oehlers & Sved (1995) proposed a model in which the shear connectors are assumed to be fully loaded i.e. under plastic conditions where bond strength is constant, while the steel and the concrete element remains linear elastic. The adoption of this mixed analysis approach greatly simplifies the partial interaction analysis process, from which closed form solutions are derived.

2.2.4.3 Nonlinear Analysis

In the nonlinear analysis of composite beams, the slip-strain ds/dx variation, such as shown in Figure 2.13c, is unknown for beams with partial interaction, and so an iterative segmental analysis procedure is required. When the shear connection is elastic, such as for the case with high degrees of shear connection, non-linear techniques are required to account for the plasticity in the steel and concrete elements, and the tensile cracking of the concrete in the analysis. The non-linear analysis of partial interaction can be carried out using the “shooting technique” (Oehlers et al. 1995), whereby analysis is performed starting from a certain position, such as at the support, and modelling continues along the

beam using a segmental analysis until a point with known boundary conditions is reached. For example, for the simply supported composite beam illustrated in Figure 2.13a under uniformly distributed loading UDL and with evenly distributed shear connectors along the beam, the slip is maximum s_{max} at the supports, and is zero at midspan by symmetry as shown in Figure 2.13b. This, hence, forms one of the boundary conditions in the non-linear analysis. After reaching a boundary point, that is the position of a known boundary condition, the boundary condition is checked. If the condition is not satisfied, the analysis is repeated by changing the initial guesses. The nonlinear analysis procedure is iterative and can be difficult to perform, however it gives a better representation of the local deformation behaviour along the beam than those obtained from the mixed analysis approach.

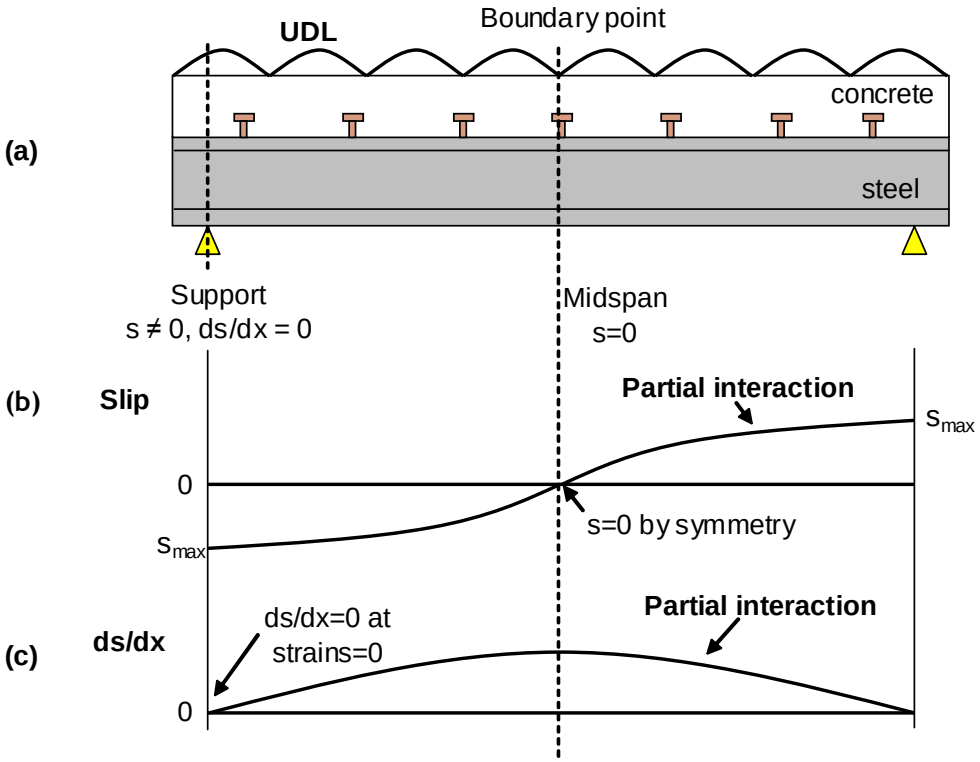

Figure 2.13 Nonlinear partial interaction analysis of composite beam

2.2.4.4 Application to Reinforced Concrete Beams

By comparing the behaviours of composite, plated and unplated RC beams under loading in Figure 2.14, it can be seen that these three types of structures are similar in that they are all dependent on three major force components: [1] the force in the concrete F_c; [2] the force in the reinforcement F_R and; [3] the bond force τ_b represented by the τ_b-slip relationships shown on the right hand side of Figure 2.14. For the composite beam in Figure 2.14a, the bond is provided by the shear connectors, whereas for the RC beam in Figure 2.14b it is provided by the ribs of the bar, and for the plated beam

in Figure 2.14c it is provided by the adhesive at the plate-concrete interface. For both plated and unplated RC beams, before cracking there is full interaction at the reinforcement/concrete interface, that is the strains in the reinforcement and the adjacent concrete at the interface are the same. Further increase in the applied load results in cracking of the concrete in the vicinity of the reinforcement. When these flexural or flexural-shear cracks intercept the reinforcement, in theory infinite strain is required in the reinforcement ε_R to accommodate this crack. As this is impossible to achieve, slip occurs at the interface between the reinforcement and the adjacent concrete, hence resulting in a difference in the strains of the two elements at the interface as illustrated by the strain profiles ε in Figure 2.14(b) and (c). This shows that the theory of partial interaction can also be applied to both plated and unplated reinforced concrete beams to account for the effects of slip on the members. Furthermore, Ferretti and Savoia (2003) found that the plate strain at a cracked section can be more than three times that of the bar at the same section. This suggests that the classical assumption of linear varying strain profile is invalid and that step changes in strains may have occurred in a section due to partial interaction.

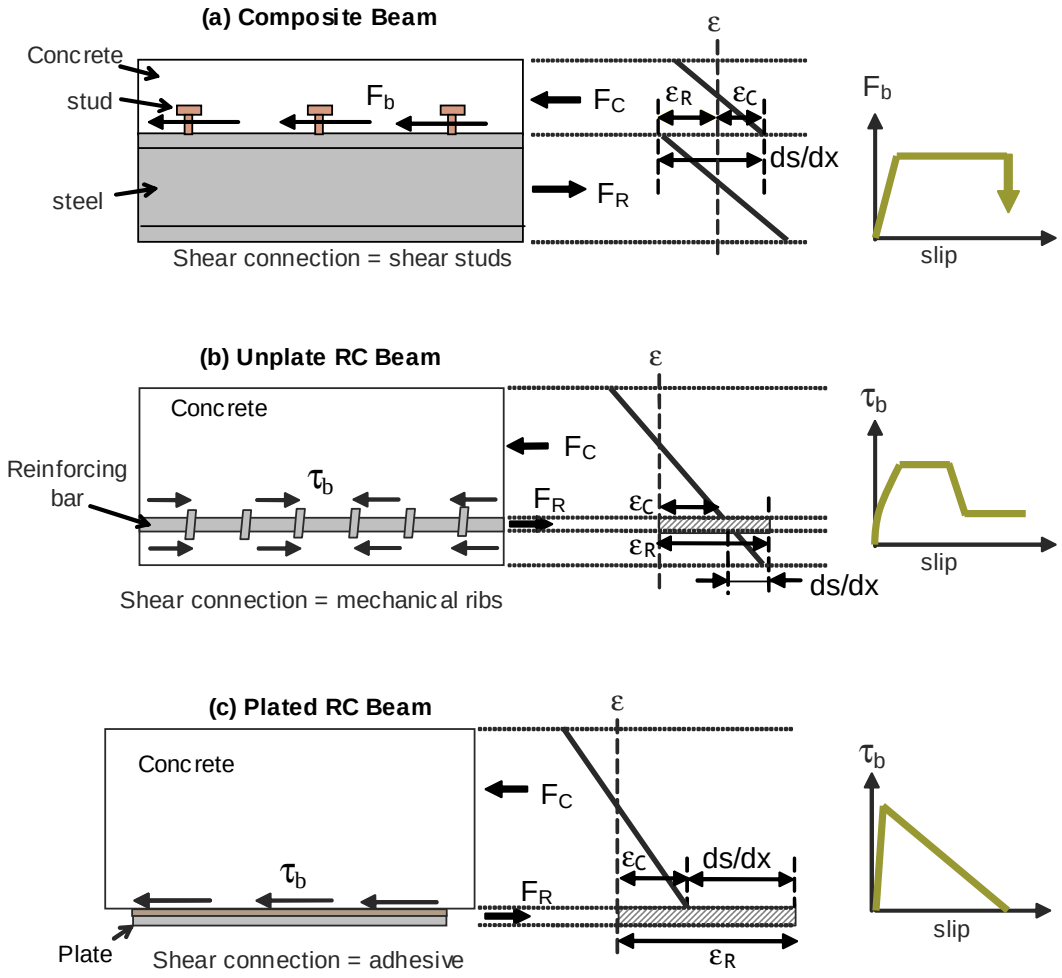

Figure 2.14 Internal forces of (a) Composite (b) Unplated RC (c) Plated RC beams

2.3 GENERAL PARTIAL INTERACTION PRINCIPLES

In Section 2.2.4.4, it has been shown that the partial interaction principles, originally developed for composite beams, is applicable for analysing the local deformation of cracked plated and unplated reinforced concrete members. However the boundary conditions for nonlinear analysis of RC beams is totally different and much more complex than those of the composite beams (Section 2.2.4.3). In the following section, it will be illustrated how the partial interaction principles can be applied to the cracked regions of a RC beam, and the boundary conditions in these regions will be identified.

As discussed in Section 2.2.4.4, the behaviour of composite, plated and unplated RC beams are largely dependent on the bond at the reinforcement/concrete interface (Figure 2.14). For plated and unplated RC beams, before flexural cracking of concrete, there is no slip at the concrete-steel/FRP interface and so the strain is linearly distributed along the cross-section such as that illustrated in Figure 2.15b for a plated beam without internal bars. Therefore the assumption of plane sections remaining plane holds, so there is *full interaction* between the steel/FRP and the concrete i.e. steel/FRP strain at the interface is equal to the strain in the concrete adjacent to it. However, when flexural cracking occurs, this causes high bondstress to develop near the crack, and as a result, sliding occurs between the concrete and the reinforcement, so there is *partial interaction*.

Therefore to analyse the cracked regions of a RC beam, the slip at the reinforcement/concrete interface needs to be accounted for in the analysis. Consider the simply supported plated beam without internal bars in Figure 2.15, where the plate is treated as a layer of reinforcement. Before loading, section AB in the concrete element is in line with section CD of the reinforcement element as shown in Figure 2.15a, resulting in the linearly varying strain profile in Figure 2.15b. When a load *P* is applied such that a flexural crack forms beneath the load, to accommodate this crack infinite strain in the plate is required, which is impossible, hence causing a sliding action across the interface, as illustrated by the positions of B and C in Figure 2.15c. The relative movement across the interface that is induced by this sliding action is referred to as slip *s*, which is resisted by the interface longitudinal shear forces i.e. the bond force. This is illustrated in Figure 2.15c, where as a crack of width w_{cr} forms, this causes slip to occur over the length *L*, and that the right hand side of *L* is at a position of zero slip. The interface slip *s* is given by the difference between deformation of the reinforcement u_r and concrete element u_c shown in Figure 2.15c. The applied load causes a strain distribution in the concrete element adjacent to the interface, ε_c, that varies over the length *L* as shown in Figure 2.15e, and the integral of this strain distribution over *L* is equal to the deformation of the concrete u_c. Same applies to the strain distribution in the reinforcement element adjacent to the interface, ε_r. Therefore,

the interface slip is given by Equation 2.24. The derivative of Equation 2.24 gives the slip-strain ds/dx in Equation 2.25, which is the difference between the strains in the reinforcement ε_r and in the adjacent concrete ε_c, as shown in Figure 2.15d. This means that full interaction analysis can no longer apply to the structure and this is now a *partial interaction* problem. When there is slip-strain, this indicates that there are two strain profiles, concrete and plate, in the section with a step change in strain at the interface as illustrated in Figure 2.15d. It is assumed that there is no separation at the interface, therefore the strain profiles are parallel, that is the curvatures in the concrete and plate are the same.

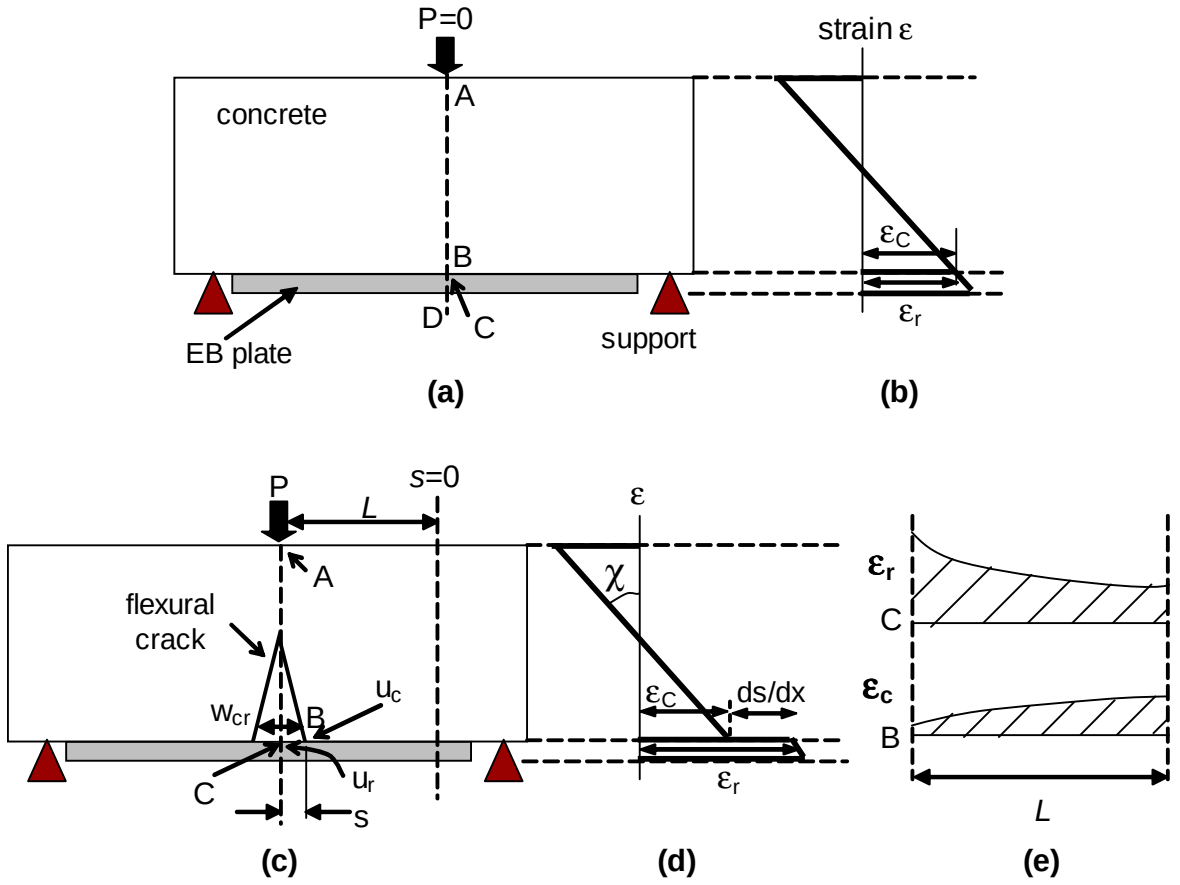

Figure 2.15 (a) Unloaded beam; (b) full interaction; (c) loaded beam; (d) partial interaction; and (e) strain distributions at interface

$$s = u_r - u_c = \int_L \varepsilon_r - \int_L \varepsilon_c \qquad \textbf{Equation 2.24}$$

$$\frac{ds}{dx} = \frac{du_r}{dx} - \frac{du_c}{dx} = \varepsilon_r - \varepsilon_c \qquad \textbf{Equation 2.25}$$

The local behaviour in a segment or 'tooth' between adjacent cracks is affected by the uncracked regions next to it. That is the total bond force at the interface between the concrete and steel/FRP is given by the sum of the resultant bond forces at each segment between adjacent cracks as discussed in Section 2.2.3.9 (Figure 2.11). This is why the local slip distributions between adjacent cracks changes when new cracks occur such as illustrated in Figure 2.16. Therefore the specimen needs to be reanalysed once new cracks form.

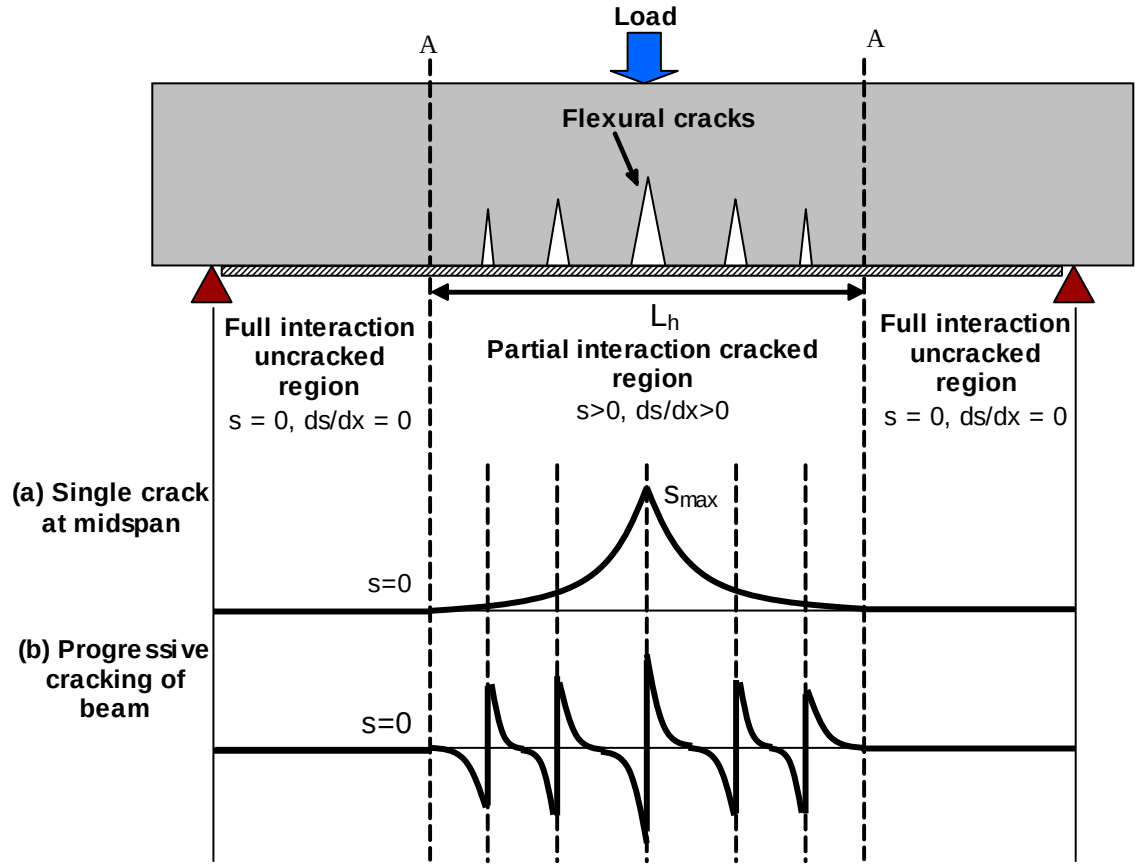

Figure 2.16 Nonlinear analysis of plated RC beam with (a) single crack at midspan; (b) progressive cracking of beam

To perform the nonlinear partial interaction analysis on tensile specimens, plated and unplated RC beams, the "shooting technique" described in Section 2.2.4.3 is adopted. This involves performing a segmental analysis along the member at fixed increments to a point where the boundary conditions are known. Iterative procedures are carried out until the boundary conditions are satisfied. Before performing the analysis, the location of the first crack needs to be chosen such as at the position of maximum moment, or at the line of symmetry. For tensile specimens, the cracks are equally spaced along the entire specimen due to zero internal moment. For beams under flexure, flexural cracks will occur at regions of high moment and at varying spacings. Due to the flexural cracks there will be slip *s*

and hence slip-strain ds/dx between the reinforcement and the adjacent concrete. Therefore this cracked region is the partial interaction region (or partial interaction hinge) such as that shown in Figure 2.16. To illustrate, consider the simply supported beam in Figure 2.16 with an externally bonded tension face plate over the length of the beam where the internal bars are neglected. The beam is subjected to a point load at midspan which is where the first flexural crack is expected to form. For the case shown in Figure 2.16a where only a single crack has formed at midspan, slip is maximum at the crack s_{max} and reduces away from the crack until a point is reached where there is no more slip and slip-strain at the plate/concrete interface, such as point A in Figure 2.16. Therefore at this point and from there to the support full interaction occurs with zero slip and slip-strain. This point with known conditions forms the boundary point which the model iterates against.

Although points of zero slip can occur in between adjacent cracks, such as illustrated in Figure 2.16b for a beam with multiple cracks, within the cracked region where partial interaction applies there is always slip-strain at the interface i.e. ds/dx>0. Therefore full interaction will only occur from the boundary of the partial interaction region to the support. This assumption is later verified with analysis examples presented in Sections 2.5 and 2.6.

2.4 PARTIAL INTERACTION ANALYSIS OF TENSILE SPECIMENS

In the early stages of developing the model, partial interaction theory was used to analyse the behaviour of plated tensile specimens, which is the easiest case scenario. These tensile specimens behave in a similar fashion to that of RC and plated beams with the difference in that there is no curvature involved. The application of the partial interaction theory to a plated specimen without reinforcing bars, which is similar to the behaviour of a simple shear test (Section 2.2.2), is first discussed in Section 2.4.1 where a non-linear model has been developed based on the "shooting technique" described in Section 2.2.4.3. This model is then modified to allow for a layer of reinforcing bars in Section 2.4.2. Also included in Sections 2.4.1 and 2.4.2, are examples of the model applications using fortran programming, where the local deformation behaviour of a plated tensile specimen with and without internal bars is studied. The modelling procedures for the partial interaction analysis of plated tensile specimens with any number of reinforcing layers based on the fortran code developed is summarized by the flow chart presented in Appendix A.1. In Section 2.4.3, a mathematical model has been proposed for plated tensile specimens based on the mixed analysis approach developed for composite beams previous discussed in Section 2.2.4.2.

2.4.1 PLATED SPECIMENS WITHOUT INTERNAL BARS

In the initial stage of developing the partial interaction model, the simplest system in Figure 2.17a was studied, where a tensile specimen with identical plates adhesively bonded to the top and bottom surfaces of the concrete block with no internal reinforcement was subjected to an axial load *P*.

2.4.1.1 FUNDAMENTAL BEHAVIOUR

Before cracking of the specimen, there is no slip between the plates and the concrete, hence full interaction occurs as shown in Figure 2.17b for the strain profile at section A-A prior to cracking. When a crack of width w_{cr} forms and intercepts the plates, slip $s = w_{cr}/2$ occurs at the interface between the concrete and the plate to accommodate this crack. As a result, the strain at the plate ε_p and at the adjacent concrete ε_c is different, and so, there is a slip-strain ds/dx and partial interaction applies where the strain profile at section A-A is now given by Figure 2.17c. The slip *s* and slip-strain ds/dx is evaluated using Equation 2.24 and Equation 2.25 respectively, where u_r is the plate displacement u_p, and ε_r is the plate strain ε_p. Note that because the two plates have the same geometry and the system is symmetrical, therefore the strains of the two plates are equal.

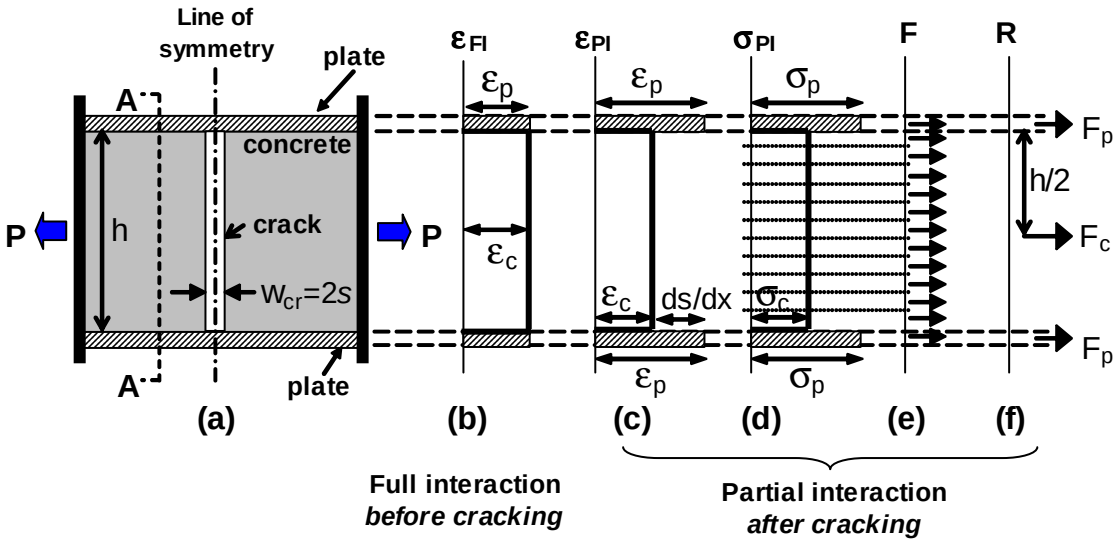

Figure 2.17 Behaviour of plated tensile specimen (no bars) before and after cracking

For a given partial interaction strain profile ε_{PI} such as Figure 2.17c, the axial forces within the beam for the section considered can be evaluated by integrating the stress in Figure 2.17d. For example, the cross-section can be divided into *n* layers with the mean stress within each layer determined from Figure 2.17d, which is obtained based on the known stress-strain relationships for each element. It is assumed that the force of each layer acts at the mid-depth of the layer, and so the magnitude and

distribution of the internal forces *F* is known, as illustrated in Figure 2.17e. Therefore the stress resultants *R* is given by Figure 2.17f, where F_c and F_p is the resultant force in the concrete and the plate acting at the centroid of the element respectively. Equilibrium requires that the total sum of the internal forces to be equal to the external longitudinal force applied *P*, which results in Equation 2.26. From the equilibrium of internal forces in the concrete element, the internal force in the plate F_p is equal to the total bond force F_{shear} at the plate/concrete interface over the shear span L_{sh}. Therefore the last component of Equation 2.26 is dependent on the bond strength P_b at the interface i.e. $F_p = F_{shear} = \sum P_b$.

$$P = F_c + 2F_p \qquad \textbf{Equation 2.26}$$

To perform nonlinear analyses along the specimen using the shooting technique (Section 2.2.4.3), boundary conditions are required. As describe in Section 2.3, outside the cracked partial interaction region full interaction occurs, and the following condition applies:

For each layer of reinforcement there is a position in the member beyond which there is no slip at the concrete/reinforcement interface, that is there is full-interaction at the extremities of the partial-interaction region where ds/dx = *s* = 0.	**Boundary Condition 1**

An assumption that is made in the analysis is that the width of a crack in a tensile specimen is constant along the crack, such as illustrated in Figure 2.17, therefore the slips of the top and bottom plates are the same. This leads to a second boundary condition where:

Crack propagates vertically along the section such that the crack width w_{cr} remains constant, and there is zero concrete tensile strain at the cracked section i.e. F_c=0 in Equation 2.26.	**Boundary Condition 2**

Using these two boundary conditions, nonlinear analysis procedures have been developed to simulate the progressive cracking of an uncracked specimen, where initially a single crack analysis is performed (Section 2.4.1.2). From the analysis, the next cracks are located (Sections 2.4.1.4), and the beam is reanalysed using multiple crack analysis (Section 2.4.1.5). This analysis procedure can also apply to precracked tensile specimens. The numerical analysis described in Sections 2.4.1.2 to

2.4.1.5 are based on load control, however, it should be noted that slip or crack width control can also be adopted.

2.4.1.2 Single Crack Analysis

To model the progressive cracking a specimen, the location of the first crack is assumed, such as at the line of symmetry, as this crack will induce a slip at the interface, and hence cause partial interaction. Consider an axial load *P* being gradually applied to the tensile specimen shown in Figure 2.18, where a single crack, crack 1, has formed at the line of symmetry and analysis is performed along the member at distance *x* away from crack 1 to locate the subsequent cracks. Note that since the tensile specimen is subjected to pure axial load *P*, theoretically cracks will form at constant crack spacing.

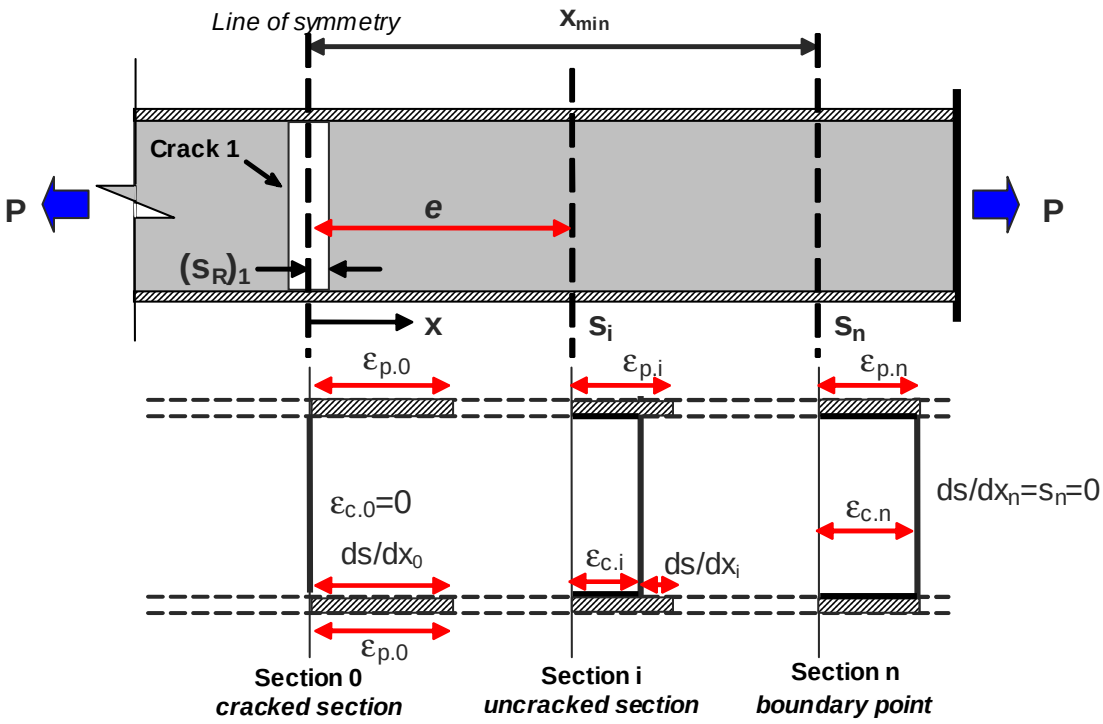

Figure 2.18 Single crack analysis of plated tensile specimen without internal reinforcement

To begin the analysis, the location of the first crack, crack 1, is assumed. As this is a tensile specimen, therefore the crack can be anywhere along the specimen. For a specimen under load control, the load *P* is fixed and the slip at the initial crack $(s_R)_1$ is guessed. Hence, one boundary condition is required to verify this guess. If the specimen was under slip or crack width control, then $(s_R)_1$ is fixed and the load *P* is iterated until a solution is obtained. Sectional analysis is performed starting at the crack, section 0 in Figure 2.18. At this cracked section, there is zero concrete tensile strain $\varepsilon_{c.0}=0$

(Boundary Condition 2 in Section 2.4.1.1), and the resultant strain profile is shown in Figure 2.18, where for zero concrete tensile strain, the slip-strain at the interface between the plate and the concrete is equal to the strain of the plate (Equation 2.25). From the applied load *P* considered, the force in the plates at the cracked section can be determined from equilibrium of forces using Equation 2.26. Note that the forces in the top and bottom plates are equal as the system is symmetrical.

After determining the forces in the plates, analysis is then performed at the next section, section *i*, at a distance *e* away from the previous section as illustrated in Figure 2.18. From the analysis of the previous section, section *i*-1, the slip-strain ds/dx_{i-1} is known, and as ds/dx is the derivative of slip, therefore the slip at section *i*, s_i, can be determined by integrating the ds/dx from the previous section over the segment *e* and subtracting it from the slip of the previous section s_{i-1} using Equation 2.27. Knowing the slip at this section, s_i, the bond force $P_{b.i}$ can be determined using the bond-slip relationship considered (i.e. Figure 2.6). The change in the force of the plate over distance *e* is due to the bond at the interface, therefore the force in the plate $F_{p.i}$ at section *i* can be evaluated using Equation 2.28 where $(F_p)_{i-1}$ is the force in the plate at the previous section. Knowing $F_{p.i}$, and from equilibrium of forces given by Equation 2.26, the force in the concrete $F_{c.i}$ can be calculated, from which the resultant strain profile of the section can be obtained and the slip-strain at this section ds/dx_i can be evaluated using Equation 2.25, as shown in Figure 2.18.

$$s_i = s_{i-1} - e\left(\frac{ds}{dx}\right)_{i-1} \qquad \text{Equation 2.27}$$

$$F_{pi} = (F_p)_{i-1} - P_{bi} \qquad \text{Equation 2.28}$$

Segmental analysis is performed along the beam at fixed increments *e* until a point is reached where both slip and slip-strain are equal to zero. This point, shown as section *n* in Figure 2.18 at a distance x_{min} from the crack, is the boundary of the partial interaction region where full interaction occurs at the plate/concrete interfaces i.e. ds/dx=*s*=0, and hence, Boundary Condition 1 given in Section 2.4.1.1 applies at this section. If slip-strain and slip are not both equal to zero at the boundary point, section *n*, this indicates that the slip $(s_R)_1$ guessed at the first crack for the fixed load *P* is incorrect. The analysis is then repeated for different values of slip $(s_R)_1$ until the boundary condition is satisfied.

2.4.1.3 Example of Single Crack Analysis

Analysis was carried out on a steel plated tensile specimen with no internal reinforcing bars as illustrated in Figure 2.17, where the specimen is 150mm in height (*h*) and 200mm in width (*b*). The

concrete has a compressive strength f_c=25MPa with the Young's modulus E_c given by Equation 2.29 (Warner et al. 1998). A linear concrete tensile stress-strain relationship is assumed with the maximum concrete tensile stress $f_{ct.max}$ calculated using Equation 2.30. Each plate is 100mm by 3mm with a yield strength $f_{p.y}$ of 400MPa, and a bilinear stress-strain relationship is assumed as illustrated in Figure 1.1, where E_s=20GPa. The simplest case of a linear ascending bond-slip model with unlimited bond strength was assumed.

Let us first consider the case of an axial load *P* of 70kN and a single crack that has formed at distance *x*=0 as illustrated in Figure 2.18. Figure 2.19 shows the slip-strain ds/dx and Figure 2.20 shows the slip *s* distribution of the specimen for different slips $(s_R)_1$ guessed at the initial crack, crack 1, whose values are listed in the legends of the figures. It can be seen that both ds/dx (Figure 2.19) and *s* (Figure 2.20) decreases as the distance from the crack increases, and eventually either ds/dx or *s* will reach 0. If the $(s_R)_1$ guessed is too small, i.e. $(s_R)_1$ = 0.02, slip will tend to zero, however slip-strain will not tend to zero as shown by line A in Figure 2.20 and Figure 2.19 respectively. Whereas if the slip guessed at crack 1 is too large, i.e. $(s_R)_1$ = 0.03 (line B in Figure 2.19 and Figure 2.20), slip-strain will tend to zero, but slip will never decrease to zero at the same point. From Figure 2.19 and Figure 2.20, it can be seen that for the case considered, slip and slip-strain both tend to zero at x_{min} for a slip $(s_R)_1$ of 0.0244. This is therefore the true slip at crack 1 and the boundary point x_{min} is at 145mm away from crack 1.

$$E_c = 5050\sqrt{f_c} \qquad \textbf{Equation 2.29}$$

$$f_{ct.\max} = 0.4\sqrt{f_c} \qquad \textbf{Equation 2.30}$$

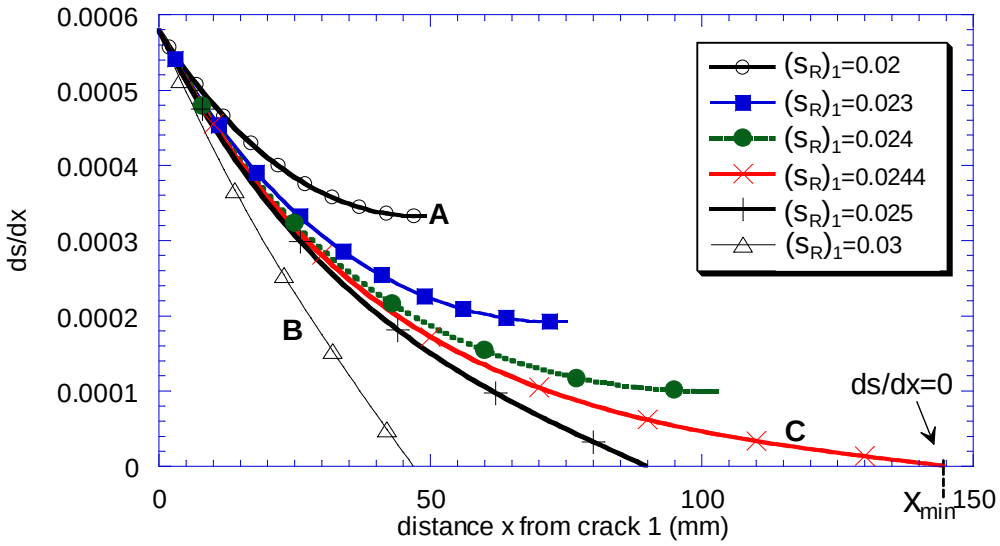

Figure 2.19 Single crack analysis: slip-strain distribution of plated tensile specimen (no bars)

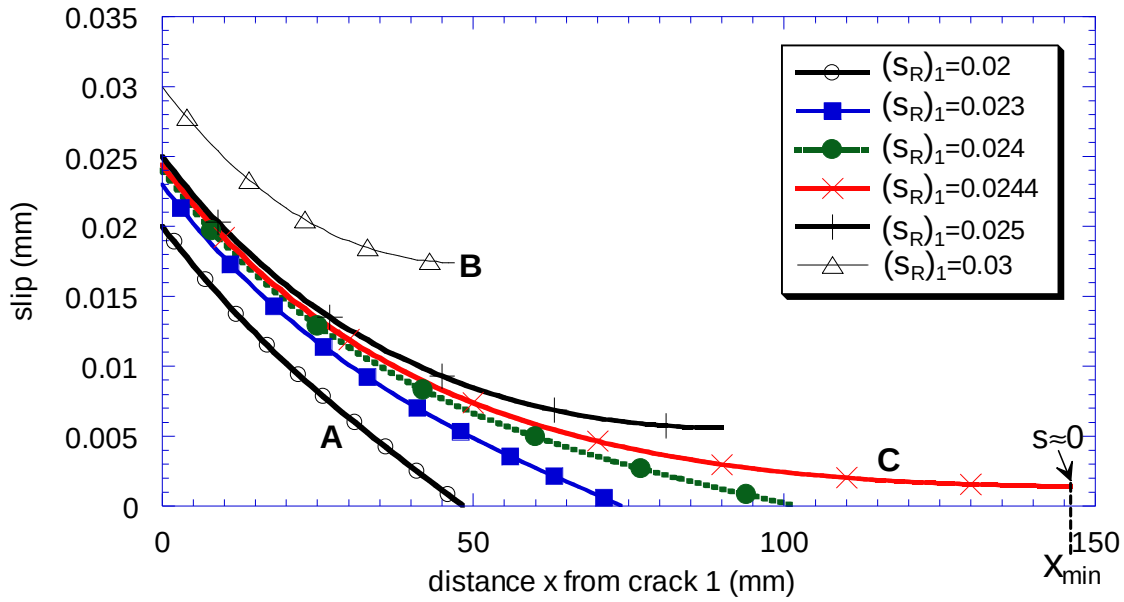

Figure 2.20 Single crack analysis: slip distribution of plated tensile specimen (no bars)

2.4.1.4 CHECK FOR CRACKING

After performing the single crack analysis and obtaining the strains and slip distributions of the tensile specimen, it needs to be check for any further cracking along the member for the load considered. From the single crack analysis, the variation in concrete strain ε_{ct} along the specimen is obtained, such as shown in Figure 2.21, for the same specimen as that considered in Section 2.4.1.3 subjected to various applied loads. From the figure, it can be seen that the tensile stress in the concrete increases when further away from the crack. If it is found that the maximum concrete tensile strain $\varepsilon_{ct.max}$ at distance x_{max} away from crack 1 exceeds the concrete cracking strain ε_{crack}, that means the first appearance of the next crack occurred at a load less than that considered. Analysis is repeated for different axial loads until $\varepsilon_{ct.max}$ equals ε_{crack}, with the position of the next crack occurring at $x_{crack} = x_{max}$. For example, in Figure 2.21 for an axial load of 80kN, it was found that the maximum concrete strain exceeds the tensile cracking strain. Therefore cracking of the beam occurred at a smaller applied load, and so to find the correct position of the next crack, analysis is repeated for a different load. For an axial load of 60kN, the $\varepsilon_{ct.max}$ is less than the tensile cracking strain. This means that for the load applied, no further cracking occurs along the beam. By further increasing the axial load to 69.5kN results in a $\varepsilon_{ct.max}$ equal to ε_{crack} at the boundary point x_{max}=145mm, therefore the next crack occurs at a load of 69.5kN, at x_{crack} = 145mm from crack 1.

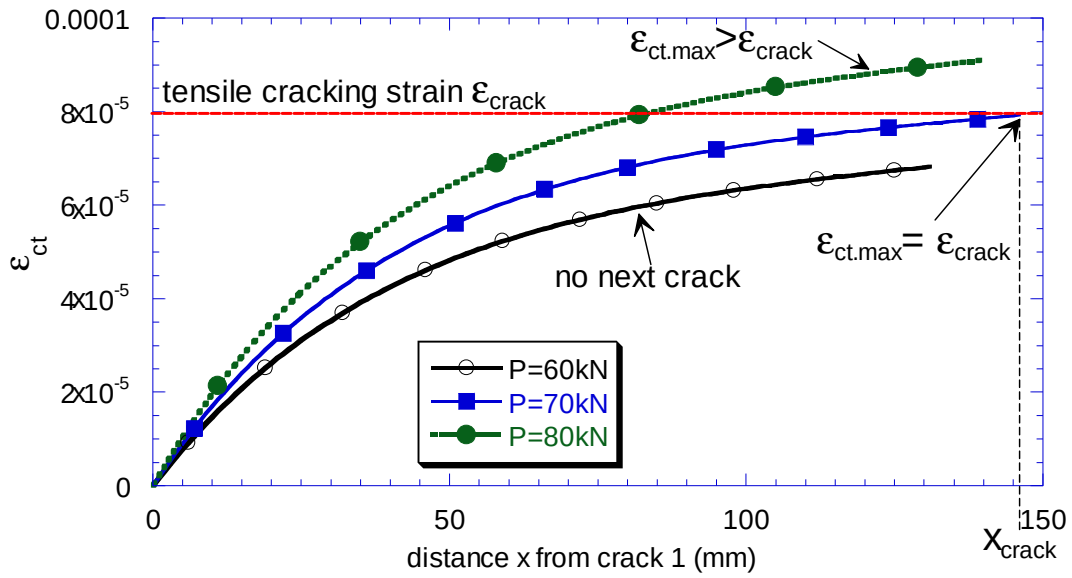

Figure 2.21 Plated tensile specimen (no bars) – check for cracking

2.4.1.5 Multiple Crack Analysis

After locating the next subsequent crack, crack 2, the specimen is reanalysed for the same applied load *P*, as the occurrence of a new crack will result in different stress and strain distributions along the member. The history of the beam is not considered in the analysis, therefore after new cracks form, the beam is reanalysed assuming it was previously unloaded. To perform partial interaction analysis on a beam with multiple cracks, each uncracked concrete segment between cracks, such as between cracks 1 and 2 in Figure 2.22, needs to be analysed.

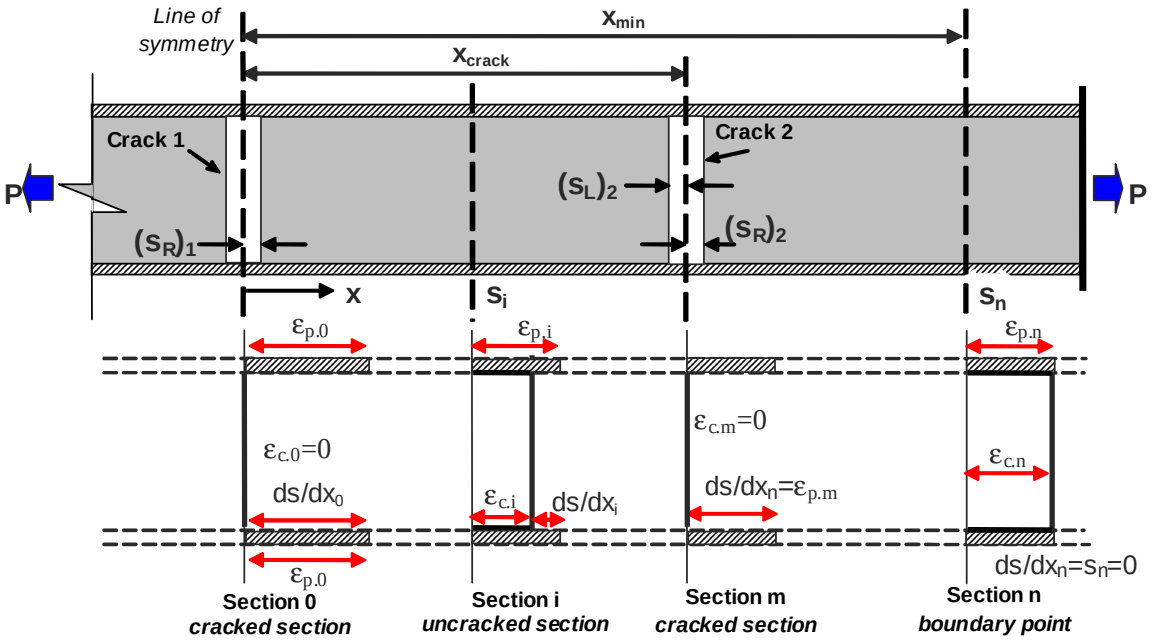

Figure 2.22 Multiple crack analysis of a plated tensile specimen (no bars)

The procedure for analysis between cracks is similar to the analysis of a single crack (Section 2.4.1.2), where a slip $(s_R)_1$ is assumed at crack 1 and a segmental analysis at fixed increments e is carried out starting from crack 1 at section 0 in Figure 2.22, but this time analysis is performed until crack 2 is reached at x_{crack}. At crack 2, shown as section *m* in Figure 2.22, Boundary Condition 2 (Section 2.4.1.1) applies where at a cracked section, there is zero tensile strain in the concrete, such that F_c=0 in Equation 2.26. If this condition is not satisfied, the analysis is repeated for a different slip guess $(s_R)_1$ at crack 1.

For a specimen with multiple cracks, segmental analysis is performed between cracks where at each crack, the slip at the right crack face s_R is iterated until Boundary Condition 2 (Section 2.4.1.1) is satisfied. If it is found that after crack *N*, no further cracking occurs, then single crack analysis, described in Section 2.4.1.2 and illustrated in Figure 2.18, is performed from crack *N*, where the s_R at crack *N* is iterated until Boundary Condition 1 (Section 2.4.1.1) is satisfied. For example, for the tensile specimen shown in Figure 2.22 with 2 cracks formed for an applied load *P*, segmental analysis is performed between cracks 1 and 2 where $(s_R)_1$ is iterated until boundary condition at crack 2 is satisfied. Single crack analysis described in Section 2.4.1.1 is then performed from crack 2 where $(s_R)_2$ is iterated until the boundary condition is satisfied at section *n* at distance x_{min} from crack 1. From the partial interaction analysis, the concrete strain along the beam is obtained, and the specimen needs to be checked for further cracking (2.4.1.4), either between cracks or in the uncracked region from the last crack to the plate end. If new cracks have formed, then the beam is reanalysed.

As tensile specimens are subjected to axial force only, i.e. there is no internal moment, the cracks will be equally spaced along the specimen, and the local strain and slip distribution of each uncracked concrete segment between 2 adjacent cracks will be the same along the specimen. Therefore each crack will have the same crack width w_{cr}, given by Equation 2.31 as illustrated in Figure 2.22, where s_R is the relative slip of the right crack face, which is the slip guessed at each crack, and s_L is the relative slip of the left crack face obtained from the segmental analysis between cracks using Equation 2.24. In fact, since the specimen has zero moment s_L= s_R. Note that as the resultant axial force at each section is constant, therefore all the cracks will appear at the same applied load, that is the specimen will be either uncracked or fully cracked at a constant crack spacing of x_{crack}.

$$w_{cr} = s_L + s_R \qquad \textbf{Equation 2.31}$$

2.4.1.6 EXAMPLE OF ANALYSIS BETWEEN CRACKS

Multiple crack analysis was carried out on the plated tensile specimen considered in Section 2.4.1.3 at a pure axial load *P* of 69.5kN, based on a linear ascending bond-slip model, and assuming that cracks had formed at a constant crack spacing x_{crack} of 145mm throughout the beam of unlimited length. To illustrate the local behaviour between cracks, analysis was carried out in uncracked regions between three cracks. The local slip-strain ds/dx, slip *s*, bondstress τ_b, plate strain ε_p, and concrete tensile strain ε_{ct} distributions are shown in Figure 2.23 to Figure 2.27 respectively, where it can be seen that ds/dx, *s*, τ_b, and ε_p reduces away from cracks, while ε_{ct} increases away from cracks. This is distinctly different from classical full interaction analysis, where ε_{ct} is equal to ε_p such that ε_{ct} reduces away from cracks as ε_p decrease. As ε_{ct} increases away from cracks, therefore cracks may form in between cracks when the concrete cracking strain is exceeded. These cracks are defined as secondary cracks.

The width of each crack w_{cr} is given by the sum of the crack face slip s_L and s_R as shown in Figure 2.24. For the local slip variation between 2 adjacent cracks shown in Figure 2.24, there is a point in between the cracks where slip equals zero, and beyond this point, slip changes direction. This point of zero slip coincides with the points of minimum ds/dx (Figure 2.23) and plate strain (Figure 2.26), and the point of maximum concrete tensile strain (Figure 2.27). It is worth noting that although the point of zero slip occurs between cracks, as ds/dx at that point is greater than zero (Figure 2.23), therefore full interaction does not occur. This verifies the assumption (Section 2.4.1.1) that full interaction only occurs at the boundaries of the partial interaction region. For a specimen under zero or constant moment with constant crack spacing, the local slip and strain behaviours are the same for each segment between adjacent cracks. Therefore for tensile specimens, the point of zero slip will always occur at the midpoint between 2 adjacent cracks.

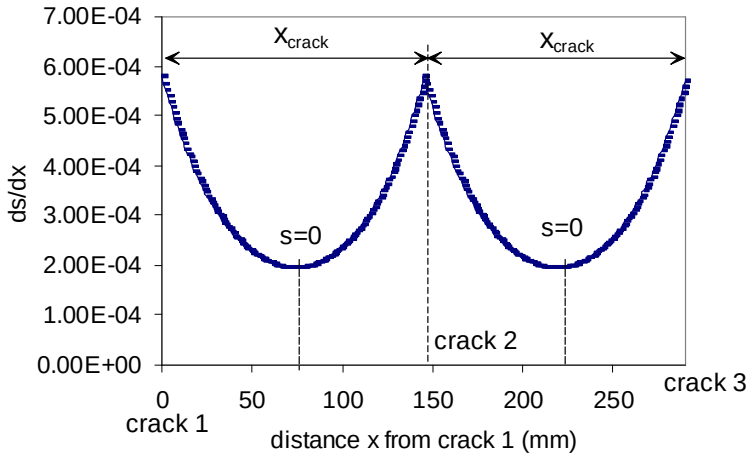

Figure 2.23 Multiple crack analysis: slip-strain distribution of plated tensile specimen (no bars)

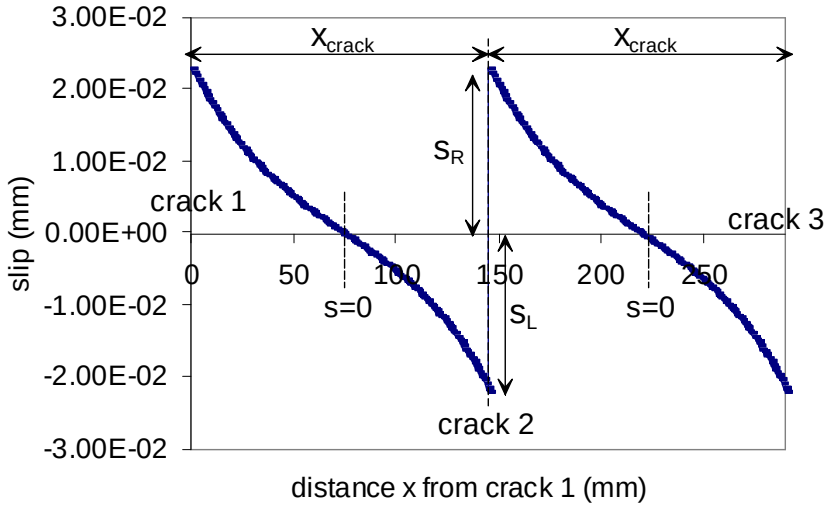

Figure 2.24 Multiple crack analysis: slip distribution of plated tensile specimen (no bars)

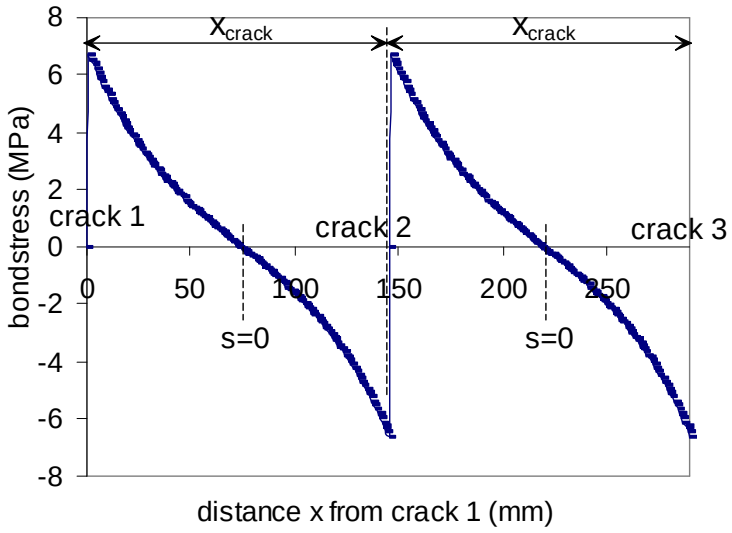

Figure 2.25 Multiple crack analysis: bondstress distribution of plated tensile specimen (no bars)

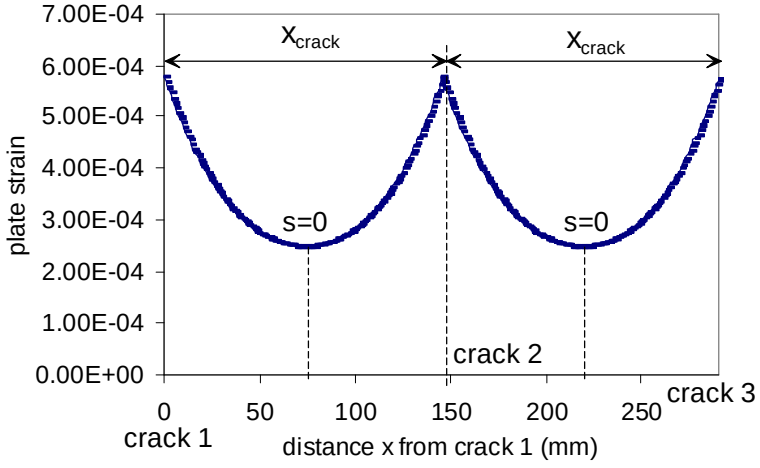

Figure 2.26 Multiple crack analysis: plate strain distribution of plated tensile specimen (no bars)

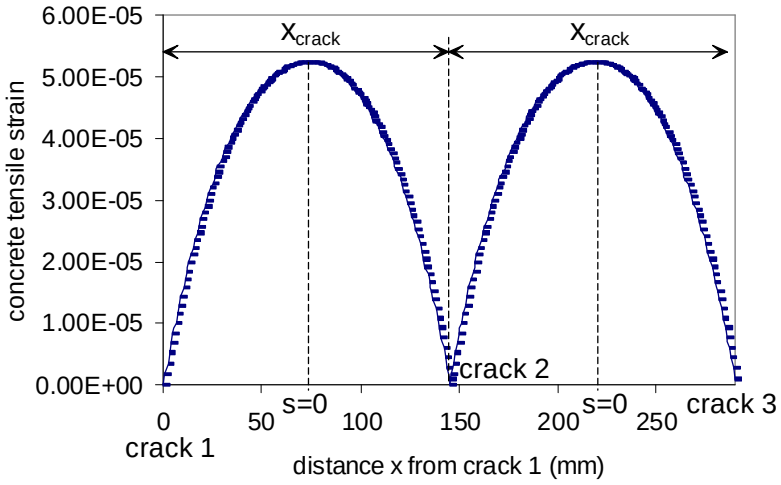

Figure 2.27 Multiple crack analysis: concrete tensile strain distribution of plated tensile specimen (no bars)

2.4.1.7 Behaviour of Plated Specimens (No Bars) With Trilinear Bond-Slip Relationship

To study the debonding behaviour of plated tensile members without bars, a trilinear bond-slip model (illustrated in Figure 2.6) is considered as it has been shown in Section 2.2.2.1 to be a better representation of the actual bond behaviour at the plate/concrete interface. The specimen analysed is 200mm wide by 150mm high with a shear span *L* of 700mm and consist of two externally bonded FRP plates as illustrated in Figure 2.18. The concrete has a compressive strength f_c of 34MPa with the Young's modulus E_c given by Equation 2.29 (Warner et al. 1998). A linear concrete tensile stress-strain relationship is assumed with the maximum concrete tensile stress $f_{ct.max}$ calculated using Equation 2.30. Each FRP plate is 50mm wide by 1.2mm thick with a linear stress-strain relationship as illustrated in Figure 1.1, where fracture strength f_{frac}=3050MPa and Young's modulus E_p =144000MPa. A peak bondstress $\tau_{b.max}$ of 6MPa is assumed at a relative slip s_{max}=0.02mm, and macro debonding begins at a slip s_f of 0.2mm. Progressive cracking of the specimen is studied, where it is assumed that a single crack, crack 1, has formed at the line of symmetry at distance *x*=0 and the specimen is loaded under slip control. This is similar to the double shear test illustrated in Figure 2.3 where the concrete edge at the loaded end is equivalent to a flexural crack.

Figure 2.28 shows the bondstress distribution along the specimen as the slip at crack 1 $(s_R)_1$ increases. Initially, prior to micro-debonding of the plate, maximum bondstress is achieved adjacent to the crack i.e. at $(s_R)_1$=0.02mm. As the slip at crack 1 $(s_R)_1$ increases, micro-debonding occurs propagating away from crack 1 i.e. at $(s_R)_1$=0.1mm. Macro-debonding is initiated at $(s_R)_1$=0.2mm, where further increase in slip results in the formation of visible debonding cracks, which is indicated

by the zero bondstress near the crack in Figure 2.28. It can be seen from Figure 2.29 that the plate strain ε_p is maximum at a cracked section, and before debonding, as the slip at crack 1 increases, so does the strain in the plate. However, as macro-debonding occurs causing a loss of bond close to the crack i.e. for $(s_R)_1$>0.2mm in Figure 2.28, the plate strain no longer increases and remains constant in the region of zero bond. That is a maximum plate strain is reached as s_{max} is reached, after which immediate IC debonding failure follows. From the non-linear analysis, debonding failure occurred at an applied load of 45.9kN, with a maximum plate strain $\varepsilon_{p.max}$ of 0.00266, which was found to correlate well with Chen & Teng's model (Section 2.2.2.3), where a debonding plate strain of 0.0029 was calculated. From the analysis of the specimen it is found that no further cracking occurs along the specimen prior to debonding failure as shown by Figure 2.30. Note how at $(s_R)_1$>0.2mm, due to zero bond near crack 1, the force cannot be transferred from the plate to the concrete, and hence, there is no force in the concrete element in the region where macro-debonding occurs.

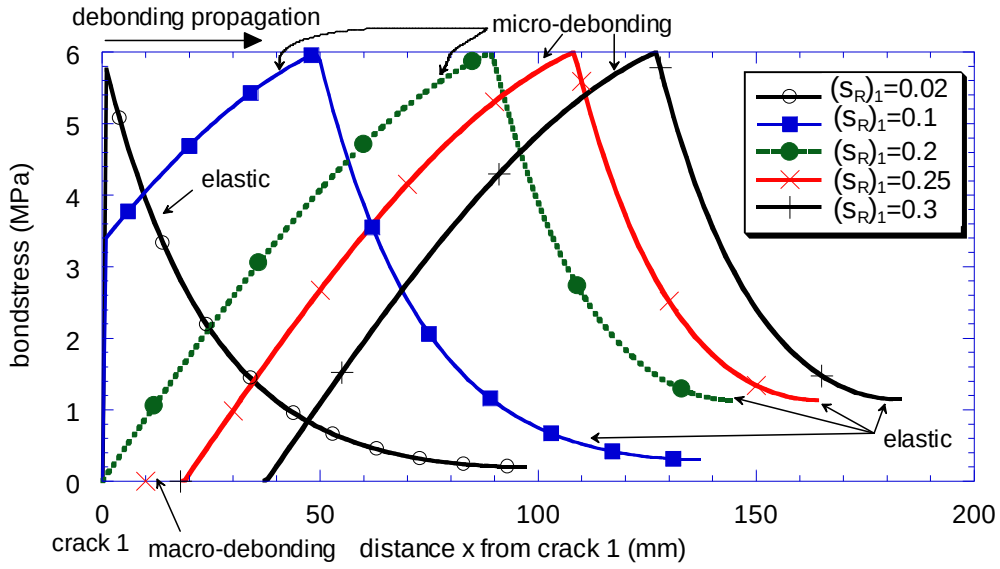

Figure 2.28 Bondstress distribution for FRP plated tensile specimen (no bars)

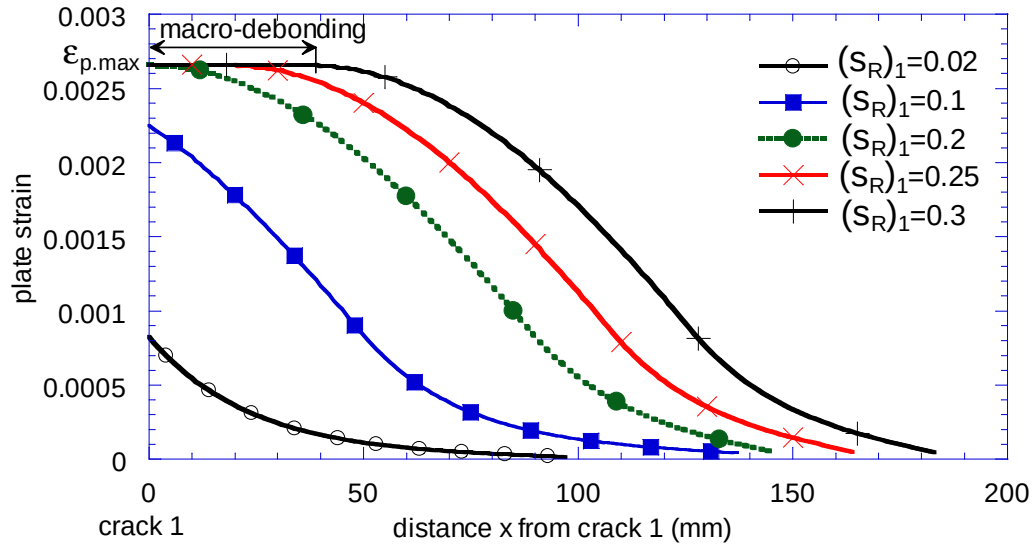

Figure 2.29 Plate strain distribution for FRP plated tensile specimen (no bars)

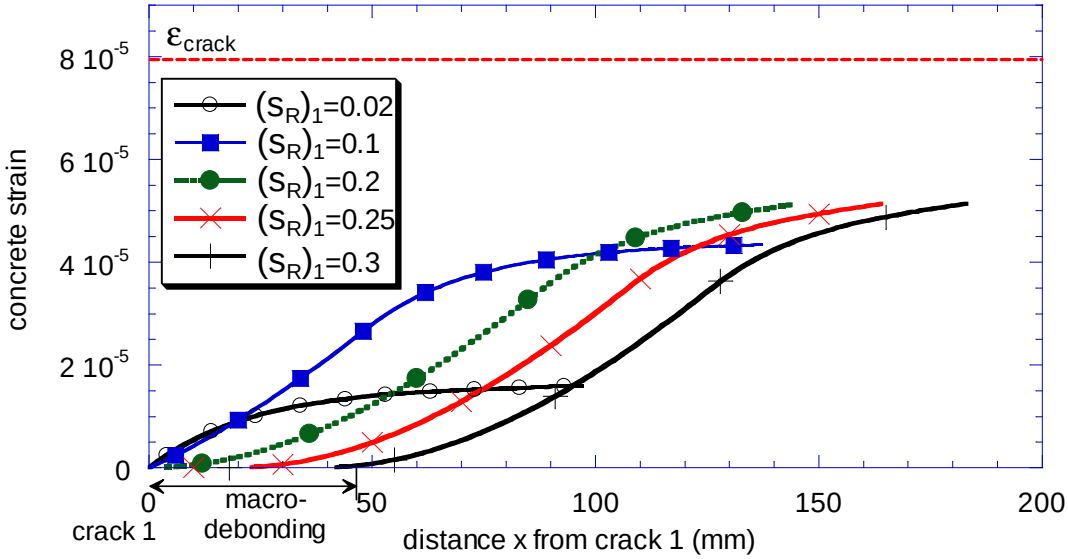

Figure 2.30 Concrete strain distribution for FRP plated tensile specimen (no bars)

2.4.2 Plated Specimens With Internal Bars

The nonlinear model proposed in Section 2.4.1 neglects the reinforcing bars in the plated tensile specimens, therefore slip will only occur at the concrete/plate interface. For plated tensile specimens with internal bars, slip will occur at both the plate/concrete and bar/concrete interfaces, and because the bonding mechanism of the plate and the bar is different, the slips at the two interfaces will differ. In the following context, partial interaction analysis of plated tensile specimens with internal reinforcing bar will be discussed.

2.4.2.1 FUNDAMENTAL BEHAVIOUR

Consider the specimen shown in Figure 2.31 which is subjected to an axial load *P*, with two identical plates adhesively bonded to the top and bottom of the concrete member, and a single reinforcing bar through the centre of the specimen. This system is similar to those having multiple reinforcing layers, that is, the model treats each layer of plate and bar as a reinforcing layer where the relevant material properties and bond-slip models are inputted. Therefore the proposed model is applicable to plated and unplated tensile specimens with several layers of reinforcement.

Before cracking there is full interaction such that the plate ε_p, bar ε_b and concrete ε_c strains are all equal as shown in Figure 2.31a for the section A-A. When a crack occurs, this induces a slip at the plate/concrete s_p, as well as at the bar/concrete s_b interface. Because the bond-slip characteristics at the two interfaces are different, the slips at each interface may differ, i.e. $s_p \neq s_b$. With different slips, and hence bond forces at the interfaces, the plate and bar strains will not be the same, resulting in different slip-strains at the concrete/plate ds/dx_p and concrete/bar ds/dx_b interface, as illustrated by Figure 2.31b. Note that because the two plates have the same geometry and the system is symmetrical, therefore the strains of the two plates are equal.

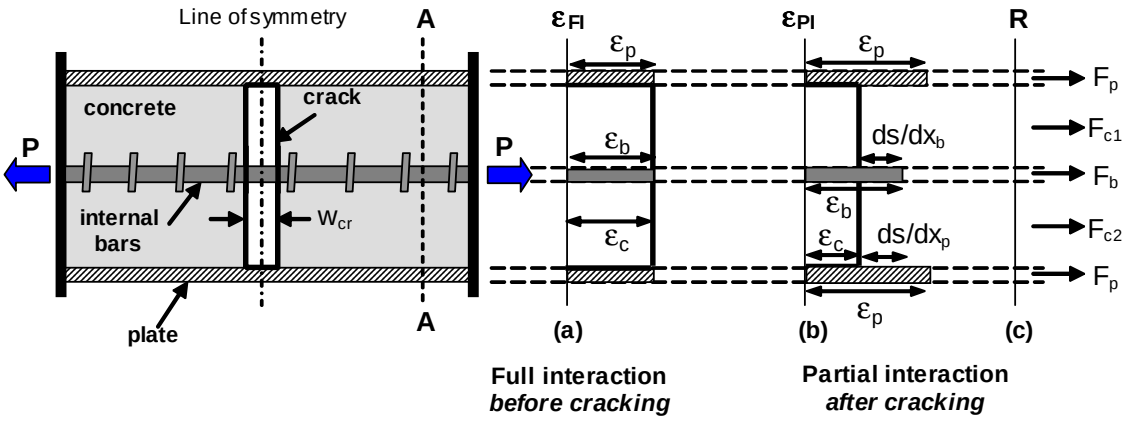

Figure 2.31 Behaviour of plated tensile specimen (with bars) before and after cracking

For a given partial interaction strain profile ε_{PI} such as Figure 2.31b, the stress distribution of the section can be determined, and hence the axial forces within the beam can be evaluated by integrating the stress. Equation 2.32 is derived from the equilibrium of axial forces shown in Figure 2.31c, where F_c, F_b and F_p are the resultant forces in the concrete, bar and plate respectively. It is assumed that each of these forces acts at the mid-depth of the element considered. Based on the equilibrium of internal forces in the concrete elements, F_p and F_b are equal to the total bond force at the plate/concrete $F_{p.shear}$ and the bar/concrete $F_{b.shear}$ interface respectively over the shear span L_{sh}.

Therefore the maximum force that can be achieved in the reinforcement is dependent on the bond strength P_b at the interfaces as shown in Equation 2.32.

$$P = F_c + 2F_p + F_b = F_c + 2\int_{L_{sh}} (P_b)_p \, dx + \int_{L_{sh}} (P_b)_b \, dx \qquad \textbf{Equation 2.32}$$

Where $F_c = F_{c1} + F_{c2}$ in Figure 2.31c; $(P_b)_p$ and $(P_b)_b$ is the bond strength at the plate/concrete and bar/concrete interfaces respectively over the element *dx*.

For tensile specimens with multiple reinforcing layers, additional boundary conditions to those given in Section 2.4.1.1 are required to solve for the unknown slips and strains of additional reinforcing layers. The boundary conditions for tensile specimens with multiple reinforcing layers are as follows:

For each layer of reinforcement there is a position in the beam beyond where no slip occurs at the concrete/reinforcement interface, that is there is full-interaction at the extremities of the partial-interaction region where ds/dx = *s* = 0 as shown by Figure 2.16. This position is not assumed to be the same at each reinforcement layer i.e. the full-interaction zone at the plate and at the bar occurs at different positions. In cases where there is no full interaction along the beam, the boundary condition is then dependent on the condition at the beam end i.e. for the specimen in Figure 2.31, at the beam end, there is zero slip at all interfaces.	**Boundary Condition 3**
Crack propagates vertically along the section such that the crack width w_{cr} remains constant, such as illustrated in Figure 2.31, and there is zero concrete tensile strain at the cracked section i.e. F_c=0 in Equation 2.32.	**Boundary Condition 4**
It is also assumed, for the case when there are multi-layers of tension reinforcement, that the crack faces act as rigid bodies. As the cracks in a tensile specimen have constant crack widths, therefore the crack width at the bar layer $(w_{cr})_b$ and that at the plate level $(w_{cr})_p$ are equal, where the crack width at each level of reinforcement is given by the algebraic sum of the slip of the left crack face s_L and right crack face s_R of the reinforcement/concrete interface considered (Equation 2.31).	**Boundary Condition 5**

Again, similar to plated tensile specimens without internal bars, the analysis procedures to simulate the progressive cracking of plated specimens with bars involves: (1) single crack analysis where an initial crack, crack 1, is assumed to form at the line of symmetry (Section 2.4.2.2); (2) from the analysis, the next subsequent crack is located (Section 2.4.2.4); and (3) the specimen is reanalysed after new cracks have formed to model the local behaviour of beams with multiple cracks (2.4.2.5).

2.4.2.2 SINGLE CRACK ANALYSIS

To study progressive cracking, consider the plated tensile specimen with a single reinforcing bar through the centre of the specimen shown in Figure 2.32, where the location of the initial crack, crack 1, is assumed to occur at the line of symmetry at x=0. Based on Boundary Condition 5 of constant crack width w_{cr} (Section 2.4.2.1), and since the system is symmetrical at crack 1, $s_L=s_R$. Hence, the crack width at each level of reinforcement is double the crack face slip at the interface considered i.e. at plate/concrete interface $(w_{cr})_p=2(s_R)_p$, and at bar/concrete interface: $(w_{cr})_b=2(s_R)_b$, and as the crack width at the bar layer $(w_{cr})_b$ equals that at the plate $(w_{cr})_p$, therefore at crack 1, the slip at the plate/concrete interface $(s_R)_{p.1}$ is equal to that at the bar/concrete interface $(s_R)_{b.1}$ as illustrated in Figure 2.32.

The following analysis procedures are described based on load control where an axial load P is considered. At this load, the slip at crack 1 at the plate/concrete interface $(s_R)_{p.1}$ and the strain in the bar at the initial crack $(\varepsilon_b)_0$ is guessed. Since two variables have been guessed, two boundary conditions are required to find a solution. As mentioned above $(s_R)_{b.1}=(s_R)_{p.1}$, therefore the slip at the bar/concrete interface is known. If slip control was considered, then $(s_R)_{p.1}$ is fixed while P and $(\varepsilon_b)_0$ are iterated in the analysis. Sectional analysis is performed starting from crack 1 at section 0, where Boundary Condition 4 of zero concrete tensile strain applies such that from Equation 2.32, the force in the plate can be evaluated, resulting in the strain profile shown in Figure 2.32. Therefore, from Equation 2.25, the slip-strain at the plate/concrete interface $(ds/dx_p)_0$ and the bar/concrete interface $(ds/dx_b)_0$ is equal to the plate strain $(\varepsilon_p)_0$ and the bar strain $(\varepsilon_b)_0$ respectively. Based on $(\varepsilon_b)_0$ guessed, the force in the plate at crack 1 $(F_p)_0$ can be determined from equilibrium of forces given by Equation 2.32. Note that the forces in the top and bottom plates are the same as the system is symmetrical.

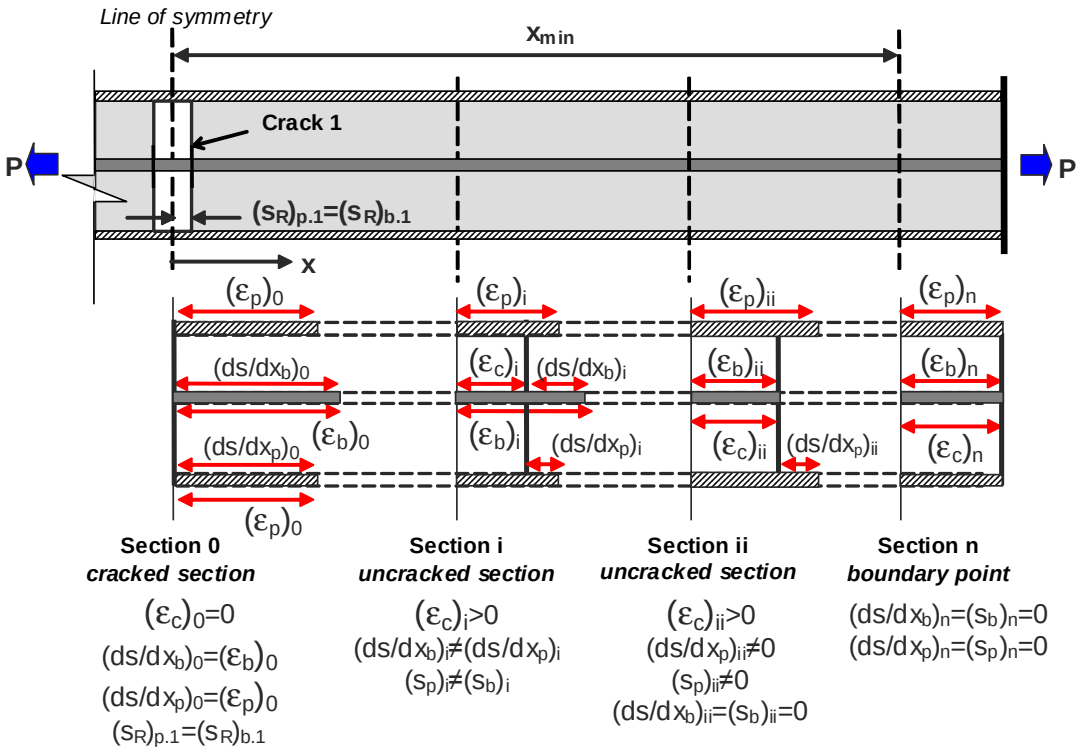

Figure 2.32 Single crack analysis of plated tensile specimen with single reinforcing bar

Analysis is then performed at the next section, section *i*, at a distance *e* away from the previous section as illustrated in Figure 2.32. From the previous section, section i-1, the slip-strains at the concrete/plate $(ds/dx_p)_{i-1}$, and at concrete/bar interface $(ds/dx_b)_{i-1}$ are known from Equation 2.25. Substituting these values and the known plate $(s_p)_{i-1}$ and bar $(s_b)_{i-1}$ slips at section i-1 into Equation 2.33 and Equation 2.34 gives the slips at section *i*, from which the bond force at the plate/concrete $(P_b)_{p.i}$ and bar/concrete $(P_b)_{b.i}$ interface can be determined using the relevant bond-slip relationships. After obtaining the bond forces at the different interfaces, the force in the plate $(F_p)_i$ and in the bar $(F_b)_i$ at section *i* can be evaluated using Equation 2.35 and Equation 2.36 respectively. From Equation 2.32, the force in the concrete $(F_c)_i$, and hence, the resultant strain profile can be obtained.

$$(s_p)_i = (s_p)_{i-1} - e\left(\frac{ds}{dx_p}\right)_{i-1} \qquad \textbf{Equation 2.33}$$

$$(s_b)_i = (s_b)_{i-1} - e\left(\frac{ds}{dx_b}\right)_{i-1} \qquad \textbf{Equation 2.34}$$

$$F_{pi} = (F_p)_{i-1} - (P_b)_{p.i} \qquad \textbf{Equation 2.35}$$

$$F_{bi} = (F_b)_{i-1} - (P_b)_{b.i}$$ **Equation 2.36**

Where $(F_p)_{i-1}$ and $(F_b)_{i-1}$ is the force in plate and in bar at section i-1 respectively.

Segmental analysis is carried out along the beam at fixed increments *e* until the boundary point x_{min} is reached where zero slip and/or zero slip-strain is obtained at each interface, i.e. section *n* in Figure 2.32. To check $(s_R)_{p.1}$ and $(\varepsilon_b)_0$ guessed initially at crack 1, Boundary Condition 3 given in Section 2.4.2.1 applies, where at the boundary of the partial interaction region x_{min} there is zero slip and slip-strain at all interfaces, i.e. at section *n* in Figure 2.32 $ds/dx_p=s_p=0$ and $ds/dx_b=s_b=0$. Therefore the shooting technique (Section 2.2.4.3) can be used where $(s_R)_{p.1}$ and $(\varepsilon_b)_0$ are iterated until this boundary condition is satisfied at all interfaces. For example, first check that $s_p=ds/dx_p=0$ at x_{min}, if not, a new $(s_R)_{p.1}$ is assumed for the same $(\varepsilon_b)_0$ guessed in Figure 2.32, and keep repeating the analysis until a solution is found. After Boundary Condition 3 is satisfied at the plate/concrete interface, the bar/concrete interface is checked. If s_b and ds/dx_b are not both equal zero at the boundary point x_{min}, this means that the $(\varepsilon_b)_0$ guessed is wrong. For each new guesses of $(\varepsilon_b)_0$, the boundary condition at the plate/concrete interface needs to be rechecked to determine the corresponding $(s_R)_{p.1}$. It should be noted that different interfaces is likely to achieve full interaction at different locations such as section *ii* in Figure 2.32 where, because the strain in the plate is greater than that in the bars, full interaction first occurs at the bar/concrete interface while there is still slip between the plate and the concrete. It is at the position where $ds/dx=s=0$ occurs at all interfaces which forms the boundary of the partial interaction region. For specimens with more than two layers of reinforcement, the same analysis procedure applies, where the unknown variables are iterated until Boundary Condition 3 is satisfied at all reinforcement/concrete interfaces.

2.4.2.3 Example of Single Crack Analysis

Analyses were carried out on the same steel plated tensile specimen as that used in Section 2.4.1.3, but with a single bar at the centre of the specimen as illustrated in Figure 2.32. The steel bar is 12mm in diameter, at a depth of 75mm from the concrete surface, where a bilinear stress-strain model is assumed with a yield strength $f_{b.y}$ of 400MPa. The dimensions and material properties of the beam and the plates are given in Section 2.4.1.3. The simplest case of a linear ascending bond-slip model at the plate/concrete interface with unlimited bond strength was assumed. The bond-slip model used for the bar/concrete interface (Huang et al. 1996; cited in *fib* 2000) is shown in Figure 2.33, where the peak bondstress $\tau_{b.max}$ is dependent on the concrete compressive stress f_c; the slips s_1=1mm, s_2=3mm, s_3=4mm and an ultimate slip s_f of $3s_3$.The specimen is under load control, where an axial load *P* of

71.1 kN was applied and a single crack, crack 1, has formed at distance x=0 as illustrated in Figure 2.32.

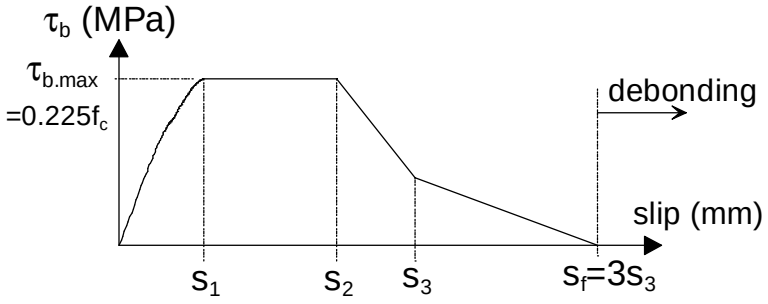

Figure 2.33 Bond-slip model for ribbed bars (Huang et al. 1996)

Figure 2.34 and Figure 2.35 show the slip and slip-strain ds/dx distributions at the plate/concrete interface for different guesses of bar strain $(\varepsilon_b)_0$ at crack 1, where for each $(\varepsilon_b)_0$ considered, the plate slip at crack 1 $(s_R)_{p.1}$ is iterated until Boundary Condition 3 is satisfied at the plate/concrete interface i.e. $ds/dx_p=s_p=0$ at the boundary point x_{min} where bar slip-strain also tends to zero. Figure 2.36 and Figure 2.37 shows the slip and ds/dx distributions at the bar/concrete interface for different guesses of bar strain $(\varepsilon_b)_0$ at crack 1. It can be seen from Figure 2.34 and Figure 2.35 that, for each $(\varepsilon_b)_0$ guessed, there is a $(s_R)_{p.1}$ which will give $ds/dx_p=s_p=0$ at x_{min}, however there is only a single value of $(\varepsilon_b)_0$ and $(s_R)_{p.1}$, which will result in zero slip and slip-strain at the boundary point at both concrete/plate and concrete/bar interfaces (Figure 2.36 and Figure 2.37). For example, when the $(\varepsilon_b)_0$ guessed is too large i.e. $(\varepsilon_b)_0=4.42\text{x}10^{-4}$, $ds/dx_p=s_p=0$ is obtained at the plate/concrete interface for a slip $(s_R)_{p.1}$ of 0.0213 (Figure 2.34 and Figure 2.35), however, at the bar/concrete interface $ds/dx_b>0$ where $s_b=0$ (Figure 2.36 and Figure 2.37). When the $(\varepsilon_b)_0$ guessed is too small i.e. $(\varepsilon_b)_0=3.98\text{x}10^{-4}$, full interaction is obtained at the plate/concrete interface for a slip $(s_R)_{p.1}$ of 0.0216 (Figure 2.34 and Figure 2.35), however, at the bar/concrete interface $s_b>0$ where $ds/dx_b=0$ (Figure 2.36 and Figure 2.37). It is at $(\varepsilon_b)_0=4.16\text{x}10^{-4}$ and $(s_R)_{p.1}$= 0.02146mm where $ds/dx_p=s_p=0$ and $ds/dx_b=s_b=0$ is obtained at the boundary point located at x_{min}=202mm from the initial crack.

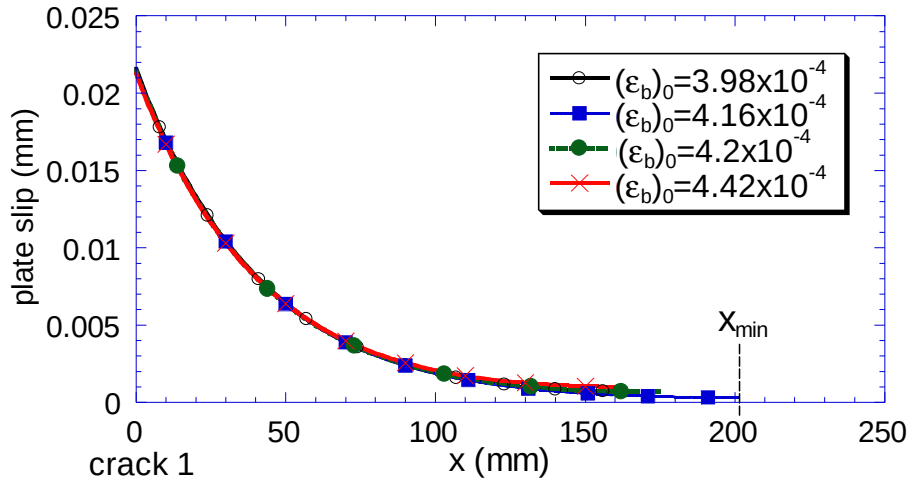

Figure 2.34 Single crack analysis: plate slip distribution of plated tensile specimen with bar

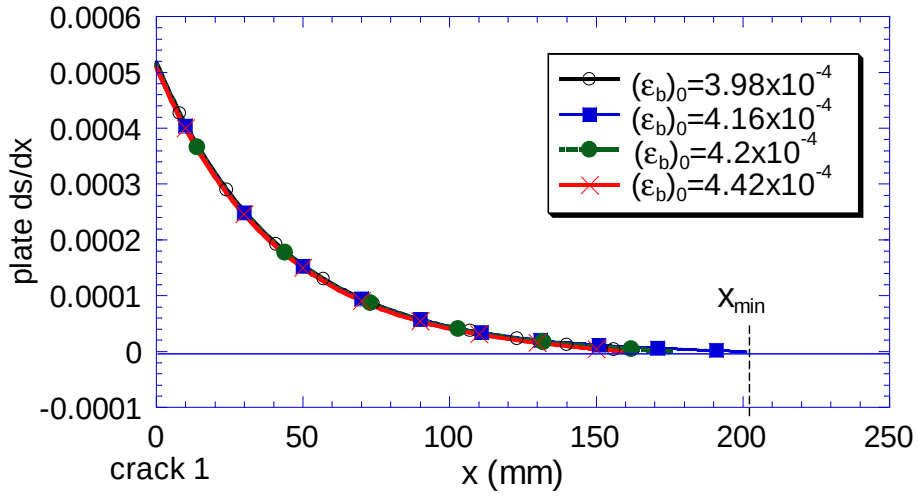

Figure 2.35 Single crack analysis: plate slip-strain distribution of plated tensile specimen with bar

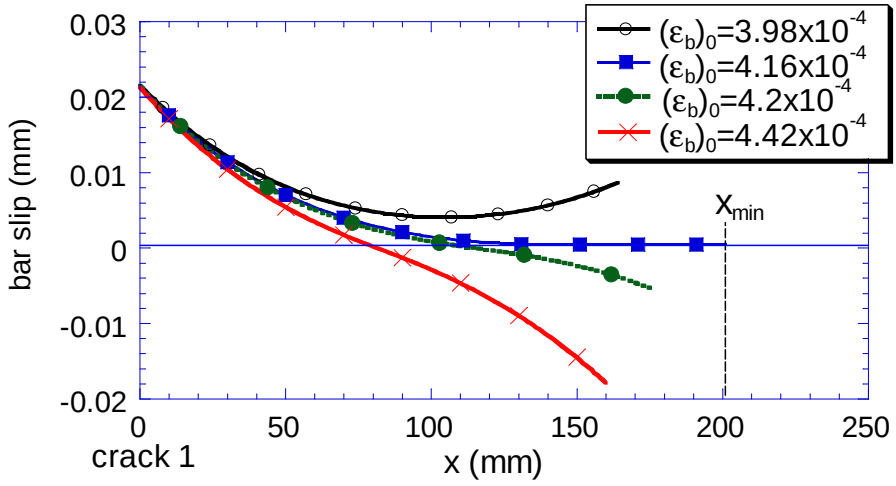

Figure 2.36 Single crack analysis: bar slip distribution of plated tensile specimen with bar

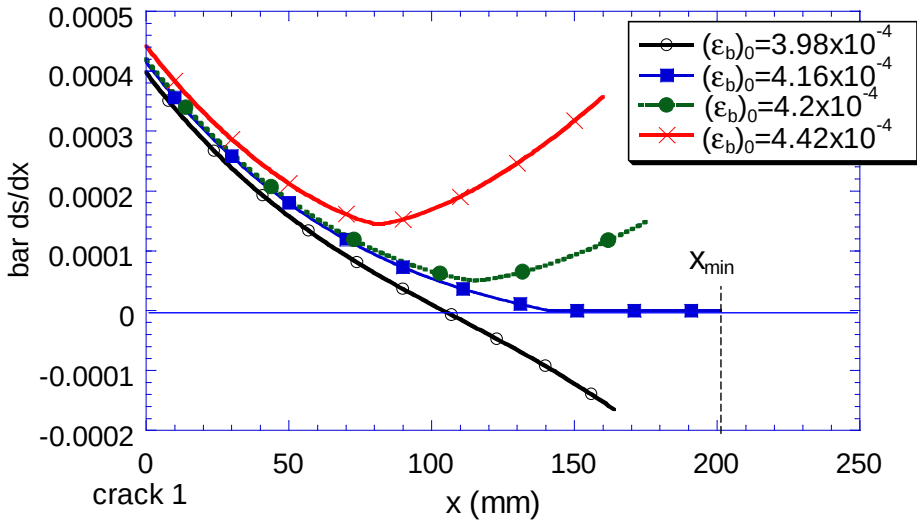

Figure 2.37 Single crack analysis: bar slip-strain distribution of plated tensile specimen with bar

From the solution found above for an applied load of 71.1kN, the behaviours of different interfaces are studied. Figure 2.38 and Figure 2.39 show a comparison between plate and bar slip-strain, and slip distributions respectively, where it can be seen that full interaction is first achieved at the bar/concrete interface at a distance of 142mm from the crack 1, however at this point there is still slip at the plate/concrete interface (Figure 2.39). It is at 202mm from the crack 1 where boundary conditions are satisfied at all reinforcing layers. A comparison between the distribution of concrete, plate and bar strains of the tensile specimen is shown in Figure 2.40, where it can be seen that as the distance from the crack increases, the concrete tensile strain increases while the strains of the plate and the bar reduce. When full interaction is reached at the interface, the concrete strain is equal to the strain of the reinforcements. Note how the plate strain at a crack can be significantly greater than that of the bar strain, which confirms that the assumption of plain strain is no longer valid.

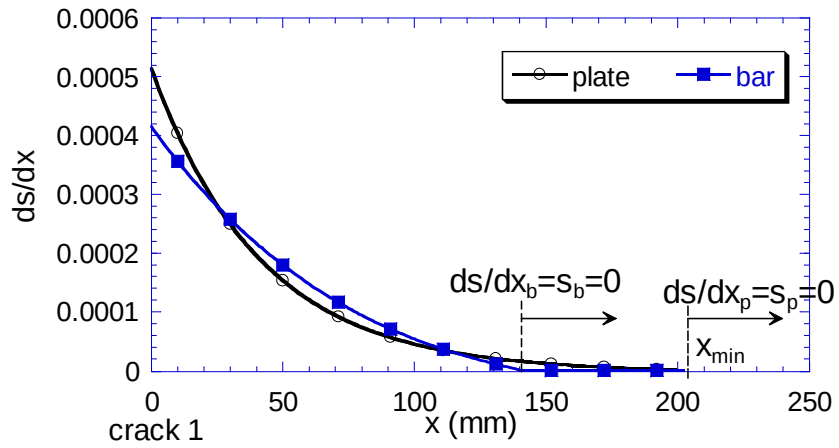

Figure 2.38 Plated tensile specimen with bars - comparison of slip-strains in single crack analysis

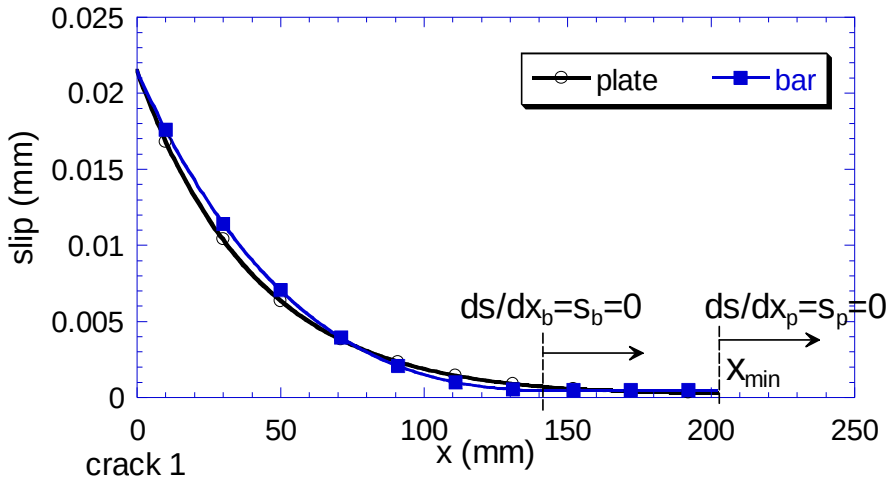

Figure 2.39 Plated tensile specimen with bars - comparison of slips in single crack analysis

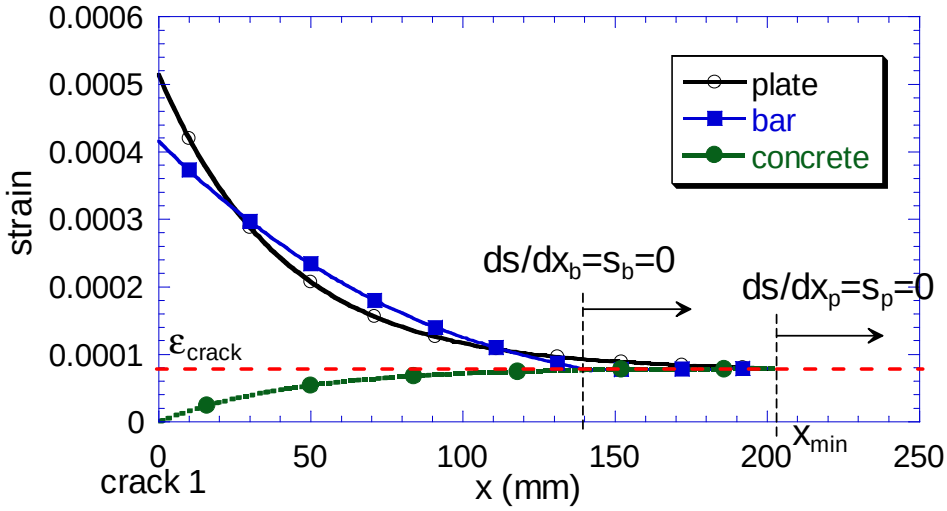

Figure 2.40 Plated tensile specimen with bars - comparison of strains in single crack analysis

2.4.2.4 Check for Cracking

From the partial interaction analysis above, the concrete strain distribution along the tensile specimen can be obtained, and the position of the next crack can be determined using the procedure described in Section 2.4.1.4. For the example considered in Section 2.4.2.3, for an axial load of 71.1kN, the maximum concrete tensile strain reached is equal to the concrete cracking strain at the boundary point x_{min} as shown in Figure 2.40. Therefore the next crack will occur at a distance x_{crack}=202mm from the initial crack. The formation of new cracks largely affects the local deformation of specimens, therefore members need to be reanalysed to allow for effects of distributed cracks.

2.4.2.5 MULTIPLE CRACK ANALYSIS

When distributed cracks occur in an initially uncracked specimen, the specimen needs to be reanalysed to model the local behaviour of the uncracked concrete between cracks. Figure 2.41 is an illustration of the analysis between adjacent cracks of a plated tensile specimen with an internal bar, where segmental analysis described in Section 2.4.2.2 for the single crack situation applies with a change in boundary conditions.

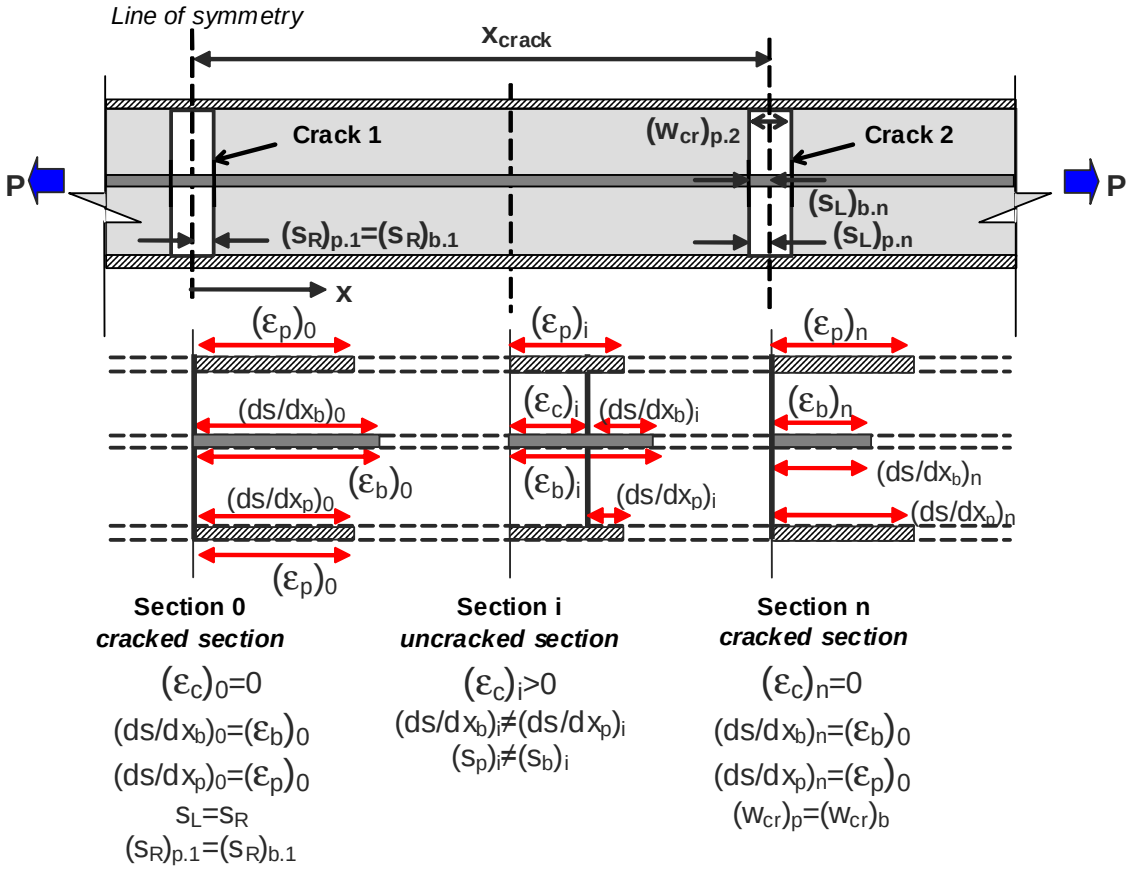

Figure 2.41 Analysis between adjacent cracks plated tensile specimen with single reinforcing bar

To illustrate the analysis between adjacent cracks, let us assume that the specimen is under load control where an axial load *P* is applied, and crack 1 is located at the line of symmetry at *x*=0 and crack 2 at a distance x_{crack} from crack 1. Analysis begins at crack 1, where the slip size $(s_R)_{p.1}$ and bar strain $(\varepsilon_b)_0$ at the crack is guessed. Therefore there are two unknowns requiring two boundary conditions for a solution. Based on the assumption of constant crack width (Boundary Condition 5 in Section 2.4.2.1) and that the system is symmetrical about crack 1, such that the left and right crack face slips are equal, $s_L=s_R$, therefore the crack face slip of the bar and of the plate are equal at crack 1 i.e. $(s_R)_{p.1}=(s_R)_{b.1}$, as discussed in Section 2.4.2.2. Also based on Boundary Condition 4 of zero

concrete tensile strain at a cracked section (Section 2.4.2.1), the force $(F_p)_0$, and hence, strain $(\varepsilon_p)_0$ in the plate at crack 1 can be determined using Equation 2.32, resulting in the strain profile of section 0 in Figure 2.41. From crack 1, a segmental analysis is carried out at fixed increments *e* until crack 2 is reached at x_{crack} where at each section considered, the slips at each level of reinforcement are calculated using Equation 2.33 and Equation 2.34, from which the bond force P_b at each interface over the increment *e* can be found, and hence, the forces in the reinforcements are evaluated from Equation 2.35 and Equation 2.36 and the strain profile is obtained. At crack 2, section n in Figure 2.41, there is zero tensile strain in the concrete i.e. $(\varepsilon_c)_n=0$ (Boundary Condition 4 in Section 2.4.2.1), and so, this forms the boundary condition for analysis between adjacent cracks. Therefore the shooting method (Section 2.2.4.3) is performed, where $(s_R)_{p.1}$ is iterated for the same $(\varepsilon_b)_0$ guessed until Boundary Condition 4 is satisfied at crack 2. After obtaining $(s_R)_{p.1}$, the guess of $(\varepsilon_b)_0$ has yet to be verified, therefore another boundary condition is required.

For beams with multiple cracks such as in Figure 2.42, the same analysis is then performed in the adjacent concrete segments between cracks, where at each crack, crack *i*, the right crack face slip at the plate/concrete interface is $(s_R)_{p.i}$ is guessed. From Equation 2.37, the crack width at the plate level $(w_{cr})_p$ is determined, where the left crack face slip at the plate/concrete $(s_L)_{p.i}$ and bar/concrete $(s_L)_{p.i}$ interface is obtained from the analysis of the previous uncracked concrete segment i.e. between crack i-1 and crack *i*. As crack width is constant i.e. $(w_{cr})_p=(w_{cr})_b$ (Boundary Condition 5), therefore $(w_{cr})_b$ in Equation 2.38 is known, and hence the right crack face slip at the bar/concrete interface $(s_R)_{b.i}$ can be evaluated. $(s_R)_{p.i}$ guessed at crack *i* is iterated and segment reanalysed until Boundary Condition 4 is satisfied at the subsequent crack, crack i+1. If it is found that no further cracking occurs after crack i+1, then the single crack analysis described in Section 2.4.2.2 is performed from crack i+1, where the $(s_R)_{p.i+1}$ guessed at crack i+1 is iterated until ds/dx=*s*=0 is obtained at the plate/concrete interface at boundary point x_{min}. The boundary condition at the bar/concrete interface at x_{min} also needs to be checked (Boundary Condition 3). If ds/dx_b and s_b are not both equal to zero at x_{min} (Section 2.4.1.1), this means that the $(\varepsilon_b)_0$ initially guessed at crack 1 is inaccurate, so that this second boundary condition is used to determine the second unknown. The beam needs to be reanalysed for different guess of $(\varepsilon_b)_0$ until all boundary conditions are satisfied in the concrete segment between adjacent cracks, and full interaction is obtained is at the boundary point x_{min} i.e. $ds/dx_b= s_b=0$ and $ds/dx_p= s_p=0$.

$$(w_{cr})_p = (s_L)_p + (s_R)_p \qquad \textbf{Equation 2.37}$$

$$(w_{cr})_b = (s_L)_b + (s_R)_b \qquad \textbf{Equation 2.38}$$

A summary of the analysis procedure for the multiple crack analysis of a plated tensile specimen with reinforcing bars subjected to load control is shown in Figure 2.42, where three cracks have formed at a constant crack spacing of x_{crack}, with crack 1 occurring at the line of symmetry.

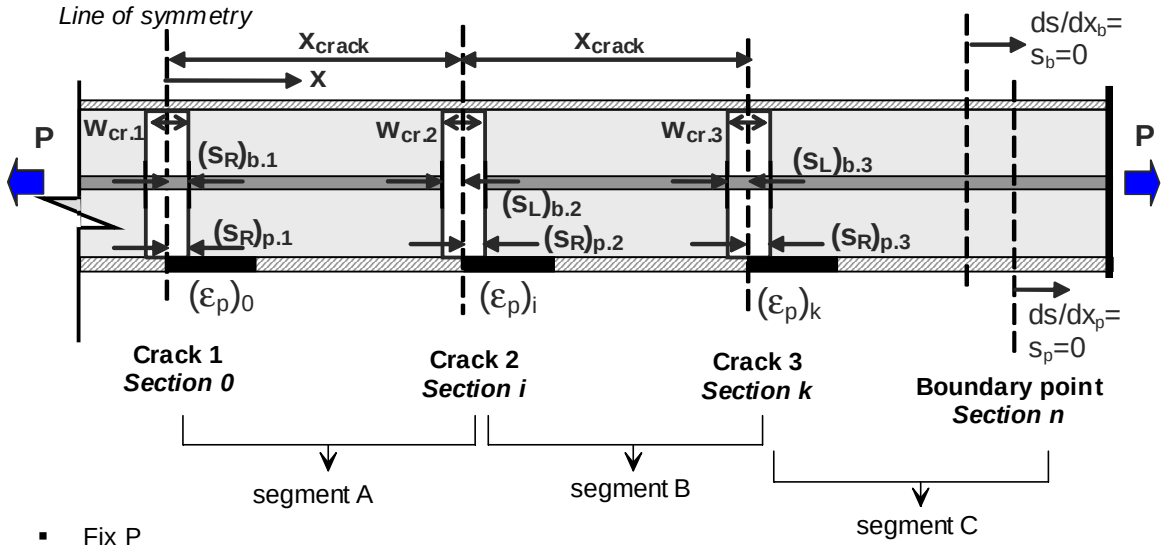

- Fix P
- Guess $(\varepsilon_p)_0$ & $(S_R)_{p.1}$
- $W_{cr.1}$=constant (boundary condition 3) & $S_L=S_R$ at line of symmetry => at crack 1: $(S_R)_{b.1}=(S_R)_{p.1}$
- At crack 1 $(\varepsilon_c)_0=0$ hence find $(\varepsilon_b)_0$ [Equation 2.30]
- apply "shooting method" along segment A
- iterate $(S_R)_{p.1}$ until $(\varepsilon_c)_i=0$ (boundary condition 2)
- evaluate $(S_L)_{p.2}$ & $(S_L)_{b.2}$
- evaluate $(\varepsilon_p)_i$ & $(\varepsilon_b)_i$

(a)

- Guess $(S_R)_{p.2}$
- from Equations 2.35 and 2.36 find $(S_R)_{b.2}$ based on boundary condition 3
- apply "shooting method" along segment B
- iterate $(S_R)_{p.2}$ until $(\varepsilon_c)_j=0$
- evaluate $(S_L)_{p.3}$ & $(S_L)_{b.3}$
- evaluate $(\varepsilon_p)_k$ & $(\varepsilon_b)_k$

(b)

- Guess $(S_R)_{p.3}$
- from Equations 2.35 and 2.36 find $(S_R)_{b.3}$ based on boundary condition 3
- apply "shooting method" along segment C
- iterate $(S_R)_{p.3}$ until $ds/dx_p=s_p=0$
- if ds/dx_b or $s_b \neq 0$ reanalyse beam changing $(\varepsilon_p)_0$ at crack 1 and repeat procedures (a)-(c)

(c)

Figure 2.42 Multiple crack analysis of plated tensile specimen with single reinforcing bar

As tensile specimens are subjected to axial force only i.e. there is no internal moment, and so, the cracks will be equally spaced along the specimen, and the local strain and slip distribution of each uncracked concrete segment between 2 adjacent cracks will be the same along the specimen. Therefore each crack will have the same crack width w_{cr}, and as the point of zero slip will always be at midpoint between 2 cracks in a zero moment region, hence $s_L= s_R$. This however does not apply to the last crack to the end of the specimen due to the different local behaviour as illustrated in Section 2.4.2.2 for single crack analysis. Note that as the total axial force is constant along the specimen,

therefore all the cracks will appear at the same applied load, that is the specimen will be either uncracked or fully cracked at a constant crack spacing of x_{crack}.

2.4.2.6 EXAMPLE OF ANALYSIS BETWEEN ADJACENT CRACKS

Analysis was carried out for the steel plated tensile specimen considered in Section 2.4.2.3, where a linear ascending bond-slip model with unlimited bond strength was assumed. From the single crack analysis previously performed, the next crack, crack 2 was found to first occur at an axial load of 71.1kN, at 202mm from crack 1 (Section 2.4.2.4). As mentioned earlier, since the specimen has zero internal moment, cracks will form at the same load such that the specimen is either uncracked or fully cracked, with cracks equally spaced throughout. Therefore, the behaviour of every uncracked concrete segment between adjacent cracks is identical, that is the local strain and slip distribution of each segment between 2 adjacent cracks will be the same along the specimen.

The local slip-strain ds/dx, slip *s*, bondstress τ_b, and strain distributions between two adjacent cracks , crack 1 and 2, are shown in Figure 2.43 to Figure 2.46 respectively. From Figure 2.43, it can be seen that slip-strains at the plate/concrete and bar/concrete interface decreases as the distance from crack 1 increases, i.e. the effect of partial interaction is reducing, however as ds/dx>0 between cracks, full interaction does not occur. Because the bond at the two interfaces are different (Figure 2.45), the distribution of the ds/dx at the two interfaces differs, but the minimum slip-strain occurs at the same location for both bar/concrete and plate/concrete interface as shown in Figure 2.43. For both interfaces, the point of zero slip occurs at the midpoint between two adjacent cracks (Figure 2.44) as the local behaviour is the same in each segment between adjacent cracks. Therefore by symmetry, the right crack face slip at crack 1, $(s_R)_1$, and the left crack face slip at crack 2, $(s_L)_2$, are equal for each interface. The point of zero slip coincides with the points of minimum ds/dx (Figure 2.43), plate ε_p and bar ε_b strains, and the point of maximum concrete tensile strain (Figure 2.46). From Figure 2.46 it can be seen the plate strain at a crack is greater than that of the bar strain, and both plate and bar strains are significantly higher than the concrete strain, which verifies that the assumption of plane section remains plane does not apply to cracked regions.

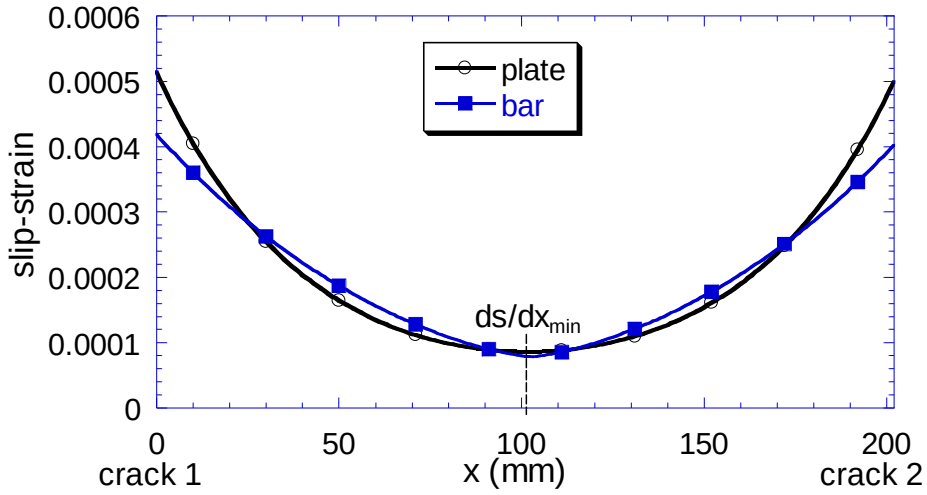

Figure 2.43 Slip-strain distributions between adjacent cracks of plated tensile specimen with bar

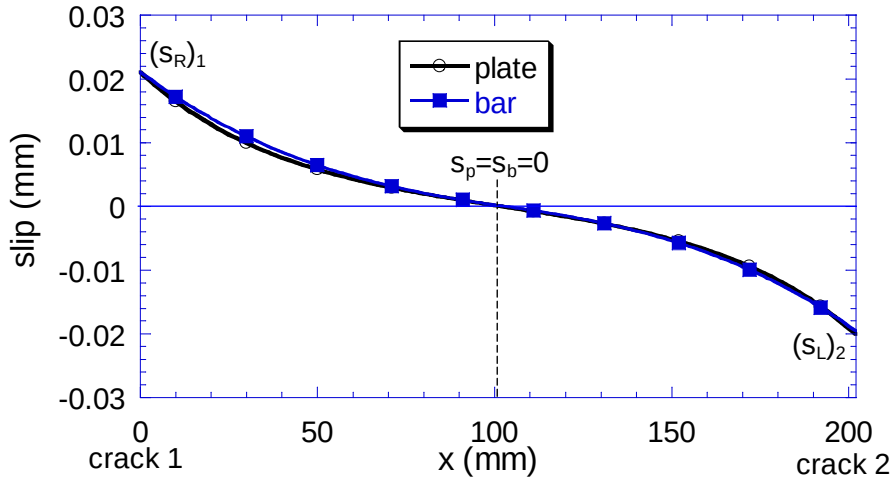

Figure 2.44 Slip distributions between adjacent cracks of plated tensile specimen with bar

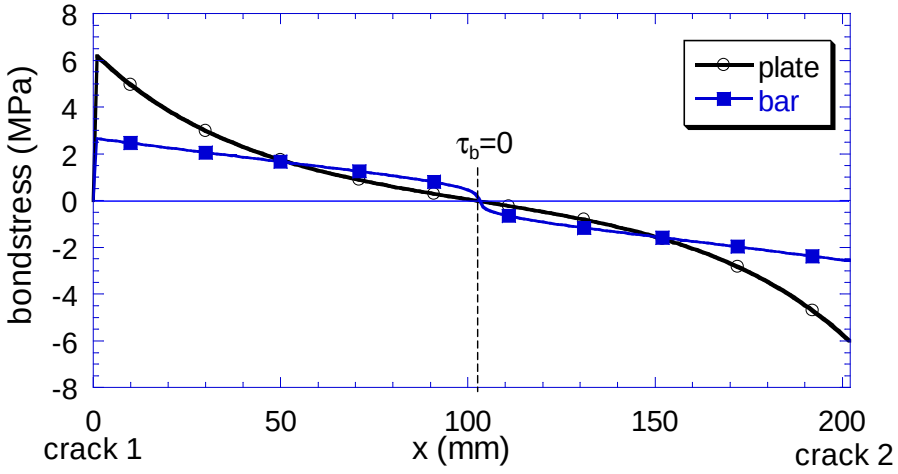

Figure 2.45 Bondstress distributions between adjacent cracks of plated tensile specimen with bar

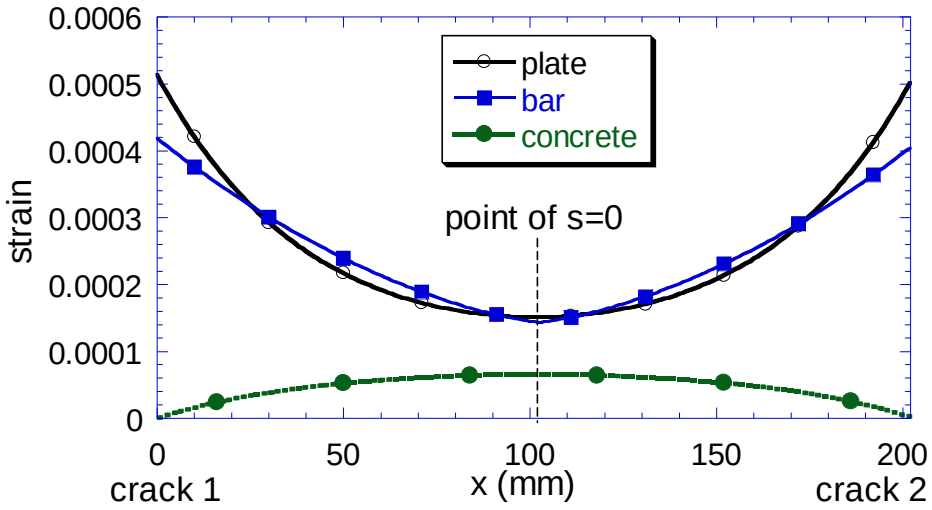

Figure 2.46 Strain distributions between adjacent cracks of plated tensile specimen with bar

2.4.2.7 Behaviour of Plated Specimens With Trilinear Bond-Slip Relationship

The specimen analysed here is the same as that in Section 2.4.1.7 with an additional steel bar of 12mm diameter, at a depth of 75mm from the concrete surface, where a bilinear stress-strain model is assumed with a yield strength $f_{b.y}$ of 400MPa. To study the local deformation of plated tensile members with bars, a trilinear bond-slip model at the plate/concrete interface (illustrated in Figure 2.6) is considered. At the plate/concrete interface, the peak bondstress $\tau_{b.max}$ of 6MPa is assumed at a relative slip s_{max}=0.02mm, and macro debonding begins at a slip s_f of 0.2mm. The bond-slip model used for the bar/concrete interface is shown in Figure 2.33, where the peak bondstress $\tau_{b.max}$ is dependent on the concrete compressive stress f_c; the slips s_1=1mm, s_2=3mm, s_3=4mm and an ultimate slip s_f of $3s_3$.

Progressive cracking of the specimen is studied, where it is assumed that a single crack, crack 1, has formed at the line of symmetry at distance x=0. As the load P was gradually applied, it was found that at P= 72.8kN, with a relative plate slip s_p of 0.12mm and a plate strain of 0.0024 at crack 1, the concrete cracking strain ε_{crack} was exceeded at 248mm from crack 1 as shown in Figure 2.47. As mentioned in Section 2.4.2.6, in a tensile specimen cracks will form at the same load at a constant spacing along the shear span, therefore for a shear span of 700mm considered, 2 more cracks will form. Compared with the plated specimen without bars in Section 2.4.1.7 where debonding failure occurred at P=45.9kN before more cracks could form, the additional bar has relieved the strain in the plate (Figure 2.47), hence delaying the debonding process at the plate/concrete interface and allowing more cracks to form.

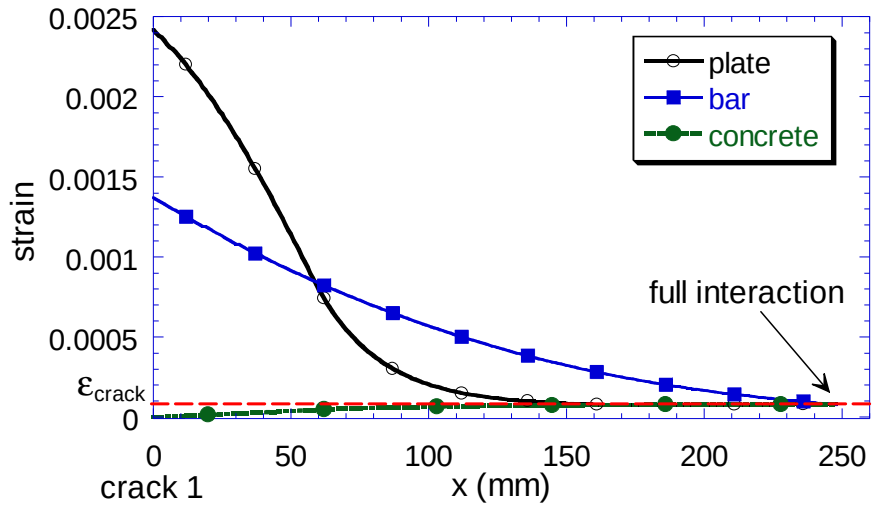

Figure 2.47 Strain distributions for FRP plated tensile specimen prior to cracking

After the formation of the cracks, the specimen is reanalysed using multiple crack analysis as illustrated in Figure 2.42 for the same applied load. From Figure 2.48, plate and bar strains are significantly higher than the concrete strain, especially for the plate strain, which is almost double that of the bar. As mentioned in Section 2.4.2.6, for a tensile specimen with multiple cracks, the point of zero slip always occur at midpoint between adjacent cracks, as shown in Figure 2.49. The slips at both interfaces are the same at the cracks, but the slip at the plate/concrete interface tend to reduce much more rapidly. Unlike the steel plated specimen analysed in Section 2.4.2.6 (Figure 2.44), the slip distributions at the two interfaces are very different for the FRP plated specimen considered. For the applied load considered, full interaction was achieved at the plate/concrete interface i.e. $ds/dx_p=s_p=0$ between the last crack and the beam end, as shown in Figure 2.49 and Figure 2.50, but not at the bar/concrete interface as indicated by the $ds/dx_b>0$ at the beam end. This is also evident from Figure 2.48, where near the beam end, the plate and concrete strains are the same, while the strain in the bar is substantially greater. From the bondstress distributions in Figure 2.51, it can be seen that micro-debonding has began at the plate/concrete interface for the applied load considered, propagating towards that midpoint between cracks, and also propagating from the last crack towards the plate end.

Through the analysis it has been shown that the local deformation at the plate/concrete interface can be very different to that at the bar/concrete interface due to the different bonding mechanisms. Therefore when studying the local behaviour of a plated reinforced concrete structure, it is necessary to account for the slip at the bar/concrete interface.

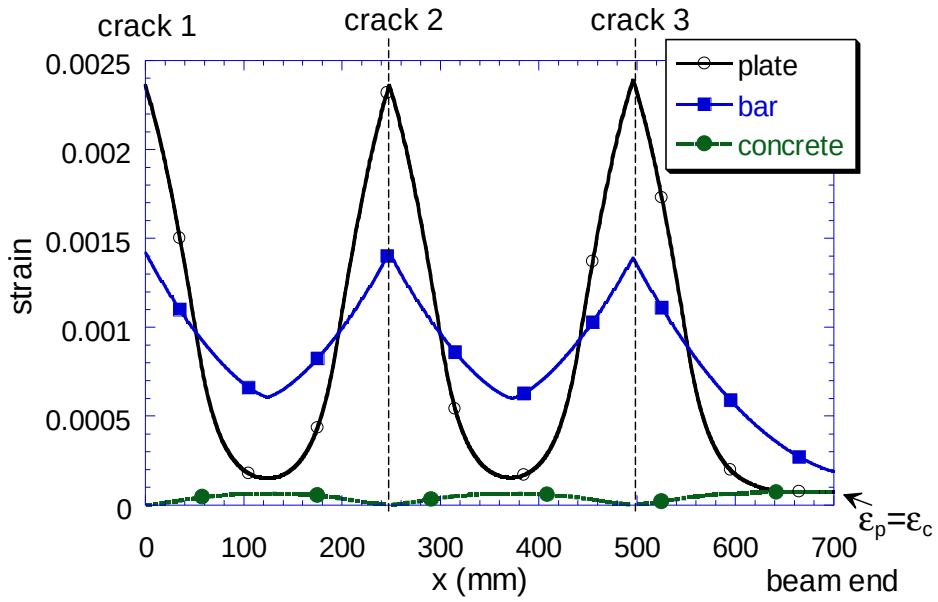

Figure 2.48 Strain distributions for FRP plated tensile specimen with multiple cracks

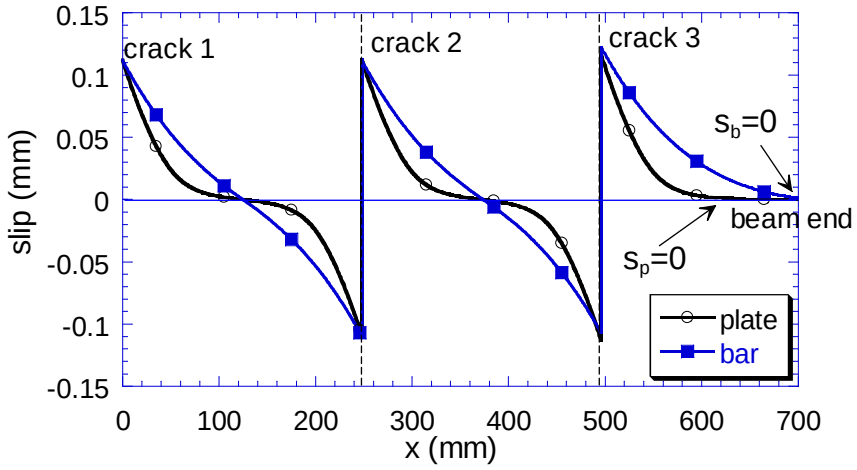

Figure 2.49 Slip distributions for FRP plated tensile specimen with multiple cracks

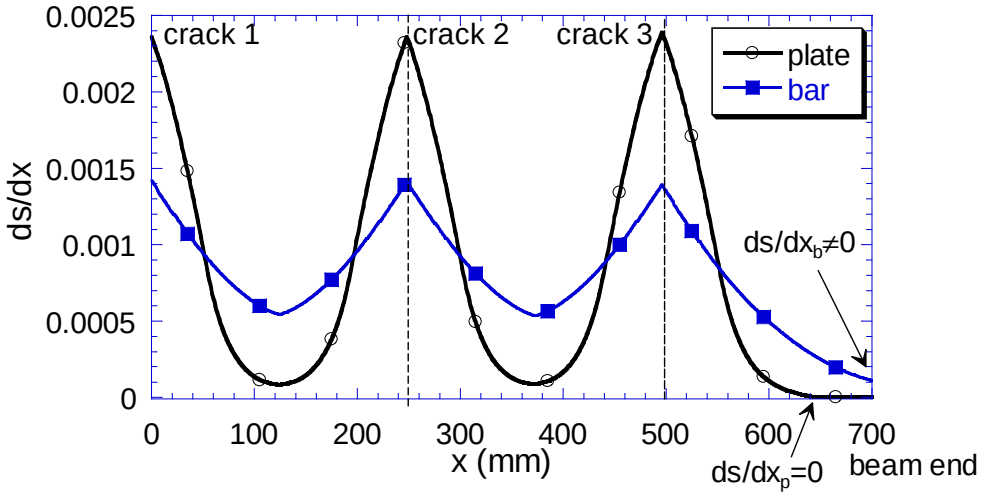

Figure 2.50 Slip-strain distributions for FRP plated tensile specimen with multiple cracks

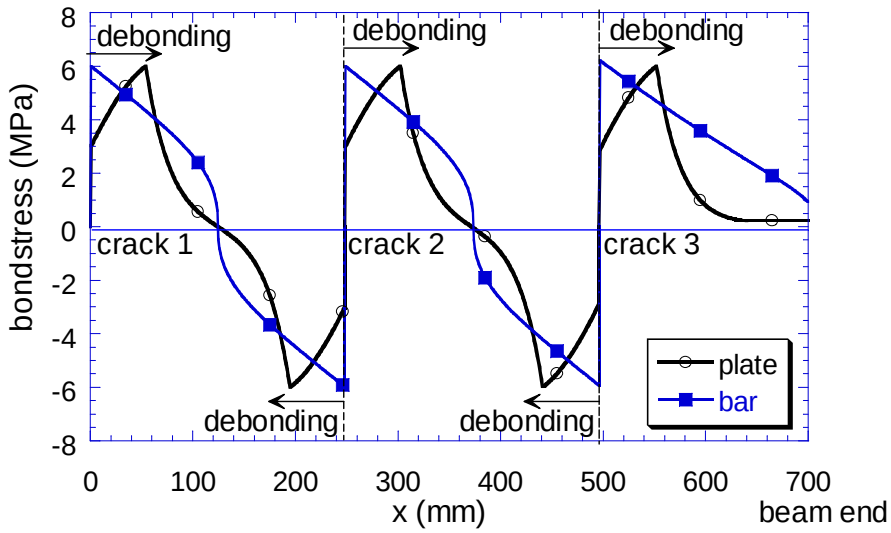

Figure 2.51 Bondstress distributions for FRP plated tensile specimen with multiple cracks

2.4.3 MATHEMATICAL MODEL FOR TENSILE SPECIMENS

In addition to the rigorous non-linear model proposed in Sections 2.4.1 and 2.4.2, a mathematical model is proposed in this Section for partial interaction analysis of tensile specimens with a single layer of reinforcement. This model is based on the mixed approach developed for composite beams in Section 2.2.4.2, where the bondstress at the interface $\tau_{b.max}$ is assumed to be constant as illustrated by the bond-slip model in Figure 2.52, that is plastic behaviour is assumed, while the other elements remain linear elastic. The adoption of this mixed analysis approach greatly simplifies the partial interaction analysis process, from which closed form solutions are derived.

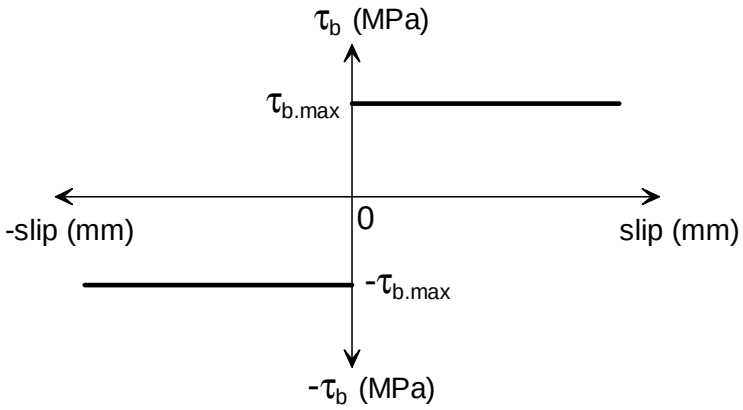

Figure 2.52 Mixed analysis approach: bond-slip model

Consider the uncracked concrete block of length *L* in Figure 2.53a, with a plate externally bonded to the top of the specimen, where an axial load *P* is applied to the plate. Therefore, at the edge of the

concrete block, such as section A-A in Figure 2.53a, there is zero force in the concrete element i.e. F_c=0, while the plate is subjected to an axial force *P*.

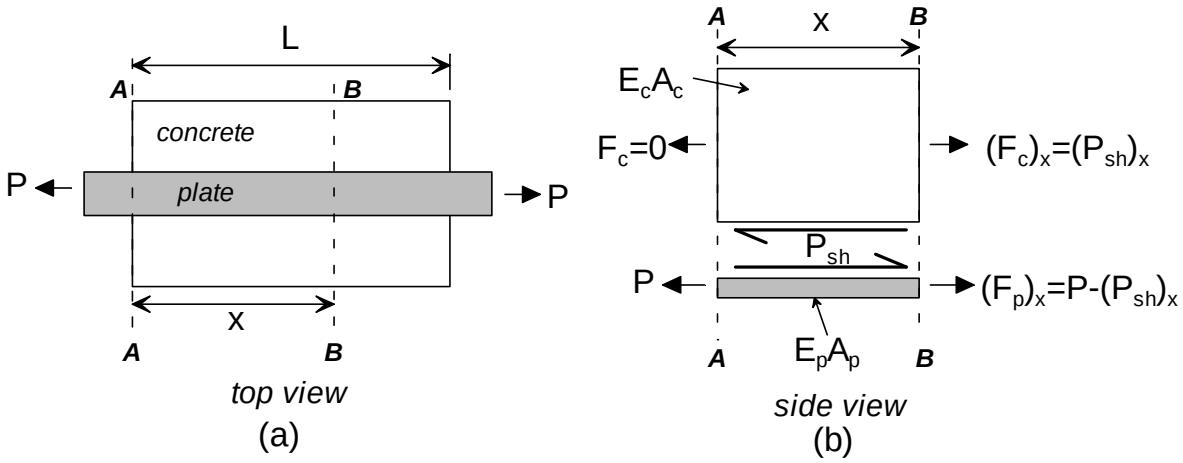

Figure 2.53 Fundamental behaviour of plated tensile specimen

Consider the free body equilibrium of segment *x* illustrated in Figure 2.53b. From equilibrium of internal forces in the plate element, Equation 2.39 is derived where $(F_p)_x$ is the force in the plate at distance *x* from the edge of the concrete block; and $(P_{sh})_x$ is the bond force over the distance *x*. Therefore, the plate strain at distance *x* can be obtained by rearranging Equation 2.39, as shown by Equation 2.40.

$$P = (F_p)_x + (P_{sh})_x \qquad \textbf{Equation 2.39}$$

$$(\varepsilon_p)_x = \frac{(F_p)_x}{E_p A_p} = \frac{P - (P_{sh})_x}{E_p A_p} \qquad \textbf{Equation 2.40}$$

Where E_p is the young's modulus of the plate; and A_p is the area of the plate element.

For the concrete element shown in Figure 2.53b, from equilibrium of internal forces, the force in the concrete at distance *x* from the edge of the concrete block, $(F_c)_x$, is equal to $(P_{sh})_x$. Therefore, the concrete strain at distance *x* is given by:

$$(\varepsilon_c)_x = \frac{(F_c)_x}{E_c A_c} = \frac{(P_{sh})_x}{E_c A_c} \qquad \textbf{Equation 2.41}$$

Where E_c is the young's modulus of the concrete; and A_c is the area of the concrete element.

By substituting the plate and concrete strains from Equation 2.40 and Equation 2.41 respectively, the slip-strain *ds/dx* at the plate/concrete interface is derived:

$$\frac{ds}{dx} = \left(\varepsilon_p\right)_x - \left(\varepsilon_c\right)_x = \frac{P - (P_{sh})_x}{E_p A_p} - \frac{(P_{sh})_x}{E_c A_c} \qquad \text{Equation 2.42}$$

Rearranging Equation 2.42 gives:

$$\frac{ds}{dx} = \frac{P}{E_p A_p} - (P_{sh})_x k_3 \qquad \text{Equation 2.43}$$

Where $k_3 = \frac{1}{E_c A_c} + \frac{1}{E_p A_p}$ Equation 2.44

As there is no internal moment, the tensile specimen in Figure 2.53a is symmetrical about the midspan, where the point of zero slip occurs at *x*=*L*/2, and there is a reverse in slip, and hence bond force, in the segment between *x*=*L*/2 and *x*=*L*. Therefore based on mixed analysis, the bond force per unit length q_{sh} is constant along the specimen between *x=0* and *x=L/2*, while the bond force between *x*=*L*/2 and *x*=*L* is of equal magnitude but opposite in direction. To evaluate the slip along the plate/concrete interface, let us firstly consider the segment between *x*=0 and *x*=*L*/2. The bond force $(P_{sh})_x$ is given by Equation 2.45, where q_{sh} is constant for $0 \le x \le L/2$. Equation 2.46 is obtained by substituting Equation 2.45 into Equation 2.43.

$$(P_{sh})_x = q_{sh}.x \qquad \text{for } 0 \le x \le L/2 \qquad \text{Equation 2.45}$$

$$\frac{ds}{dx} = \frac{P}{E_p A_p} - k_3 q_{sh}.x \qquad \text{for } 0 \le x \le L/2 \qquad \text{Equation 2.46}$$

The slip at the plate/concrete interface, s_x, at distance *x* away from the section A-A in Figure 2.53a can be obtained by integrating Equation 2.46:

$$s_x = \frac{P}{E_p A_p} x - k_3 q_{sh} . \frac{x^2}{2} + C_1 \qquad \text{for } 0 \le x \le L/2 \qquad \text{Equation 2.47}$$

Where C_1 is the integration constant.

By symmetry, there is zero slip at the plate/concrete interface at midspan of the tensile specimen in Figure 2.53a, i.e. at $x=L/2$. Therefore, based on this boundary condition, the integration constant C_1 is evaluated as follows:

$$0 = \frac{P}{E_p A_p}\frac{L}{2} - k_3 q_{sh} . \frac{L^2}{8} + C_1 \qquad \text{Equation 2.48}$$

$$C_1 = k_3 q_{sh} . \frac{L^2}{8} - \frac{P}{E_p A_p}\frac{L}{2} \qquad \text{Equation 2.49}$$

Substituting Equation 2.49 into Equation 2.47 gives:

$$s_x = \frac{P}{E_p A_p} x - k_3 q_{sh} . \frac{x^2}{2} + k_3 q_{sh} . \frac{L^2}{8} - \frac{P}{E_p A_p}\frac{L}{2}$$
$$= \frac{P}{E_p A_p}\left(x - \frac{L}{2}\right) - k_3 q_{sh}\left(\frac{x^2}{2} - \frac{L^2}{8}\right) \qquad \text{for } 0 \le x \le L/2 \qquad \text{Equation 2.50}$$

For the segment between $x=L/1$ and $x=L$ in Figure 2.53a, the bond force $(P_{sh})_x$ is given by Equation 2.51, where q_{sh} is constant for $L/2 \le x \le L$. The slip-strain between $x=L/1$ and $x=L$ is hence given by Equation 2.52, which is obtained by substituting Equation 2.51 into Equation 2.43.

$$(P_{sh})_x = q_{sh}(L - x) \qquad \text{for } L/2 \le x \le L \qquad \text{Equation 2.51}$$

$$\frac{ds}{dx} = \frac{P}{E_p A_p} - k_3 q_{sh}(L - x) \qquad \text{for } L/2 \le x \le L \qquad \text{Equation 2.52}$$

The slip at the plate/concrete interface, s_x, for $L/2 \le x \le L$ can be obtained by integrating Equation 2.52:

$$s_x = \frac{P}{E_p A_p} x - k_3 q_{sh} L x + k_3 q_{sh} \frac{x^2}{2} + C_2 \qquad \text{for } L/2 \le x \le L \qquad \text{Equation 2.53}$$

Where C_2 is the integration constant.

By symmetry, there is zero slip at the plate/concrete interface at $x=L/2$. Therefore, based on this boundary condition, the integration constant C_2 is evaluated as follows:

$$0 = \frac{P}{E_p A_p}\frac{L}{2} - k_3 q_{sh}\frac{L^2}{2} + k_3 q_{sh}.\frac{L^2}{8} + C_2 \qquad \textbf{Equation 2.54}$$

$$C_2 = k_3 q_{sh}\frac{3L^2}{8} - \frac{P}{E_p A_p}\frac{L}{2} \qquad \textbf{Equation 2.55}$$

Substituting Equation 2.55 into Equation 2.53 gives:

$$s_x = \frac{P}{E_p A_p}x - k_3 q_{sh} Lx + k_3 q_{sh}\frac{x^2}{2} + k_3 q_{sh}\frac{3L^2}{8} - \frac{P}{E_p A_p}\frac{L}{2}$$

$$= \frac{P}{E_p A_p}\left(x - \frac{L}{2}\right) - k_3 q_{sh}\left(Lx - \frac{x^2}{2} - \frac{3L^2}{8}\right) \qquad \textbf{Equation 2.56}$$

for $L/2 \le x \le L$

The mathematical model is verified by comparing it with the non-linear model proposed in Section 2.4.1, as shown in Figure 2.54 for the slip distributions obtained for the tensile specimen illustrated in Figure 2.53, where the uncracked segment between crack 1 and crack 2, at a spacing of 80mm was considered. Good correlation is observed between the two methods.

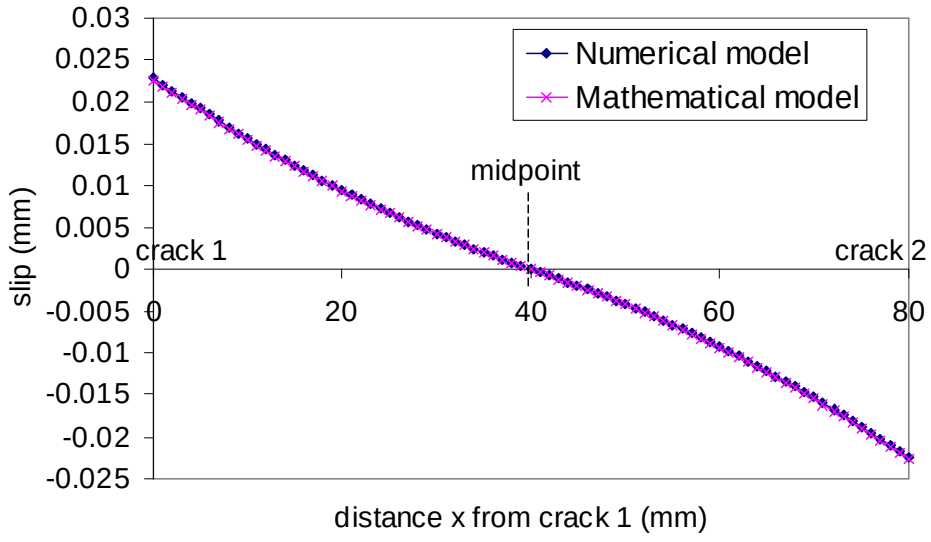

Figure 2.54 Comparison between mathematical and numerical model

2.5 INITIAL PARTIAL INTERACTION APPROACH FOR FLEXURAL MEMBERS

Based on the model developed for tensile specimens in Section 2.4, an initial attempt was made to apply the partial interaction theory to unplated reinforced concrete (RC) beams with a single layer of reinforcement in Section 2.5.1. Due to the presence of moment, the behaviour of flexural members is much more complex and the boundary conditions determined for tensile specimens need to be revised to allow the additional moment. In Section 2.5.2, it will be shown how the initial model developed for a single layer of bar is also applicable to plated beams without bars. Within the cracked region of a RC member, the area around a crack is disturbed, that is the concrete strain does not vary linearly due to the crack. The behaviour of the disturbed regions is extremely complex and difficult to analyse, therefore in the initial partial interaction model developed, this region was ignored. The shortfalls of this initial partial interaction model due assumptions made in the analysis will be discussed in Section 2.5.3, which eventually leads to the development of the modified approach presented in Section 2.6.

2.5.1 UNPLATED REINFORCED CONCRETE BEAM (SINGLE REINFORCING LAYER)

2.5.1.1 FUNDAMENTAL BEHAVIOUR

The behaviour of unplated RC beams is similar to tensile specimens (especially for those under constant moment) with the difference being that curvature is involved in flexural beams. Consider a segment of a tensile specimen with a single layer of reinforcing bar between two adjacent cracks, crack 1 and crack 2 in Figure 2.55a. As there is no moment in the specimen, the force in the bar at crack 1 and 2 must be the same, i.e. $F_{s1}=F_{s2}$. Therefore the resultant bond force ΣP_b of the segment is zero. For an unplated RC beam under constant moment illustrated in Figure 2.55b where $M_1=M_2$ at each crack, the force in the bar must also be the same so that $F_{s1}=F_{s2}$ and $F_{c1}=F_{c2}$, and so the resultant bond force ΣP_b of the segment is zero. It can be seen that the local behaviour of the beam is similar to that for tensile specimens. Therefore the partial interaction model developed in Section 2.4 can be modified to analyse flexural beams.

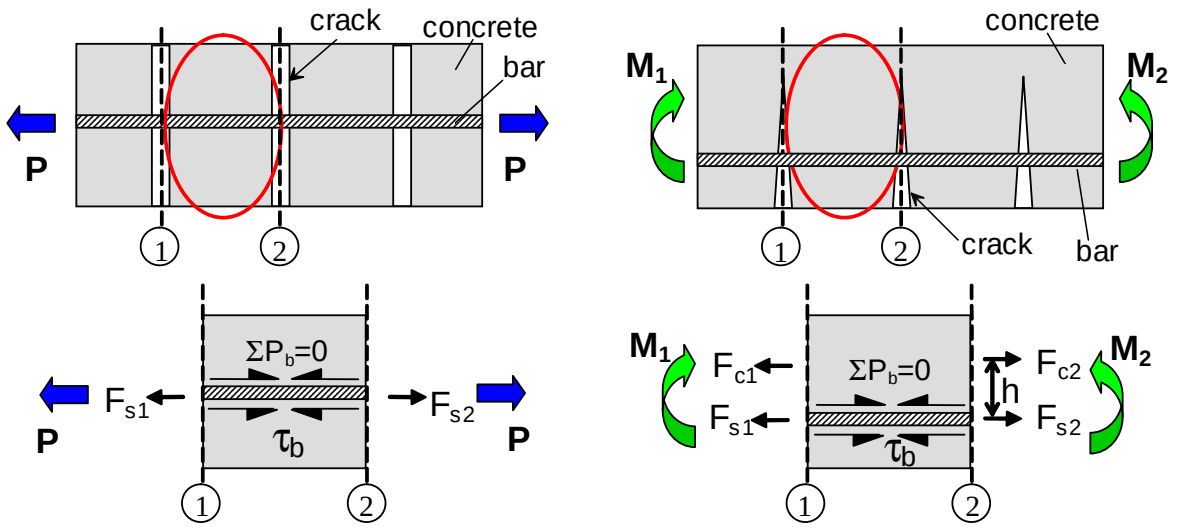

(a) Tensile specimen **(b) Unplated RC beam**

Figure 2.55 Comparison between tensile specimen and unplated RC beam

A numerical model has been developed for the non-linear analysis of an unplated reinforced concrete (RC) beam with a single reinforcement layer that is based on partial interaction theory described in Section 2.2.4.2. Unlike most of the existing non-linear RC models where either uncracked or fully cracked members are considered (Section 2.2), the model described in this Section can analyse the progressive cracking of beams.

Consider the reinforced concrete beam with a single layer of reinforcing bar illustrated in Figure 2.56a, which is subjected to a point load *P*. Before cracking, there is no slip between the reinforcing bar and the concrete. Hence, full interaction occurs at the bar/concrete interface as illustrated in Figure 2.56b for the strain profile with a curvature of χ_{FI}. When a crack of width w_{cr} forms and intercepts the bar, to accommodate this crack a slip *s* occurs at the interface between the concrete and the bar as shown in Figure 2.56a. Therefore the strain in the adjacent concrete is relieved and the strain in the bar needs to take up the additional tensile force. As a result, the strain at the bar ε_b and at the adjacent concrete ε_c is different, that is there is a slip-strain ds/dx, and partial interaction applies, where the strain profile is now given by Figure 2.56c, with a curvature in the concrete of χ_{PI}.

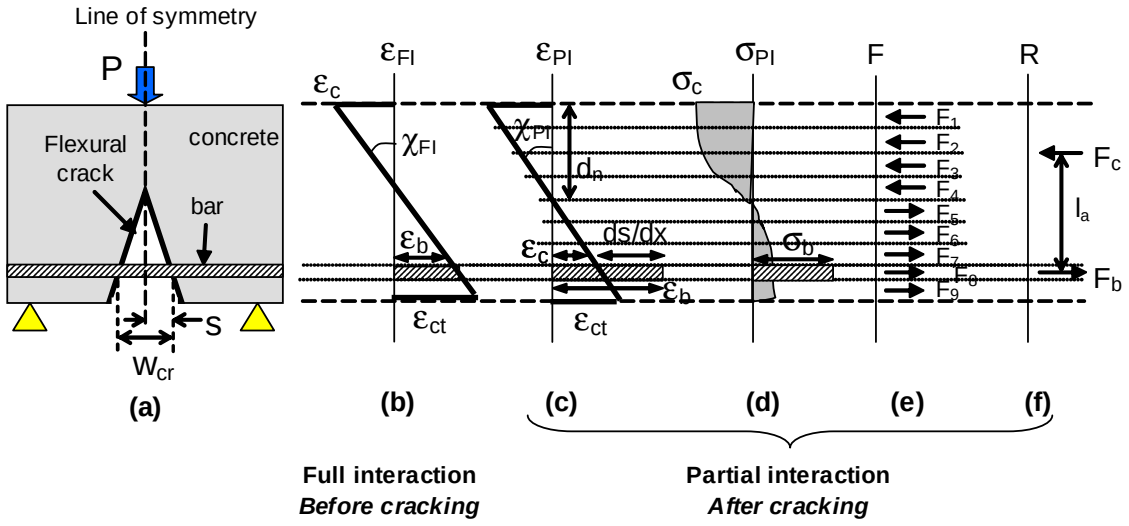

Figure 2.56 Behaviour of unplated RC beam before and after cracking

To perform sectional analysis on a partial interaction strain profile ε_{PI} such as Figure 2.56c, for the bar strain ε_b considered, the flexural stress profile σ_{PI} is firstly evaluated based on the known stress-strain relationships of the concrete and the bar. The flexural forces within the beam can hence be derived by integrating the stress over the cross-section. For example, the cross-section can be divided into *n* layers with the mean stress within each layer determined from Figure 2.56d. It is assumed that the axial force of each layer acts at the mid-depth of the layer, and so the magnitude and distribution of the internal forces *F* is known, as illustrated in Figure 2.56e. As no external longitudinal forces is being applied, equilibrium requires that the total sum of the internal forces to be equal to zero i.e. $\sum F=0$. Therefore, for a curvature in the concrete χ_{PI} guessed, the neutral axis d_n in Figure 2.56c is iterated until horizontal equilibrium is achieved, and the internal moment M_{int} can hence be evaluated. If M_{int} is not equal to the external applied moment, χ_{PI} is then iterated until rotational equilibrium with the applied moment is achieved.

Alternatively, the resultant internal force distribution of the unplated RC beam with a single layer of reinforcing bar can be expressed by the internal couple shown in Figure 2.56f, where F_c and F_b are the resultant axial forces in the concrete and bar respectively, with a lever arm l_a between the forces. Therefore based on the horizontal equilibrium of forces, F_c and F_b are of equal magnitude. From the equilibrium of internal forces in the concrete element, F_b is equal to the total bond force F_{shear} at the bar/concrete interface over the shear span L_{sh}, i.e. $F_b = F_{shear}$, which indicates that the moment of a partial interaction section is dependent on the bond strength P_b at the interface.

To perform nonlinear analyses along the specimen using the shooting technique (Section 2.2.4.3), boundary conditions are required. As described in Section 2.3, outside the cracked partial interaction region full interaction occurs. The following conditions apply:

For each layer of reinforcement there is a position along the length of the reinforcement beyond which there is no slip and no slip-strain at the concrete/reinforcement interface, that is there is full-interaction at the extremities of the partial-interaction region where ds/dx = s = 0. If there is no point of full interaction along the beam, then for the simply supported specimen in Figure 2.56 the boundary condition becomes that at the beam end where there is zero strain in all the elements.	**Boundary Condition 6**

Due to the internal moment, the flexural cracks in a RC member have varying widths such as illustrated in Figure 2.56, therefore the boundary condition 2 for tensile specimens, where constant crack width is assumed, does not apply to flexural members. Instead, when analysing flexural members, it is assumed that a linear variation in concrete strain applies immediately adjacent to a crack. That is the disturbed region surrounding a flexural crack is neglected in the analysis, and since there is zero tensile force in the concrete next to a crack, this leads to the following boundary condition:

Undisturbed region analysis applies immediately adjacent to a crack, where a linear variation in concrete strain is assumed. At the section immediately adjacent to a flexural crack, there is zero tensile force in the concrete and the point of zero concrete strain is assumed to occur at the reinforcement/concrete interface furthest from the concrete surface.	**Boundary Condition 7**

In reality, the concrete strain distribution near a crack, that is the disturbed region, is nonlinear and the strain distribution changes from nonlinear to linear at some distance away from the crack. However the transition over this disturbed region is very difficult to quantify and, furthermore, the length of the disturbed region is unknown. The aim of this model is to analyse the local deformation behaviour in the undisturbed region between cracks. Therefore in this initial partial interaction model, analysis will only be performed between cracks based on the assumption that the whole uncracked region between cracks is undisturbed such that a linear concrete strain profile applies.

Using the two boundary conditions above, nonlinear analysis procedures have been developed to simulate the progressive cracking of an uncracked specimen, where initially a single crack analysis is performed (Section 2.5.1.2). From this analysis, the next cracks are located and the beam is reanalysed using a multiple crack analysis (Section 2.5.2). The multiple crack analysis procedure is also applicable to precracked beams where the cracks are predefined.

2.5.1.2 SINGLE CRACK ANALYSIS

To model the local behaviour of an initially uncracked RC member, analysis is carried out at the position of maximum moment M_0, where it is assumed that a single flexural crack has formed at distance x=0, such as illustrated in Figure 2.57. The following analysis procedures are described based on load control where for a given bar strain $(\varepsilon_b)_0$ at x=0, the slip size s_0 at the first crack is guessed. Therefore one boundary condition is required to verify the s_0 guessed. For analysis under slip control, s_0 is fixed and $(\varepsilon_b)_0$ is iterated to obtain a solution.

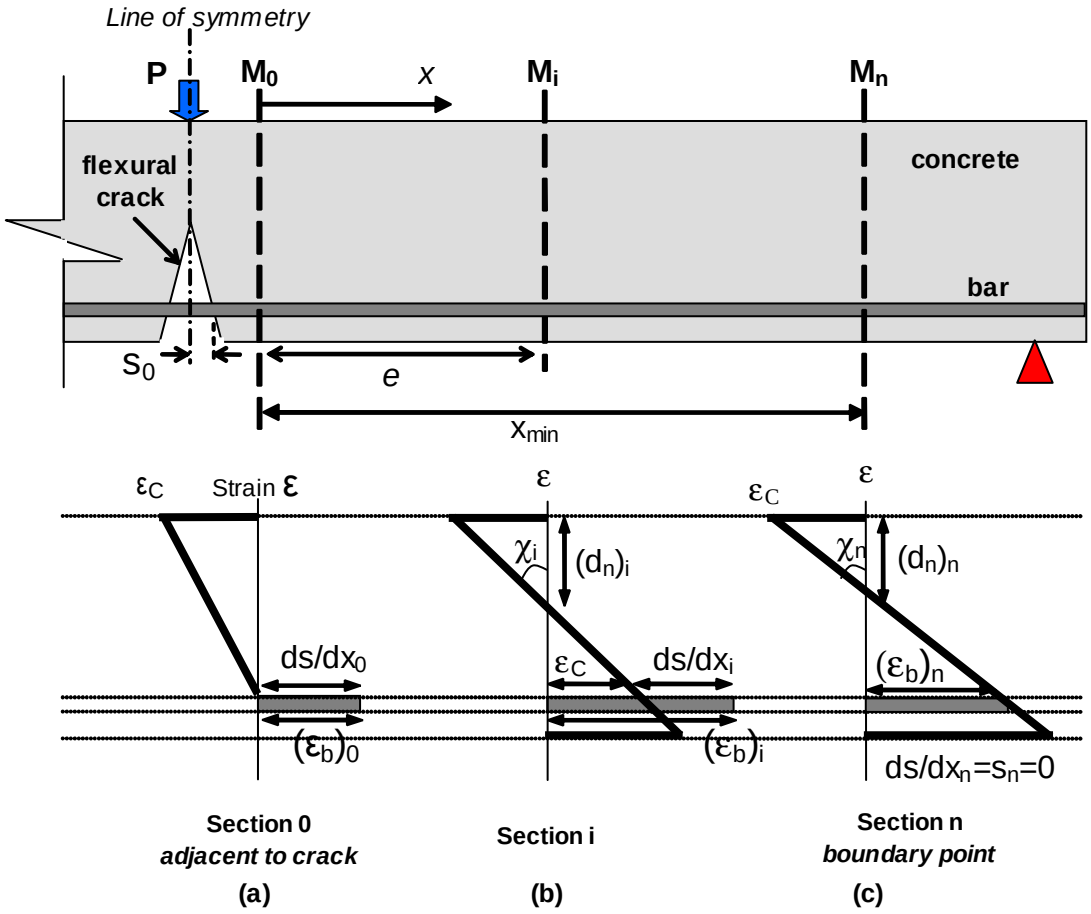

Figure 2.57 Single crack analysis of unplated RC beam

Based on Boundary Condition 7 in Section 2.5.1.1, a sectional analysis is performed at the section immediately adjacent to the crack as illustrated by section 0 in Figure 2.57a, where the bar strain is $(\varepsilon_b)_0$ and slip is s_0. Knowing that at this section adjacent to the crack there is zero tensile strain in the concrete, the concrete strain profile is idealised to vary linearly down the section with a zero tensile strain just above the reinforcement layer of the beam (Boundary Condition 7) as shown in Figure 2.57a. Sectional analysis is performed at section 0 for the $(\varepsilon_b)_0$ considered, where the curvature in the concrete χ_{PI} is iterated until from the stress and force distributions of the section, longitudinal equilibrium is obtained i.e. $F_c=F_b$. After obtaining the resultant force distribution at section 0, the moment at the section M_0, and hence, the moment distribution along the beam can be evaluated. It is worth noting that for section 0 which has zero concrete tensile strain, the slip-strain is equal to the bar strain i.e. $(ds/dx)_0=(\varepsilon_b)_0$.

The next section i.e. section *i* in Figure 2.57b, at a distance *e* away from the previous section is then analysed. The slip s_i at this section can be determined from integrating $(ds/dx)_{i-1}$ from the previous section over the segment *e* and adding it to the slip of the previous section s_{i-1} using Equation 2.27. Knowing the slip at this section, the bond force $(P_b)_i$ can be determined using a bond-slip relationship such as Figure 2.33. The force in the bar $(F_b)_i$ at section *i* can then be evaluated using Equation 2.57, where $(F_b)_{i-1}$ is the force in the bar at the previous section, section i-1. Hence at section *I* we now have M_i and F_i. A sectional analysis is performed at section *i* by iterating the two unknown: the neutral axis depth $(d_n)_i$ and the curvature in the concrete χ_i until horizontal and rotational equilibrium, F_i and M_i, (Section 2.5.1.1) are achieved. After the resultant strain profile of the section is obtained, i.e. χ_i and $(d_n)_i$ fixed in Figure 2.57b, the slip-strain at this section $(ds/dx)_i$ is evaluated as shown in Figure 2.57b.

$$(F_b)_i = (F_b)_{i-1} - (P_b)_i \qquad \textbf{Equation 2.57}$$

Segmental analysis is performed along the beam at fixed increments *e* at distance *x* away from crack 1 until a point is reached where either slip or slip-strain is equal to zero. This point, shown as section *n* in Figure 2.57c, at a distance x_{min} from the crack is the boundary of the partial interaction region where full interaction occurs at the bar/concrete interfaces i.e. $ds/dx=s=0$, and hence, Boundary Condition 6 given in Section 2.5.1.1 applies at this section. If slip-strain and slip are not both equal to zero at the boundary point, section *n*, this indicates that the slip s_0 guessed at the first crack is incorrect. The analysis is then repeated for different values of slip s_0 until the boundary condition is satisfied. It can be seen that both Boundary Conditions 6 and 7 have been used to find a solution, where Boundary

Condition 7 is used to analyse the sections adjacent to cracks, and Boundary Condition 6 is used to verify the slip s_0 guessed at crack 1.

After finding the correct slip s_o for the bar strain $(\varepsilon_b)_0$ considered at crack 1, the beam is checked for cracking using the procedure described in Section 2.4.1.4. If a new crack forms, this will largely affect the local deformation behaviour of the beam, and the Boundary Condition 6 in Section 2.5.1.1 no longer applies to the uncracked concrete segment between the cracks. Therefore the beam will need to be reanalysed using the analysis procedures described in the following Section.

2.5.1.3 MULTIPLE CRACK ANALYSIS

After locating the next subsequent crack, crack 2, from Section 2.5.1.2, the beam has to be reanalyzed for the same bar strain $(\varepsilon_b)_0$ considered, as the occurrence of a new crack changes the boundary condition, resulting in different stress and strain distributions along the beam. The slip between the concrete and the reinforcing bars will be different as the opening of the new crack reduces the width of the old crack. The procedure for the analysis between cracks is basically the same as the single crack analysis described previously, where a slip size s_0 is assumed at crack 1, and a segmental analysis is carried out starting from the section immediately adjacent to crack 1, as shown in Figure 2.58, using Boundary Condition 7 in Section 2.5.1.1. There is, however, a change in the boundary condition, Boundary Condition 6, used to verify s_0 as Boundary Condition 7 now applies at the new crack, crack *i*. Analysis is performed up to the section *i* immediately adjacent to the next crack. Based on Boundary Condition 7 in Section 2.5.1.1, at section *i*, there is zero tensile strain in the concrete, such that $\varepsilon_{ct} = 0$ at the level of reinforcement. If this condition of $\varepsilon_{ct} = 0$ is not satisfied at the second crack, the analysis is repeated for a different slip guess s_0 at crack 1 until $\varepsilon_{ct} = 0$ is achieved.

For beams with multiple cracks, the procedure described above is performed on each segment between two adjacent cracks, until no further cracking is found, that is the region between the last crack and the beam end is uncracked. Single crack analysis (Section 2.5.1.2) is then performed in this region, starting from the last crack, to evaluate the local deformation behaviour along rest of the beam. The beam is then checked for cracking, and the analysis procedure is repeated until no more cracking occurs along the beam.

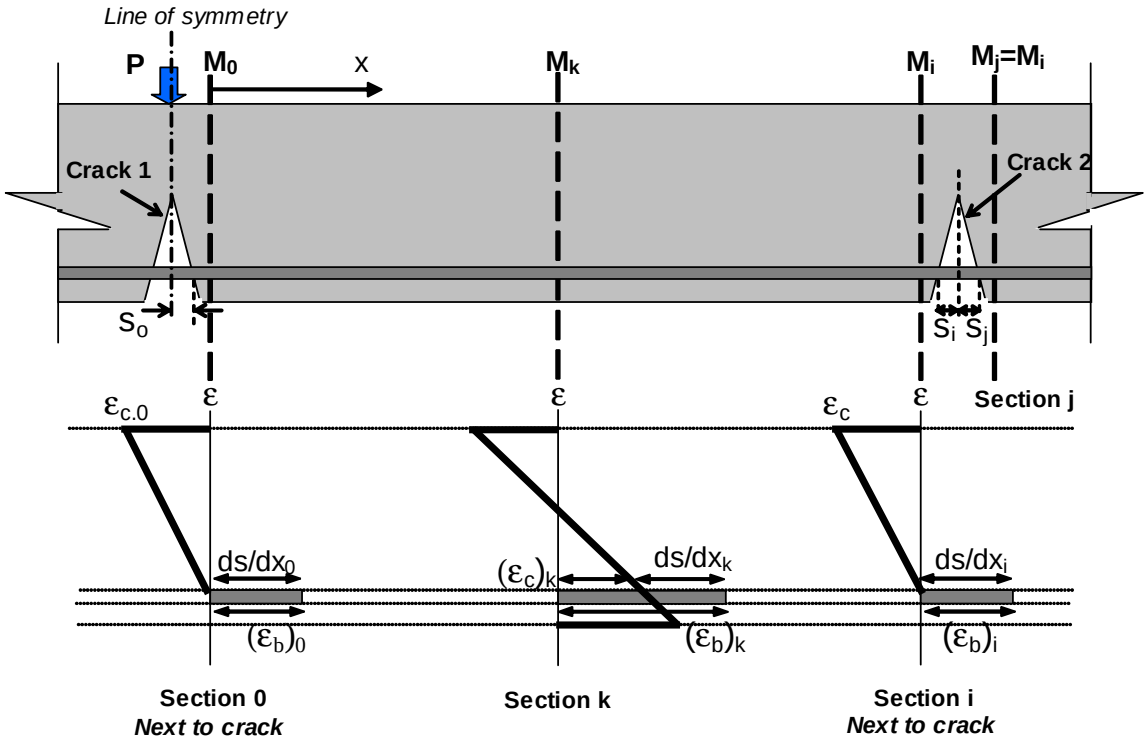

Figure 2.58 Analysis between adjacent cracks of unplated RC beams

2.5.2 PLATED REINFORCED CONCRETE BEAM (NEGLECTING INTERNAL BARS)

The initial partial interaction model developed for unplated RC beams is modified in this Section to analyse the intermediate crack (IC) debonding of RC beams with adhesively bonded external plates, and without internal reinforcing bars.

Consider the reinforced concrete beam illustrated in Figure 2.59. Before cracking, there is full interaction at the plate/concrete interface and the assumption of plane sections remaining plane applies as shown in Figure 2.59a, for the strain profile at section A-A prior to cracking with a curvature of χ_{FI}. When a flexural or flexural-shear crack forms and intercepts the plate, high longitudinal shear stress develops near the crack. As a result, debonding cracks occur and propagate from the root of the crack towards plate ends. Therefore there is slip s and hence slip-strain ds/dx between the plate and the adjacent concrete, and so the assumption of plane sections remaining plane is no longer valid. Partial interaction analysis will now apply and an illustration of the variation in strain down the section is given in Figure 2.59b. This behaviour is the same as that in an unplated RC beams, therefore the model developed in Section 2.5.1 for can be applied directly to plated flexural members to simulate IC debonding behaviour, where the plate is simply idealised as a layer of reinforcement

with the material properties the plate and a bond-slip model for the plate/concrete interface inputted into the simulation.

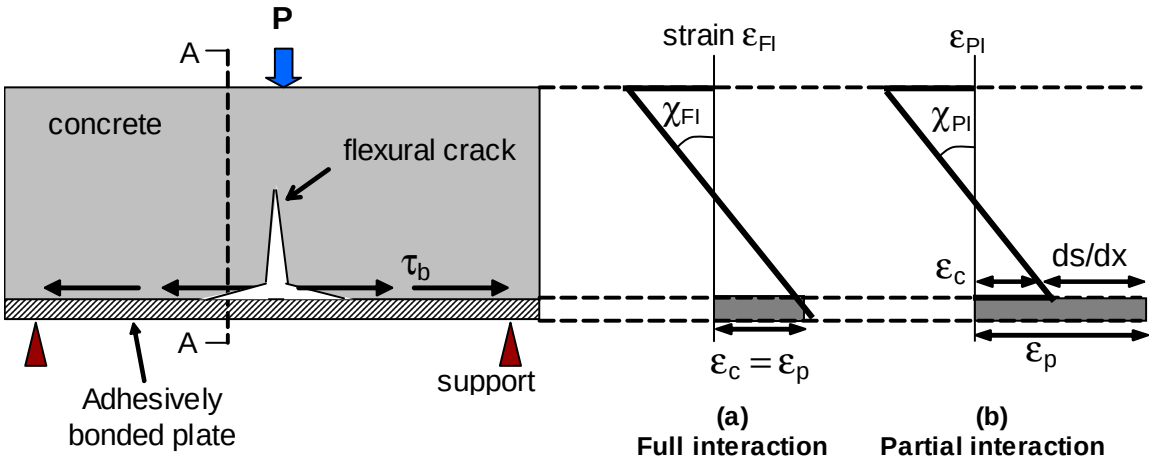

Figure 2.59 (a) Full interaction and (b) partial interaction of adhesively plated beam

Example of applications of the initial partial interaction approach on plated RC members without reinforcing bars can be found in Liu et al. 2004 (refer to Appendix A.2).

2.5.3 Disadvantage of Initial PI Approach

Within the cracked region of an RC member, the area around a crack is disturbed, that is the concrete strain does not vary linearly due to the crack. The behaviour of the disturbed regions is extremely complex and difficult to analyse, therefore in the initial partial interaction model, this region was ignored, such that linear variation in concrete strain applies immediately adjacent to the crack. The local slip and strain behaviour of RC specimens obtained from the initial approach (Liu et al. 2004) was found to be similar to those reported by other researchers (Niu & Wu 2001a,b; Rebentrost 2003). This shows that neglecting the disturbed regions only has minor effects on the local deformation behaviour in the uncracked concrete away from the cracks, especially when small load is applied. However, the magnitude of the moment for a given load can be significantly different to that obtained from analyses of a cracked section, due to the linear strain profile assumed at the section immediately adjacent to a crack. To properly model the cracked region of an RC beam, it is necessary to analyse the disturbed region adjacent to the cracked sections as it is at the cracks where the strains in the plate and the bars are at their maximum; therefore, the cracked sections will govern the magnitudes of the moment and forces in the specimen. This led to the development of the modified PI model discussed in the following Section.

2.6 MODIFIED PARTIAL INTERACTION APPROACH FOR FLEXURAL MEMBERS

Modifications were made to the initial partial interaction model proposed in Section 2.5 to overcome the shortfalls of the model discussed in Section 2.5.3. This modified approach takes into account the disturbed regions around a crack by identifying the disturbed and undisturbed regions. The partial interaction approach described previously in Section 2.5 still applies to the undisturbed region, but with different boundary conditions, while a new disturbed region analysis is performed at a crack. The model also allows for the widening of the disturbed regions around cracks as the applied load increases. The fundamental behaviour of an unplated RC beam with a single layer of reinforcing bars previously discussed in Section 2.5.1.1 still applies to the modified model, but with a change in the boundary conditions to account for the disturbed region around a crack.

In developing the model, unplated reinforced concrete beams with single and multiple reinforcing layers were studied initially, and the details are covered in the journal paper presented in Section 2.6.1. Also included in the paper is the local deformation behaviour of the RC beams obtained from the model. Since an externally bonded plate can be considered as an additional layer of reinforcement with a different bond-slip behaviour at the interface, the modified model is also applicable to plated beams with and without reinforcing bars. A description of the proposed partial interaction model for plated members and discussions on the local deformation behaviour of these members are presented in the journal paper included in Section 2.6.2. A flow chart of the modelling steps of the fortran code developed for the modified partial interaction model can be found in Appendix A.3. In Section 2.6.3, details on the proposed partial interaction model that are not covered in the journal papers in Sections 2.6.1 and 2.6.2, such as the development of the governing equations based on equilibrium and compatibility of plated RC beams, are presented.

2.6.1 JOURNAL PAPER: THE GRADUAL FORMATION OF HINGES THROUGHOUT REINFORCED CONCRETE BEAMS

The journal paper presented this Section includes a description of the modified partial interaction model developed for unplated reinforced concrete beams with multiple reinforcing layers, and in particular, the identification of the governing boundary conditions. Using the proposed model, analyses were performed to study the local deformation behaviour of unplated RC beams with the results presented in the paper. A flow chart of the modelling steps of the fortran code developed for the modified partial interaction model can be found in Appendix A.3.

THE GRADUAL FORMATION OF HINGES THROUGHOUT REINFORCED CONCRETE BEAMS

Shortened title: GRADUAL FORMATION OF HINGES THROUGHOUT RC BEAMS

*Oehlers, D.J., **Liu, I.S.T., and ***Seracino, R.

Corresponding author
*Dr. D.J. Oehlers
Associate Professor
School of Civil and Environmental Engineering
The University of Adelaide
Adelaide
SA5005
AUSTRALIA
Tel. 61 8 8303 5451
Fax 61 8 8303 4359
email doehlers@civeng.adelaide.edu.au

**Ms. I.S.T. Liu
Postgraduate student
School of Civil and Environmental Engineering
The University of Adelaide

***Dr. R. Seracino
Senior Lecturer
School of Civil and Environmental Engineering
The University of Adelaide

Mechanics Based Design of Structures and Machines – Accepted for publications September 2005

Statement of Authorship

THE GRADUAL FORMATION OF HINGES THROUGHOUT REINFORCED CONCRETE BEAMS

Mechanics Based Design of Structures and Machines – Accepted for publications September 2005

LIU, I.S.T. (Candidate)

Performed all analyses, interpreted data and co-wrote manuscript.

Signed _____ Date _____

OEHLERS, D.J.

Supervised development of work, co-wrote manuscript and acted as corresponding author.

Signed _____ Date _____

SERACINO, R.

Supervised development of work and manuscript review.

Signed _____ Date _____

Oehlers, D.J., Liu, I.S.T., and Seracino, R. (2005)
The gradual formation of hinges throughout reinforced contrete beams
Mechanics Based Design of Structures and Machines, accepted for publications September 2005

NOTE: This publication is included on pages 95 - 114 in the print copy of the thesis held in the University of Adelaide Library.

2.6.2 JOURNAL PAPER: PARTIAL INTERACTION NUMERICAL SIMULATION OF HINGES IN FRP PLATED REINFORCED CONCRETE BEAMS

The journal paper attached in this Section presents the modified partial interaction model developed for plated reinforced concrete beams with and without internal bars. The paper also contains results and discussions on the local deformation behaviour of plated RC beams obtained from the proposed model. Examples of application of the modified partial interaction approach on plated RC members with a layer of reinforcing bars can also be found in Liu et al. 2005 (refer to Appendix A.4). A flow chart of the modelling steps of the fortran code developed for the modified partial interaction model can be found in Appendix A.3.

PARTIAL INTERACTION NUMERICAL SIMULATION OF HINGES IN FRP PLATED REINFORCED CONCRETE BEAMS

*Liu, I.S.T., **Oehlers, D.J., and ***Seracino, R.

*Ms. I.S.T. Liu
Postgraduate student
School of Civil and Environmental Engineering
The University of Adelaide

Corresponding author
**Dr. D.J. Oehlers
Associate Professor
School of Civil and Environmental Engineering
The University of Adelaide
Adelaide
SA5005
AUSTRALIA
Tel. 61 8 8303 5451
Fax 61 8 8303 4359
Email: doehlers@civeng.adelaide.edu.au

***Dr. R. Seracino
Senior Lecturer
School of Civil and Environmental Engineering
The University of Adelaide

Submitted to Computers and Structures 22 March 05

Statement of Authorship

PARTIAL INTERACTION NUMERICAL SIMULATION OF HINGES IN FRP PLATED REINFORCED CONCRETE BEAMS

Submitted to Computers and Structures 22 March 05

LIU, I.S.T. (Candidate)

Performed all analyses, interpreted data and wrote manuscript.

Signed _____ Date _____

OEHLERS, D.J.

Supervised development of work and manuscript evaluation, and acted as corresponding author.

Signed _____ Date _____

SERACINO, R.

Supervised development of work and manuscript review.

Signed _____ Date _____

PARTIAL INTERACTION NUMERICAL SIMULATION OF HINGES IN FRP PLATED REINFORCED CONCRETE BEAMS

Liu, I.S.T., Oehlers, D.J., and Seracino, R.
School of Civil and Environmental Engineering, The University of Adelaide

ABSTRACT

Reinforced concrete (RC) structures are commonly retrofitted for strength or stiffness using adhesively bonded steel or fibre reinforced polymer (FRP) plates as the technique is unobtrusive and inexpensive. However, FRP plated RC beams behave differently from unplated beams as FRP is a brittle material. Furthermore, FRP plates usually debond before the concrete crushes. Hence, the established RC beam design techniques for ductility, such as the neutral axis depth factor for moment redistribution and the plastic hinge concept for the rotation capacity, cannot be used directly requiring an alternative approach. A partial interaction numerical model has been developed that simulates the behaviour of plated RC hinges and, thereby, quantifies both the rotation of a plated RC hinges as well as the plate debonding resistance required in developing design rules for both strength and ductility.

Keywords: Retrofitting; reinforced concrete beams; externally bonded plates; IC debonding; partial interaction; slip

NOMENCLATURE

ε	strain
ε_{crack}	concrete tensile capacity
ε_{ct}	peak concrete tensile strain
D	disturbed region
dM/dx	moment gradient
d_n	depth of neutral axis
ds/dx	slip strain
E_p	Young's moduls of plate
F	force; force profile
f_{cm}	maximum concrete compressive stress
$f_{p.frac}$	plate fracture stress
h	depth of beam
k_2	strain ratio
L	shear span
M	moment
s	slip
s_f	ultimate slip
UD	undisturbed region
w	crack width
x	distance from maximum moment
x_{dis}	length of disturbed region
φ	curvature
σ	stress

τ_b interface shear stress/bond stress

Subscripts

b bar layer
c concrete
d at disturbed region
l at left crack face
p plate layer
r at right crack face

1. INTRODUCTION

There is much good research on recognising and quantifying the four major debonding mechanisms in plated structures that has allowed guidelines[1-4] to be established for strengthening or stiffening reinforced concrete structures. Plate debonding can occur through flexural deformations of a beam and also through vertical shear deformations of a beam. The most important debonding mode for flexural deformation is intermediate crack (IC) debonding and it is the effect of this mechanism of debonding on the behaviour of hinges which is the subject of this paper.

An example of the IC debonding mechanism in a reinforced concrete slab with tension face externally bonded (EB) plates is shown in Fig.1. Wherever a flexural crack or flexural/shear crack (in fact any type of intermediate crack) intercepts a plate, interface cracks occur that propagate away from the intermediate crack and often in both directions. These IC interface cracks eventually join up so that the plate debonds between adjacent cracks and a succession of plate debonding between intermediate cracks can reduce the strains in the plate which signifies debonding even though the plate ends may still be anchored. Although IC debonding is the most common failure mode [5-8], there is a lack of research into this debonding behaviour. A few researchers such as Teng [3], Niu & Wu [5-7], Aiello & Ombres [9] have developed models for IC debonding, but most only determine the strength at which debonding occurs and do not attempt to model the IC debonding behaviour as it propagates along the beam. In order to simulate the IC debonding behaviour accurately, discrete cracking needs to be modelled taking into account the slip at the interfaces [8].

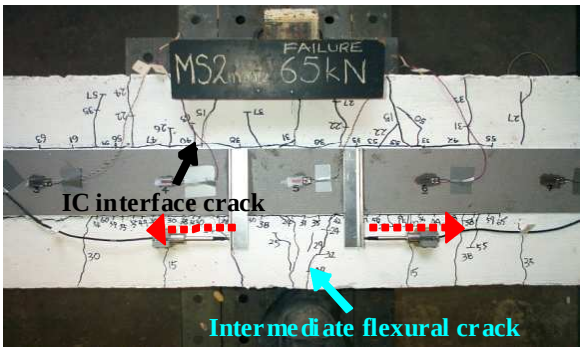

Fig. 1 Intermediate crack (IC) debonding

The interface shear material characteristics associated with propagation of the IC interface crack in Fig.1 is often assumed to have the form shown in Fig.2 where the slip s is zero when the interface shear stress τ_b is zero. The shear stress increases with slip to a peak value of $\tau_{b.max}$ at slip s_{max} after which the shear stress diminishes to zero at a slip of s_f so that for slips greater than s_f complete debonding is assumed to have occurred. The τ_b/s characteristic can be considered as a material

characteristic, it is usually measured directly in pull-tests[3] and is often idealised as bi-linear as shown. It is this material characteristic that governs the propagation of the IC intermediate crack, and, hence the IC debonding mechanism and its effect on ductility. The shear/slip material characteristic in Fig.2 that occurs across a plate/concrete interface signifies a partial interaction problem where there is a step-change in the strain profile at the interface. This has been known to occur in composite steel and concrete beams [10-11] where the mechanical shear connectors slip and the problem was first solved in 1951 [10]. However the boundary conditions of the IC partial interaction debonding mechanism illustrated in Fig.3 will be shown in this paper to be totally different from that which occurs in composite steel and concrete beams.

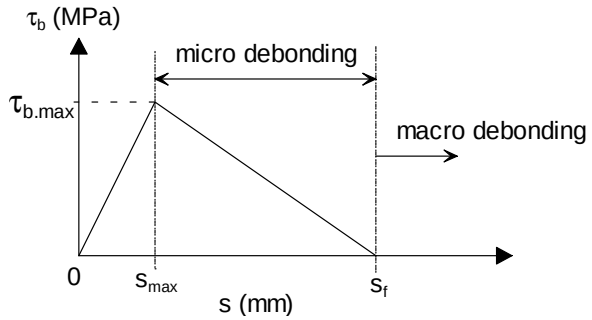

Fig. 2 Bond-slip model for plate/concrete interface

The ductility or rotational capacity of reinforced concrete beams is a complex problem which was first studied in depth in the 1960s through tests [12-13] and through the introduction of the finite hinge concept [14-16]. More recently in the eighties and nineties, the hinge region of unplated reinforced concrete beams has been numerically simulated by considering the blocks between flexural cracks as discrete and independent elements [17-19]. The discrete block approach has now been taken a step further [20] by allowing for the interaction between adjacent blocks and the gradual formation of the hinge along the beam as the applied load increases. The rotational capacity of unplated reinforced concrete beams is generally limited by concrete crushing and it is on this basis of concrete crushing that ductility rules for unplated RC beam, such as for moment redistribution are based. There is an additional complexity in plated beams because the plates generally debond prior to the concrete crushing and over a very wide range of debonding strains that depend on: the plate material properties such as the wide range of FRP plate materials as well as steel or aluminium plates; the geometry such as plate width and thickness; and the type of plate such as externally bonded plates or near surface mounted plates. In this paper, the numerical model for simulating the formation of hinges in unplated beams [20] is first further adapted to allow for the gradual debonding of plates; this partial interaction numerical model is then used to illustrate the generic behaviour of plated RC hinges, and, in particular the interaction between the partial interaction reinforcing bars and the partial interaction hinges.

2. PARTIAL INTERACTION SIMULATION OF A HINGE

When a flexural crack forms intercepting the bars and the plate, there is theoretically an infinite strain in the reinforcement which cannot occur. This strain is relieved by slip between the reinforcement and the concrete which is shown as horizontal interface cracks in Fig.1. As the strain in the bars and in the plate are different, the slip at each interface will differ. Where slip occurs, the strain in the reinforcement and the adjacent concrete will no longer be the same, and the difference is defined as the slip-strain ds/dx as illustrated in Fig.3 in the strain profile at (A). Therefore in the regions along the

beam where there is slip, there is partial interaction and this is referred to as the *partial interaction hinge*. The partial interaction model which was developed to analyse the hinge of an unplated reinforced concrete beam [20] has now been modified to allow for beams with externally bonded plates in order to model the IC debonding behaviour of plated RC beams. The external plate can simply be considered as another layer of reinforcing bars but with a different bond characteristic and, hence, it can be easily incorporated into the original partial interaction model [20].

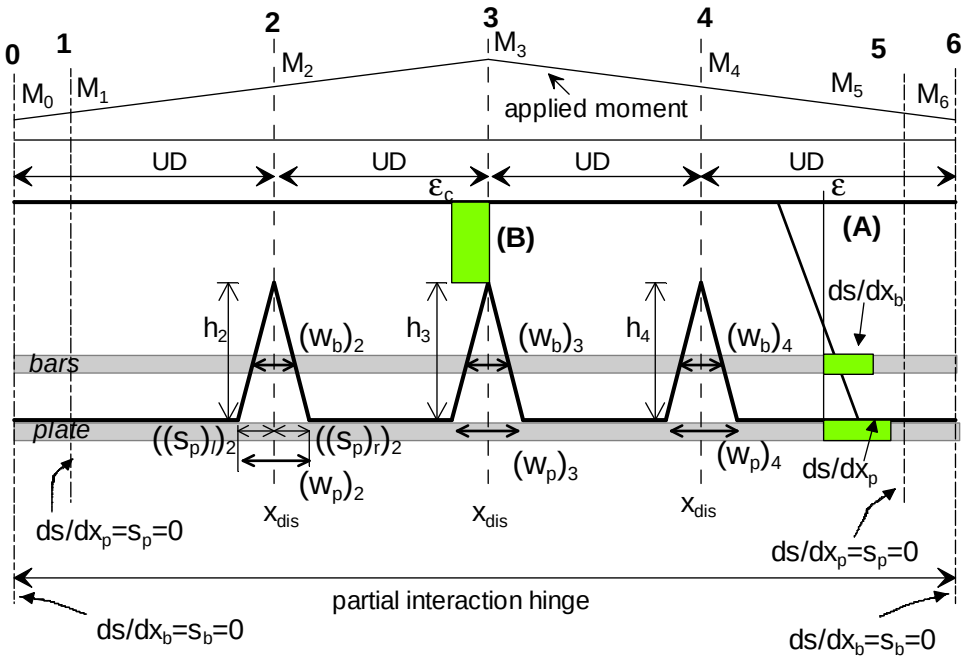

Fig. 3 Partial interaction hinge boundary conditions

The analysis involves firstly identifying the cracked region of the beam shown as the *partial interaction hinge* in Fig.3. This is the region adjacent to the position of maximum moment where slip occurs at the bar/concrete and plate/concrete interface, such that partial interaction takes place in this region and so the partial interaction model applies here. Outside this region where there is no slip at the interfaces, standard full interaction analyses apply. The model developed [20-21] allows for the *disturbed* region around a crack of width x_{dis} in Fig.3 where the concrete strain does not vary linearly through the section. In areas away from the cracks where concrete is uncracked, the region is *undisturbed*, UD in Fig.3, where it can be assumed that there is a linear variation in concrete strain along the cross-section, but as there is slip at the bar/concrete and plate/concrete interfaces, partial interaction analysis applies in this undisturbed region. The disturbed region around a crack forms a boundary for the partial interaction analysis of the undisturbed region, so in order to analyse the partial interaction hinge, the disturbed regions around the cracks need to be solved to determine the moment distribution along the beam.

In the initial stages of loading, when the stress in the concrete is low, the length of the disturbed region x_{dis} in Fig.3 surrounding the flexural crack can be assumed to be very small [20-21] in comparison to the length of the undisturbed region; that is the disturbed region can be assumed to be of zero length and just a section through the flexural crack. To determine the *boundary moment* at these cracked sections it is necessary to determine the crack height h based on elastic analysis of the second moment of area of the cracked section in which the tensile strength of the concrete is assumed to be zero. Curvature in the uncracked concrete above the crack is neglected and a compressive strain adjacent to the crack tip is allowed as illustrated in Fig.3 at (B). In cases when no solutions can be

found for the undisturbed region, this signifies a widening of the disturbed region and the new length of the disturbed region is accounted for in the analysis [20-21].

To perform the partial interaction analysis in the undisturbed region, segmental analyses are applied at fixed increments along the beam and the procedures are iterative until all the boundary conditions along the beam are satisfied. Therefore, the crucial part of the modelling is to identify the boundary conditions. The boundary conditions consist of the following:

1. For each layer of reinforcement there is a position in the beam beyond which there is no slip at the concrete/reinforcement interface, that is there is full-interaction at the extremities of the partial-interaction region where ds/dx = s = 0 in Fig.3. This position is not assumed to be the same at each reinforcement layer as shown at Sections *5* and *6* where the full-interaction zone at the plate and the bar is shown to occur at different positions. In cases where there is no full interaction along the beam i.e. slip has propagated to end of beam, the boundary condition becomes that at the beam end where there is zero strain in the beam.
2. At each crack, the applied moment M and crack height h are known from the analysis of the *boundary moments*, in the disturbed regions as previously described.
3. It is also assumed, for the case when there are multi-layers of tension reinforcement, that the crack faces act as rigid bodies so that there is a linear variation in crack width from the crack tip. When the crack widens and slip increases at the plate/concrete interface, the crack width adjacent to the plate w_p is equal to the algebraic sum of the slip of the left crack face s_l and the slip of the right crack face s_r as shown in Fig.3, that is $w_p = s_l - s_r$. The same applies to the bar layers. The variation in crack widths at each reinforcement layer being linear from the crack tip.

3. SIMULATION OF INITIALLY UNCRACKED BEAM

To illustrate the numerical model, let us consider an initially uncracked reinforced concrete beam with a single layer of reinforcing bars and an externally bonded plate on the tension face that is subjected to a point load at midspan as shown in Fig.4. A flexural crack first forms at the position of maximum moment, which is in the disturbed region and which is assumed to be of zero length upon initial loading. The standard shooting method[11] of analysis in the undisturbed region is depicted in Figs.4 (c) to (e). The analysis will be described in terms of plate strain so that the distribution of moment along the hinge is known for a particular bar strain, alternatively other forms such as crack width control can be also used.

Let the strain in the plate at the disturbed region be fixed at $(\varepsilon_p)_d$ as shown in Fig.4(b) and the strain in the bar layer in the disturbed region be $(\varepsilon_b)_d = k_2(\varepsilon_p)_d$ so that the unknown is k_2. Hence guess or assume a value for k_2 so that $(\varepsilon_p)_d$ and $(\varepsilon_b)_d$ and, therefore, the bar forces are now known. The moment in the disturbed region M_{max} can now be derived from the *boundary moment* at the flexural crack which fixes the distribution of moment in Fig.4(a) for a fixed value of $(\varepsilon_p)_d$. At the position of maximum moment and only for the case of a line of symmetry, the magnitude of the crack face slips are the same for the left and right faces, that is $(s_p)_l = (s_p)_r$ and $(s_b)_l = (s_b)_r$, so that for this case only there is a linear variation in the crack face slips $(s_p)_d$ and $(s_b)_d$ as shown in Fig.4(b). As the slips at the concrete/plate and concrete/bar interfaces are unknown, we need to guess the crack face slip at one of the interfaces, eg. $(s_p)_d$ and from the linear variation of crack face slip at line of symmetry, the slip at the other interface can be determined in terms of $(s_p)_d$.

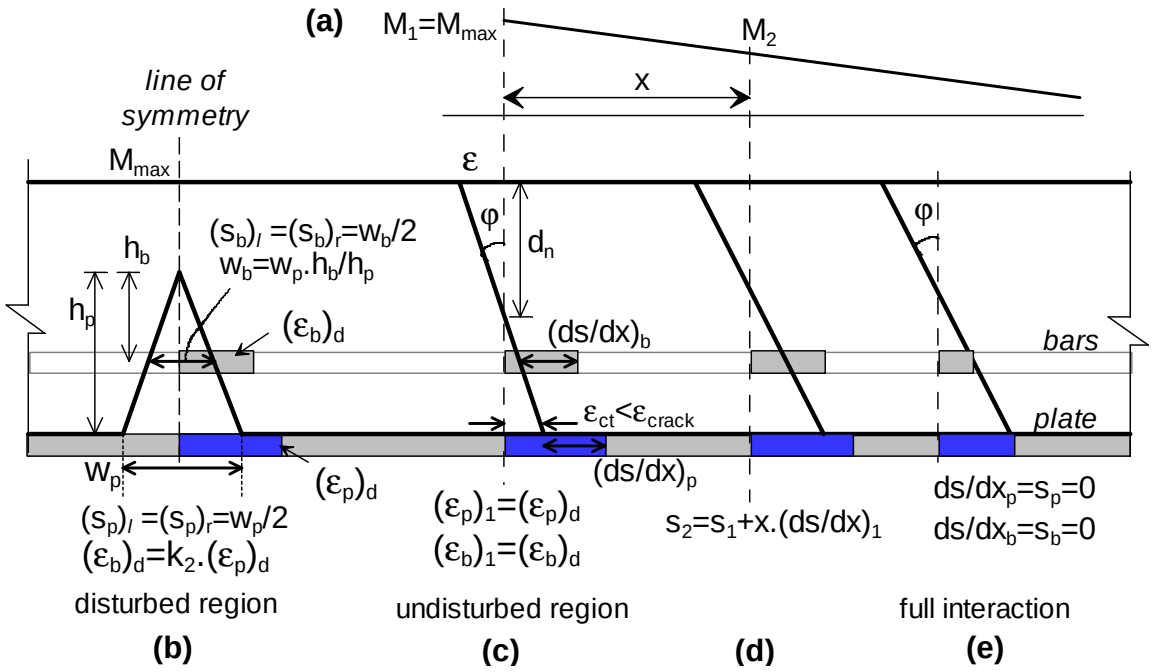

Fig. 4 Standard undisturbed region analysis of single crack beam

Now consider the strain profile in the undisturbed region immediately adjacent to the disturbed region, which is shown in Fig.4(c), so that the plate and bar strains are the same as in the disturbed region. As the longitudinal force in the section (from both $(\varepsilon_p)_d$ and $(\varepsilon_b)_d$) and the applied moment M_1 are known, curvature φ and depth of the neutral axis d_n can be iterated until both rotational and longitudinal equilibrium is achieved. This gives the strain profile of the section, from which the slip strains ds/dx at the concrete/plate and concrete/bar interfaces can be evaluated as shown in Fig.4(c). Sectional analyses are carried out along the beam at fixed increments of distance x. Integrating the slip-strains between sections such as at (c) and (d) gives the change in slip between sections (c) and (d). Knowing the slip distribution and the interface bond material characteristics gives the change in force in the plate and in the bar and, hence, the longitudinal force. As both the longitudinal force and moment at section (d) are known, the standard iterative analysis depicted at (c) can be applied at (d) and the procedure repeated along the undisturbed region. As the crack face slip $(s_p)_d$ and the strain layer relationship k_2 were both guessed at the start two boundary conditions are required to iterate towards a solution. These boundary conditions are shown at Sections *5* and *6* in Fig.3, that is at the point of full-interaction ds/dx = s = 0 at each interface. Once a solution is found, the results of the analyses can be used to determine if a further flexural crack has occurred and where it has occurred within the partial-interaction hinge region.

4. SIMULATION OF PREVIOUSLY CRACKED BEAM

The generic analysis procedure is further illustrated in Fig.5 for half of a hinge where the first crack at (a) is at a line of symmetry. The analysis is shown for the case where three flexural cracks have formed at (a), (b) and (c), and for a plated beam with a single layer of reinforcing bars. The analysis is applied under bar strain control so that the distribution of moment along the beam is known as shown in (e). In the initial stage of analysis, where the applied load is small, the length of the disturbed region is assumed to be negligible i.e. $x_{dis} = 0$. The flexural cracks divide the beam into bays as shown. The

analysis between flexural cracks (a) and (b) that is in bay a-b is shown in (f), that in bay b-c in (g) and that in bay c-d in (h).

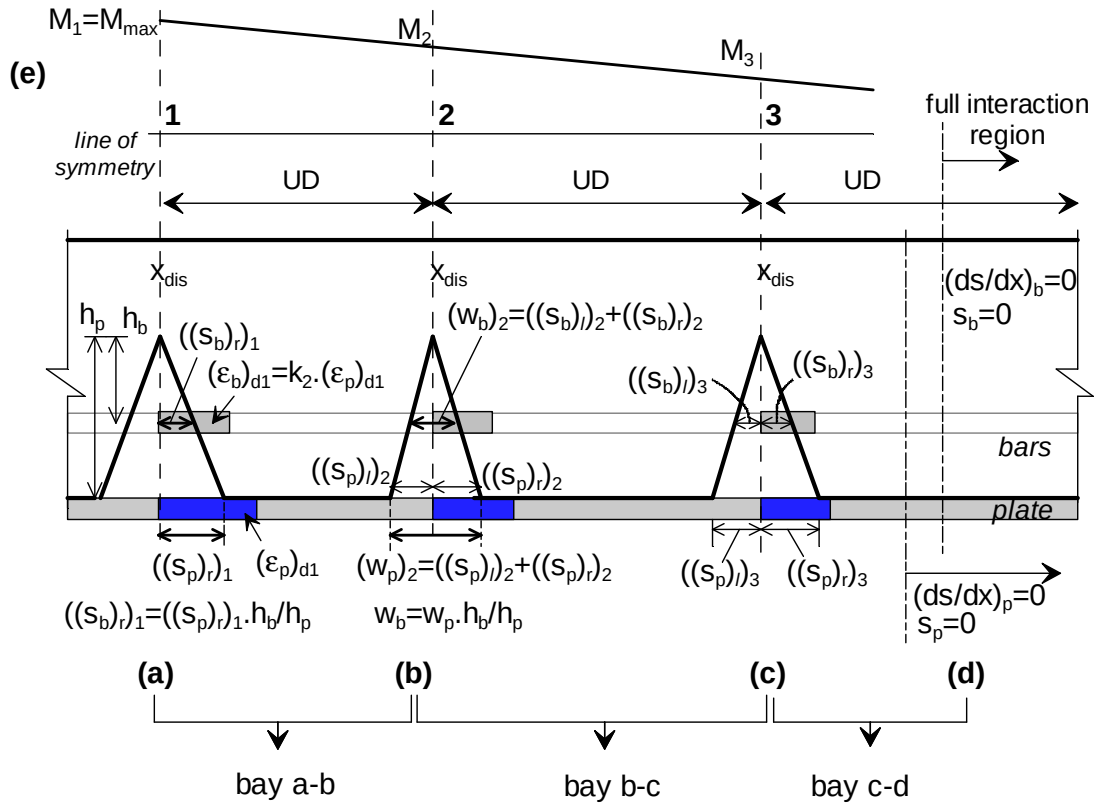

- Fix $(\varepsilon_p)_{d1}$
- $(\varepsilon_b)_{d1}=k_2(\varepsilon_p)_{d1}$
- guess k_2
- calculate M_1
- guess $((s_p)_r)_1$
- find $((s_b)_r)_1$ from linear variation of slip
- apply "shooting method" along bay 1
- iterate $((s_p)_r)_1$ until M_2 achieved
- evaluate $((s_p)_l)_2$ &$((s_b)_l)_2$
- evaluate $(\varepsilon_p)_{d2}$ & $(\varepsilon_b)_{d2}$

(f)

- guess $((s_p)_r)_2$
- find $((s_b)_r)_2$ from linear variation of crack width
- apply "shooting method" along bay 2
- iterate $((s_p)_r)_2$ until M_3 achieved
- evaluate $((s_p)_l)_3$&$((s_b)_l)_3$
- evaluate $(\varepsilon_p)_{d3}$&$(\varepsilon_b)_{d3}$

(g)

- guess $((s_p)_r)_3$
- find $((s_b)_r)_3$ from linear variation of crack width
- apply "shooting method" along bay 3
- iterate $((s_p)_r)_3$ until $(ds/dx)_p=s_p=0$
- if $(ds/dx)_b\neq 0$ at $s_b=0$ or vice versa, reanalyse beam changing k_2 at (f)

(h)

Fig. 5 Standard undisturbed region analysis of beams with multiple cracks

In cases where there is no point of full-interaction along the beam, the boundary condition will become that at the end of the beam, where for a simply supported beam the strain is zero at all reinforcing layers i.e. $((s_p)_r)_1$ and k_2 are iterated until $\varepsilon_p = \varepsilon_b = 0$ at the beam end. If w_b at any of the disturbed regions tends to zero because $(s_b)_l + (s_b)_r = 0$ then this signifies crack closure so that this boundary or disturbed region disappears and the analysis is then repeated without this boundary condition.

If it is found that upon further loading, the peak tensile strain ε_{ct} occurs immediately adjacent to a crack, and when it exceeds the concrete tensile capacity ε_{crack}, this signifies that the length of the disturbed region x_{dis} is now significant and can no longer be assumed to be of zero length. This means that the beam needs to be reanalysed for the same $(\varepsilon_p)_d$ considered, but taking into account the new length of the disturbed region x_{dis}. The analysis of the disturbed region at a distance x from the flexural crack is shown in Fig.6(b) at Section 2. It is assumed that within the disturbed region compressive stress blocks remain rectangular, the bar and the plate bond stresses are zero, and that the plate and the bar strains are much larger than the adjacent concrete strains. Therefore, the forces in the plate and bar remain unchanged over the disturbed region so that at Section 2 the forces are known as well as the boundary moment M_2, hence α_2 and $(d_n)_2$ can be determined. The extent of the disturbed region x_{dis} is increased until an adjacent undisturbed analysis as shown in Fig.6(c) gives $\varepsilon_{ct} < \varepsilon_{crack}$ from which the standard undisturbed analysis proceeds. Full details of the numerical approach are given elsewhere [20-21].

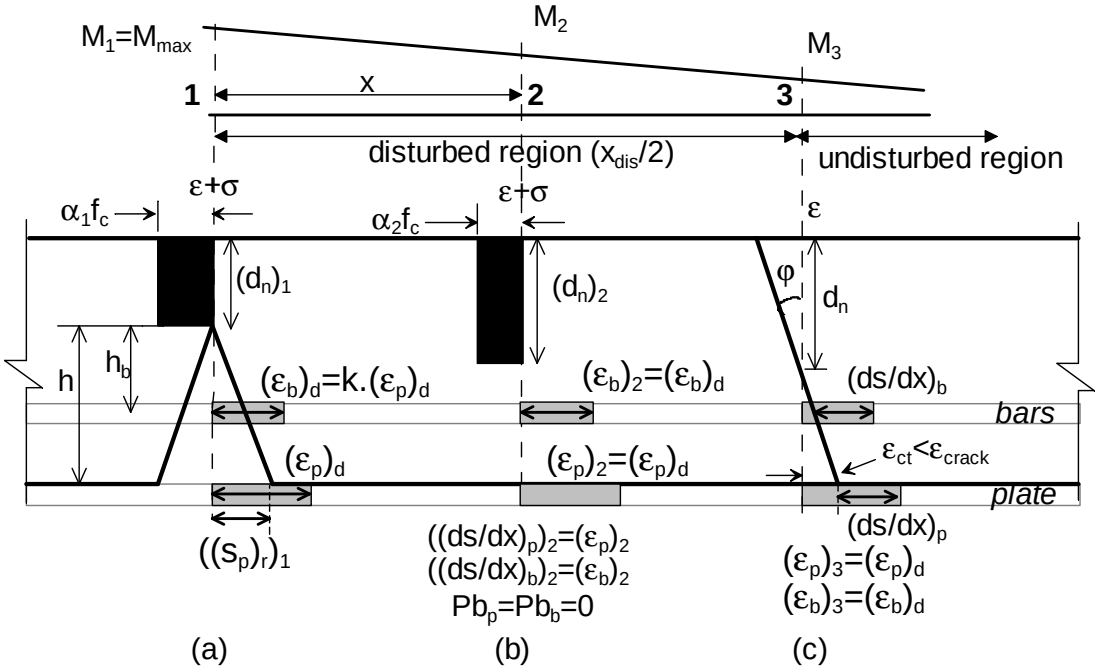

Fig. 6 Disturbed region analysis

5. PARTIAL-INTERACTION HINGE BEHAVIOUR OF PLATED CONCRETE BEAM

To illustrate the application of the numerical model and to study the debonding behaviour of plated beams, the partial interaction analysis is applied to a precracked concrete beam that is plated with carbon fibre reinforced polymer (CFRP) plates on the tension face, and where the cracks are evenly spaced at 100mm throughout the beam. The beam is 220mm wide and 240mm deep, with a 50mm wide and 1.2mm thick CFRP plate adhesively bonded on the tension face along the full length of the beam. The plate has a fracture stress $f_{p.frac}$ of 3050MPa and a Young's modulus E_p of 144GPa. The bilinear bond-slip model shown in Fig.2 was used in the analysis where a maximum bond stress τ_{bmax} of 6MPa was used, with a corresponding slip s_{max} of 0.02 and an ultimate slip of s_f = 0.2. A point load was applied at midspan of the beam, where shear spans L of 250mm and 1000mm were considered. As the beam is symmetrically loaded, only half of the beam will be considered in the following

analysis. This beam does not have reinforcing bars, which is considered in the following section, and, hence is analogous to a plated masonry beam where the crack positions are at the mortar joints.

5.1 Single Crack

5.1.1 Debonding Behaviour

Let us first consider a beam with a shear span L of 250mm, that is the distance from the position of maximum moment to the point of contraflexure is 250mm, and where a single crack, crack 1, has formed at midspan. The variation in the slip, slip-strain and plate strain along the beam are shown in Figs. 7-9 for increasing plate slip $(s_p)_d$ at crack 1. It can be seen in Figs.7 and 8 that both s_p and ds/dx decrease away from the crack.

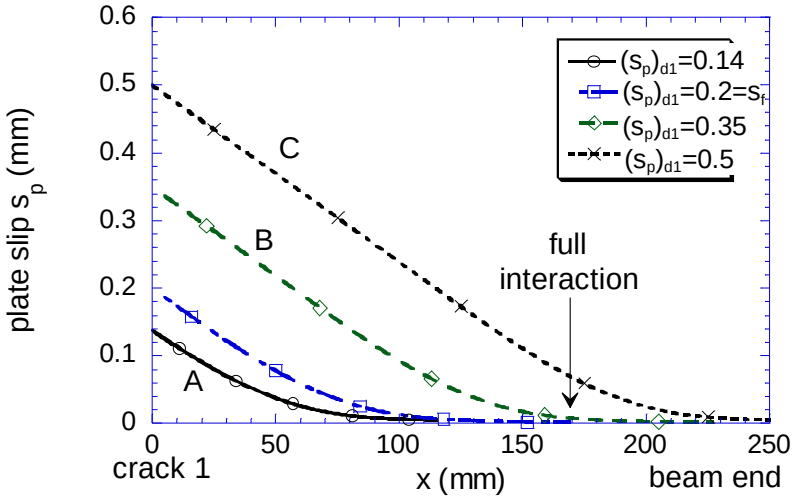

Fig. 7 Slip s distribution for single crack plated beam without bars [L=250mm]

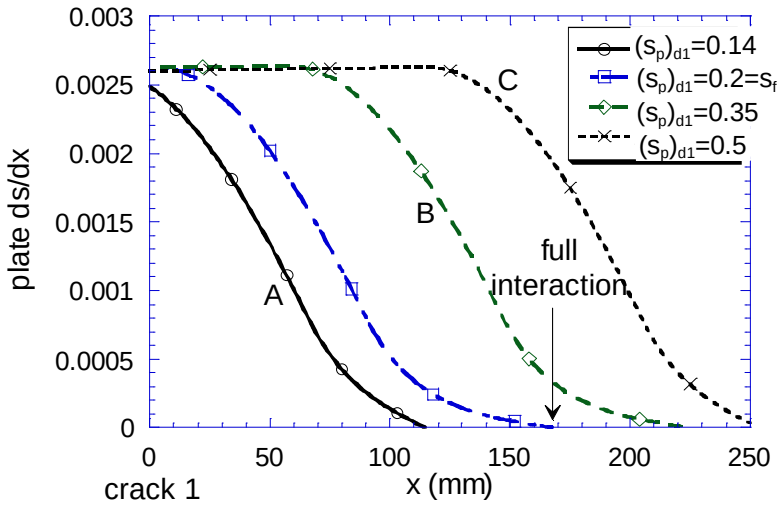

Fig. 8 Slip strain ds/dx distribution for single crack plated beam without bars [L=250mm]

When $(s_p)_d < s_f$ e.g. $(s_p)_{d1}$=0.14 in Fig.9, strain in the plate reduces towards the plate end. When $(s_p)_d > s_f$ there is zero bond at the plate/concrete interface in the region where $s>s_f$, and so the plate strains remain constant along the beam until the slip reduces to less than s_f e.g. line B in Fig.9. At low $(s_p)_d$, e.g. line A, full-interaction (ds/dx=s=0) is achieved before reaching the end of the beam. As $(s_p)_d$

increases, this point of full interaction propagates towards the beam end and when there is no point of full-interaction along the beam, debonding failure occurs e.g. line C.

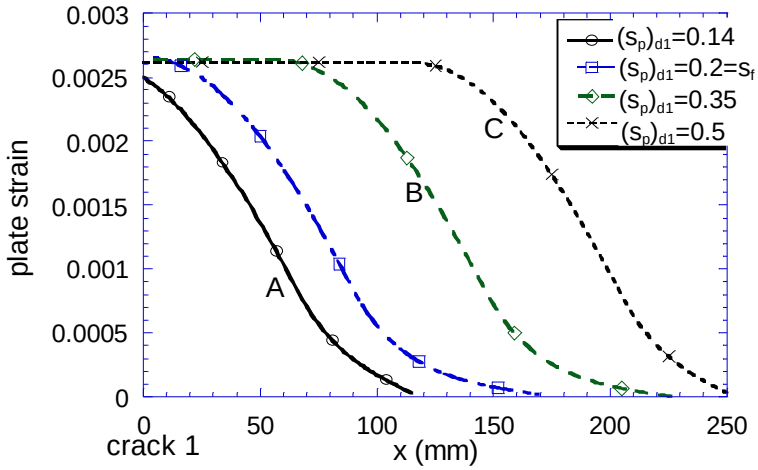

Fig. 9 Plate strain ε_p distribution for single crack plated beam without bars [L=250mm]

A maximum strain of 0.0027 in the plate is reached when slip reaches s_f at the point of maximum moment at x=0. As slip further increases to above s_f, the strain in the plate remains almost constant until debonding failure occurs due to slip propagating to the plate end e.g. line C. From the analysis, it can be seen that the debonding behaviour of a single crack plated beam is similar to that of a pull test, where rapid debonding failure occurs immediately after the maximum plate strain is reached.

5.1.2 Negative Curvature

Figures 10 and 11 show the distribution of the peak concrete tensile strain ε_{ct} as defined in Fig.6(c) and curvature in the concrete element φ also defined in Fig.6(c) for increasing plate slip $(s_p)_d$ at crack 1. At small $(s_p)_d$ such as lines A in Figs.10 and 11, ε_{ct} and φ increase away from the crack even though the plate strain is reducing as in A in Fig.9, but ε_{ct} and φ soon reduce again as the end of the beam is approached. As $(s_p)_d$ is further increased, the large slip near midspan of the beam causes a loss of bond which results in high plate strains in this region as shown by line B in Fig.9 between x=0 and x=75mm. These higher plate strains mean higher plate forces, which allow the reduction in curvature as shown for B in Fig.11 and reduction in ε_{ct} as shown for line B in Fig.10.

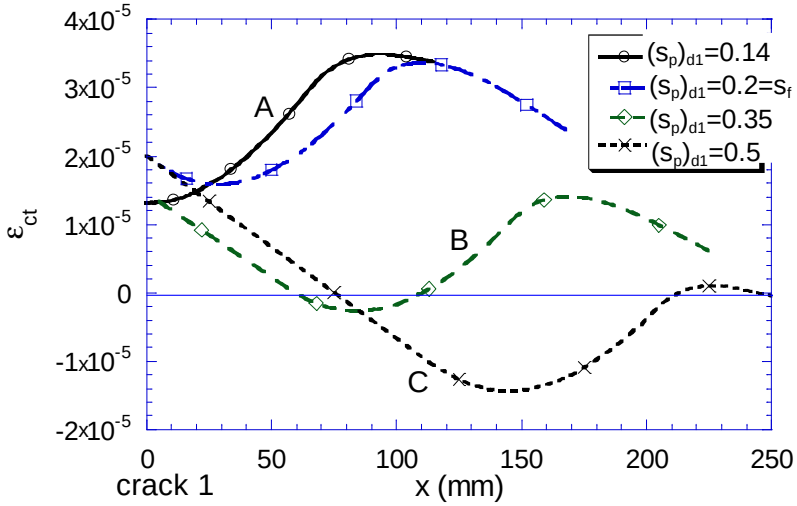

Fig. 10 Peak concrete tensile strain ε_{ct} distribution for single crack plated beam without bars [L=250mm]

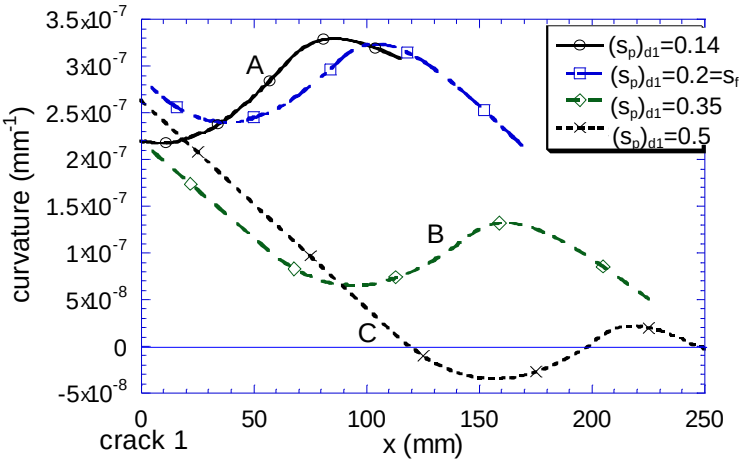

Fig. 11 Curvature φ distribution for single crack plated beam without bars [L=250mm]

In cases where excessive debonding occurs, e.g. line C in Fig.9, plate strain remains very high along the beam even when there is a rapid reduction in moment along the beam from the position of maximum moment to the point of contraflexure. Hence to maintain longitudinal equilibrium of forces it is found that in some parts of the beam, the entire concrete element is under compression, which is represented by negative ε_{ct} in Fig.10 for line C which occurs because of the reversal in curvature shown for line C in Fig.11. This behaviour is analogous to a prestressed concrete beam. It can be seen that for plated beams where large amounts of debonding have occurred, the debonded plate acts as an external prestressing rod and from prestress theory it can be seen that this may cause reversal in curvature. It is worth noting in Fig.10 that as ε_{ct} adjacent to the crack is less than the cracking strain, the disturbed region x_{dis} remains at zero length.

5.2 Multiple Cracks

5.2.1 Debonding Behaviour

To study the difference between the behaviour of beams with single and multiple cracks, analyses were carried out on the same beam as described above with a shear span L of 250mm, but this time with two cracks at 100mm spacing. The occurrence of the second crack significantly affects the slip, slip-strain, bond stress, plate stress and curvature distributions along the beam as illustrated in Figs.12-15 respectively for different plate strains at crack 1, where (L) and (S) represents loading and softening of the beam respectively, which will be explained in the following paragraphs.

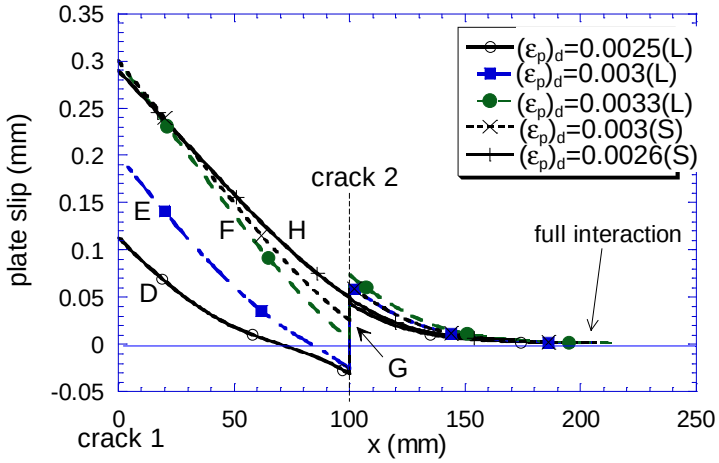

Fig. 12 Slip distribution of plated beam, no bars, 2 cracks at 100mm spacing [L=250mm]

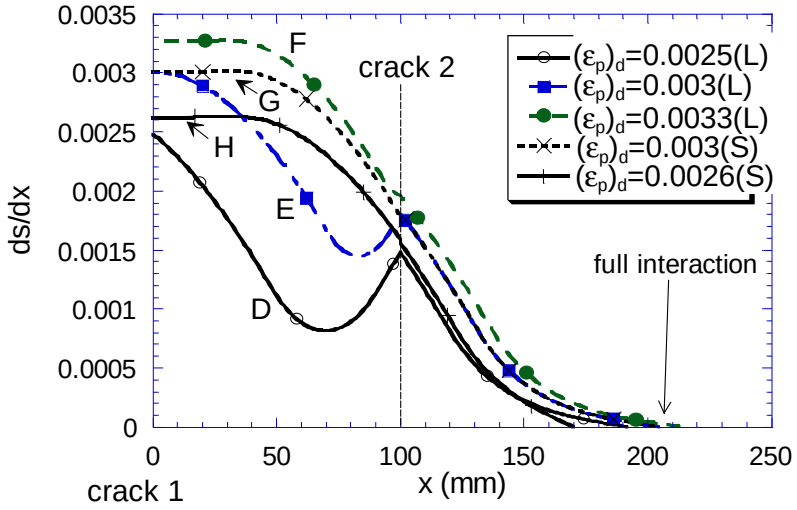

Fig. 13 Slip strain distribution of plated beam, no bars, 2 cracks at 100mm spacing [L=250mm]

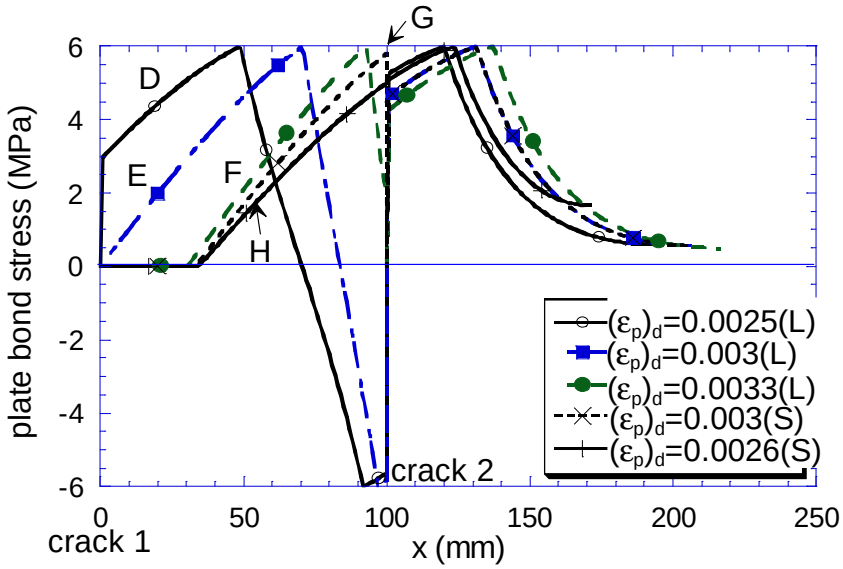

Fig. 14 Bond stress τ_b distribution of plated beam, no bars, 2 cracks at 100mm spacing [L=250mm]

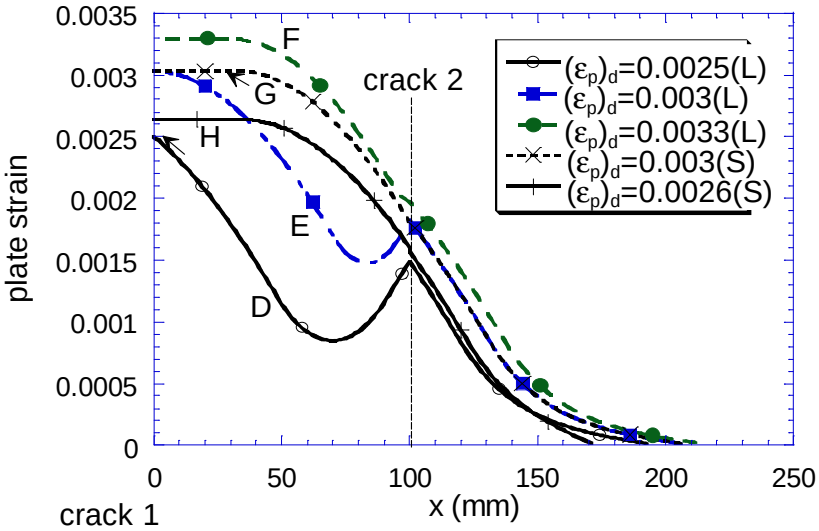

Fig. 15 Plate strain ε_p distribution of plated beam, no bars, 2 cracks at 100mm spacing [L=250mm]

At low plate strains e.g. line D Fig.15, when there is little slip at the plate/concrete interface, the occurrence of the second crack caused an increase in the plate strain around the second crack, as well as a reversal in slip, line D in Fig.12, and hence bond direction, line D in Fig.14. As the plate strain increases, slip will increase causing the point of zero slip to move towards the second crack (line E in Fig.12). Eventually, there will be no more reversal in slip direction as shown by line F, which indicates that the uncracked concrete segment is now sliding towards the second crack.

It can be seen in Figs.12 and 13 that there is only one point where full interaction, that is ds/dx=s=0, can be achieved which is in the uncracked concrete between the last crack and the plate end. It is worth noting that as the beam is precracked, when the plate strain is very low, it may be found that slip only occurs locally around that cracks which means full interaction still takes place in the uncracked concrete between the cracks. When this happens, each crack can be treated separately which is equivalent to the analysis of a single crack, as the local behaviour around one crack is independent of the adjacent cracks.

In analysing uncracked concrete in between cracks such as in a bay in Fig.5, it is found that two solutions of slip at crack 1 $((s_p)_r)_1$ can be obtained for each plate strain $(\varepsilon_p)_{d1}$ considered; one with reversal in bond direction between cracks, and the other with bond in one direction only, such as shown by lines E and G respectively in Fig.14. This is because the resultant bond force between the two cracks, which is given by the area under the bond stress graphs, is the same for both situations. The same applies to analyses based on crack width control, where for the same $((s_p)_r)_1$, two different $(\varepsilon_p)_{d1}$ are found which give different bond stress distributions but the same resultant bond force.

As can be seen in Fig.15, the plate strain at crack 1 is the same for lines E and G, however, the slip at crack 1 of line G in Fig.12 is much greater than that of line E. What is happening is that as the beam is gradually loaded, the slip at crack 1 gradually increases, and as debonding has not yet propagated along the beam, there is a reversal in slip direction between the cracks. So as we gradually load the beam up to $(\varepsilon_p)_{d1}$= 0.003, a slip of 0.2 occurs at crack 1, which is represented by line E in Fig.12-15. When the beam is further loaded such that the point of zero slip moves towards crack 2, it is found that as this point of zero slip occurs at crack 2, maximum bond is achieved between the two cracks and so the maximum plate strain of 0.0033 is obtained, as shown by line F in Fig.15. After the maximum plate strain is reached, due to extensive debonding occurring, indicated by the zero bond between cracks in Fig.14, the bond between the cracks weakens hence resulting in a reduction in plate strain. This is defined as the *softening* behaviour of the beam, such as illustrated by line G, where the plate strain has reduced to the same as line E during loading. Therefore in general, for each plate strain considered, except for the case of the maximum possible $(\varepsilon_p)_{d1}$, two slips can be found; the smaller slip represents the *loading* (L) of the beam and the larger slip is during *softening* (S) of the beam.

Looking at lines E and G in Fig.15 it can be seen that although $(\varepsilon_p)_{d1}$ is the same for the two cases, during softening the plate strain along the beam between the two cracks (line G) is greater than while the beam is loaded (line E) owing to the weakened bond caused by debonding. When softening occurs, due to the reduction in $(\varepsilon_p)_{d1}$, slip at crack 1 reduces slightly, however the slip on the left of crack 2 $((s_p)_l)_2$ increases at a much faster rate. With the slip on the right of crack 2 $((s_p)_r)_2$ also decreasing as the beam softens, this causes the width of crack 2, given by $((s_p)_r)_2$ - $((s_p)_l)_2$, to reduce, eventually closing the crack at $(\varepsilon_p)_{d1}$=0.00264 (line H). The closing of crack 2 is also evident in the bond stress and plate strain distributions (Figs.14 and 15), whereby the beam is found to behave like a beam with a single crack. When crack 2 closes, the beam is reanalysed ignoring crack 2, which means that single crack analysis is performed giving the same results as Figs.7-11. Therefore,

debonding failure occurs at $(\varepsilon_p)_{d1}$=0.00264, which is slightly less than the maximum plate strain (0.0033) reached.

It is worth noting that crack closure may not always happen. For example, if crack 2 does not close, then softening will continue where the bond between the cracks will keep reducing until all bond is lost between the cracks. It is also worth noting how the debonding cracks between cracks, which is represented by the zero bond in Fig.14, propagates along the beam up to a certain point then stops as softening occurs and does not propagate further until complete debonding occurs over that region.

5.2.2 Ductile Behaviour

Analyses were carried out on the same beam as described above, but with a shear span L of 1000mm, and uniform cracks of 100mm spacing spread along the whole beam. Figure 16 shows the variation of the plate strain at crack 1 $(\varepsilon_p)_{d1}$ with the slip at crack 1 $((s_p)_r)_1$ for the 3 beams considered. Behaviour of this beam with L=1000mm is similar to that described above with L=250mm, whereby the slip in the plate increases as the plate strain increase until a maximum plate strain is reached.
For the beam of L=1000mm the maximum plate strain was 0.006 as compared to 0.0033 for L=250mm as shown in Fig.16. After which softening of the beam occurs due to large debonding at the plate/concrete interface, causing the plate strain to reduce as shown in Fig.16. This eventually causes crack 2 to close and the beam was reanalysed neglecting crack 2. As the bond between crack 2 and crack 3 is still relatively strong, this allowed the plate strain to increase again until significant debonding occurs causing crack 3 to close. As more and more cracks close, which in effect increases the crack spacing of the beam, the plate strain continues to reduce until all the cracks have closed, after which debonding failure immediately follows with a strain in the plate that is the same as that for beam with a single crack.

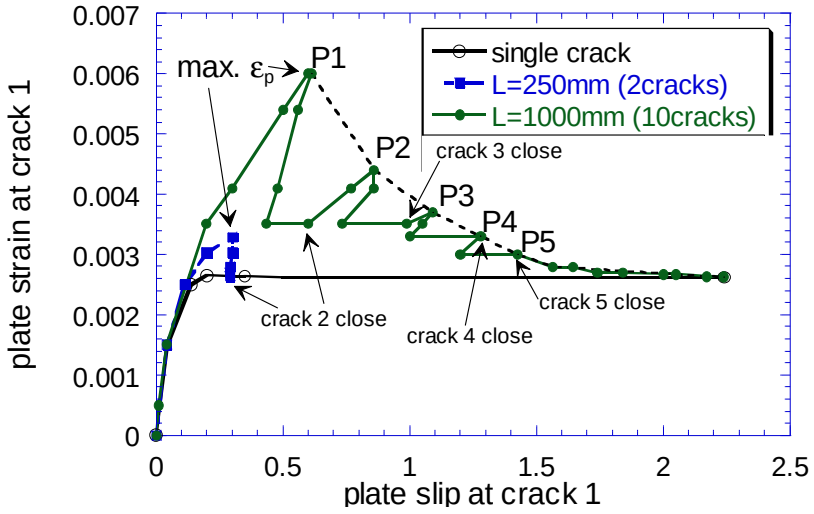

Fig. 16 Comparison between different L for plated beam without bars

Basically after the maximum $(\varepsilon_p)_{d1}$ is reached, shown by P1 in Fig.16, the plate starts to debond between cracks 1 and 2 and when the plate is completely debonded in this region, the plate strain will reduce to a maximum achieved when maximum bond is obtained between cracks 2 and 3, i.e. P2, after which debonding will occur between cracks 2 and 3, eventually causing crack 3 to close and so on until failure occurs. Therefore, the maximum plate strain achieved in a beam with a single crack, which is similar to that of a pull test, can be considered as a lower bound of the IC debonding strain.

From Fig.16, it can be seen that a much higher plate strain and ductile behaviour occurs in a beam with a shallow moment gradient where a lot of cracks have formed.

6. PARTIAL-INTERACTION HINGE BEHAVIOUR OF PLATED RC BEAM

In this section, partial interaction analyses were applied to an initially uncracked reinforced concrete beam with 2Y12 internal bars and which was plated with CFRP on the tension face. The beam was 220mm wide and 240mm deep, with a 50mm wide and 1.2mm thick CFRP plate adhesively bonded along the full length of the beam. The material properties of the plate and the bond characteristic at the plate/concrete interface is the same as in the beams above. The bond-slip model[22] used for the bar/concrete interface is shown in Fig.17 where $\tau_{b.max}=0.225f_{cm}$, $s_1=1$mm, $s_2=3$mm, $s_3=4$mm and $s_f=3s_3$. A point load was applied at midspan of the beam, where shear spans L of 250mm, 500mm and 1000mm were considered.

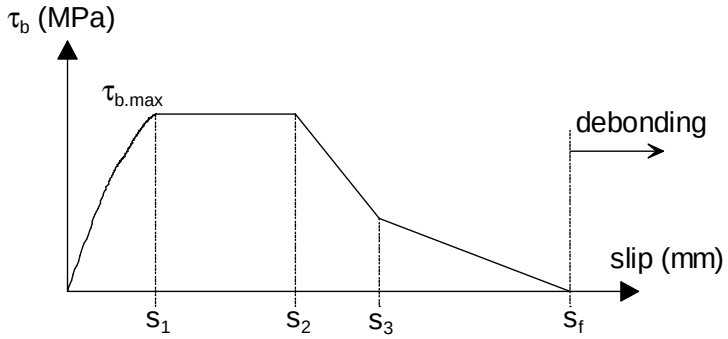

Fig. 17 Bond-slip model for bar/concrete interface

6.1 Single crack

In the analysis of the beam with a shear span L of 250mm, due to the steep moment gradient, no further cracking was found along the beam and there was no sign of widening of the disturbed region up to failure. Figures 18-20 illustrate respectively the slip, slip-strain, plate strain, and bar strain distributions along the beam for a plate strain $(\varepsilon_p)_{d1}$ at crack 1 of 0.00268 at a plate slip $((s_p)_r)_1$ of 0.25, and in which debonding failure had not yet occurred. Note how full interaction was achieved at the plate/concrete interface at x=200mm, however, slip of the bar propagated to the end of the beam, that is there is no full interaction at the bar layer. This does not mean that debonding failure of the bar occurred as the bond of ribbed bars is much stronger than that of the plate. With plates, macro-debonding initiates at a very small slip of $s_f = 0.2$, therefore we can assume that once slip propagates to the end of the plate, debonding failure follows immediately. For bars the slip at which debonding begins is far much greater i.e. at 3 times the rib spacing [22], therefore slip can occur at the beam end while a strong bond remains.

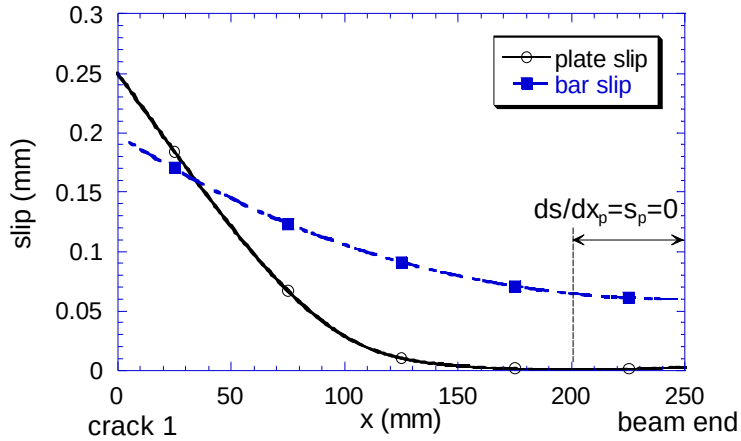

Fig. 18 Slip s distribution for single crack plated beam with 2Y12 bars $(\varepsilon_p)_{d1}$=0.00268, $((s_p)_r)_1$=0.25 [L=250mm]

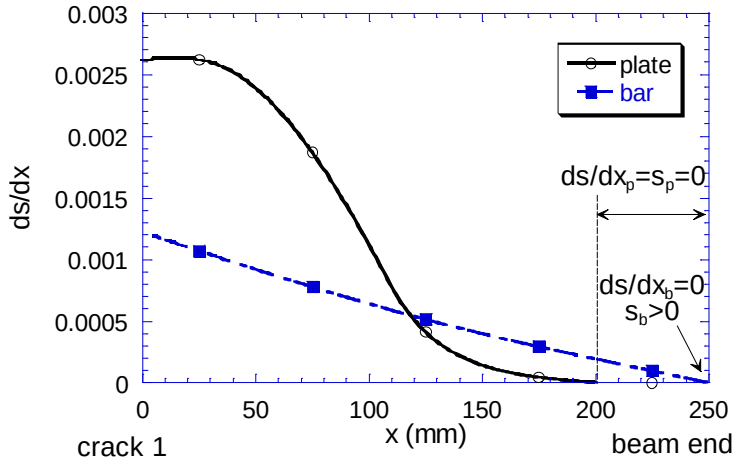

Fig. 19 Slip-strain ds/dx distribution for single crack plated beam with 2Y12 bars $(\varepsilon_p)_{d1}$=0.00268, $((s_p)_r)_1$= 0.25 [L=250mm]

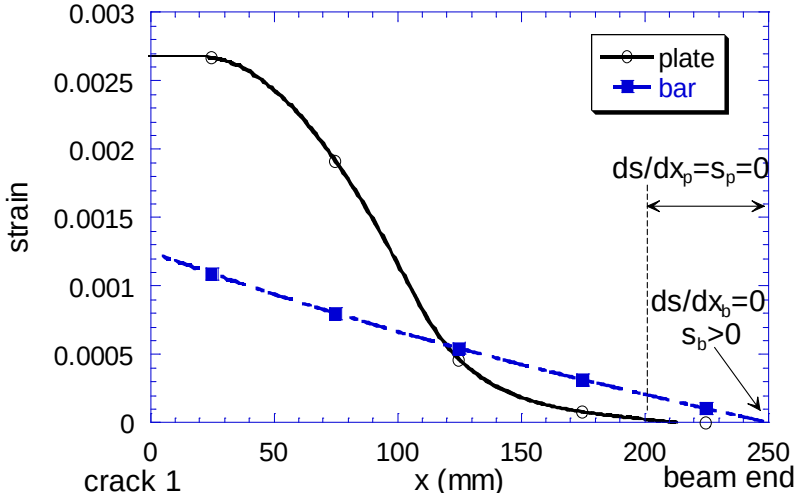

Fig. 20 strain ε distribution for single crack plated beam with 2Y12 bars at $(\varepsilon_p)_{d1}$=0.00268, $((s_p)_r)_1$= 0.25 [L=250mm]

From Fig.20, it can be seen that the plate strain ε_p is significantly greater than the bar strain ε_b in regions with large slip at the plate/concrete interface indicating that partial interaction allows higher

plate strain to be achieved, as opposed to beams with full interaction at all interfaces where the difference between ε_p and ε_b is caused only by the depth of the bar and the plate which is very small. The large difference between ε_p and ε_b is due to the different bond models. Although the maximum bond stress $\tau_{b.max}$ in the bars (Fig.17) is greater than the plates (Fig.2), the relative slip at which $\tau_{b.max}$ is achieved is a lot smaller for the plates. This means that much larger bond develops at the plate/concrete interface resulting in a much greater force in the plate than in the bars in the area where large slip occurs. Note how towards the plate end, the bar strain is greater than the plate strain, which is caused by the rapid rate of reduction of plate force. That is, as the plate slip reduces to less than s_{max} towards the plate end, the steep ascending branch of plate bond model (Fig.2) causes great reduction in the plate force. However, at the bar/concrete interface, slip propagates to the point of contraflexure, that is full interaction does not occur at the bar/concrete interface, as shown in Figs.18 and 19. Therefore, significant amount of bond at the bar/concrete interface occurs near the point of contraflexure, such that the force in the bar becomes greater than the rapidly reducing plate force. This behaviour is similar to that of a prestressed beam where bars are anchored at the ends.

For the beam with L=250mm, a maximum plate strain $(\varepsilon_p)_{d1}$ of 0.0027 is reached. The debonding failure is very rapid, such that when debonding initiates as the maximum plate strain is reached, failure follows immediately.

6.2 Multiple Cracks

6.2.1 Brittle Behaviour

Analyses were carried out on the same beam as above but with a shear span L of 500mm and in which the load was gradually applied to observe the behaviour of the beam as cracks form. Figures 21-23 show the plate strain, bar strain, and plate slip distribution respectively, along the beam for various $(\varepsilon_p)_{d1}$ considered. Due to the steep moment gradient, cracks form mainly near the midspan of the beam. As more and more cracks form, it is found that the tensile strain becomes highest near crack 1, but since the cracking strain is not exceeded, widening of the disturbed region did not occur. It is worth noting that due to the bond model for bars (Fig.17) assumed in this numerical simulation, which ignores the reduction in bond around a crack, the analysis showed the formation of a lot of secondary cracks near crack 1 that does not occur in reality. This discrepancy can be eliminated by adopting a more realistic bond model.

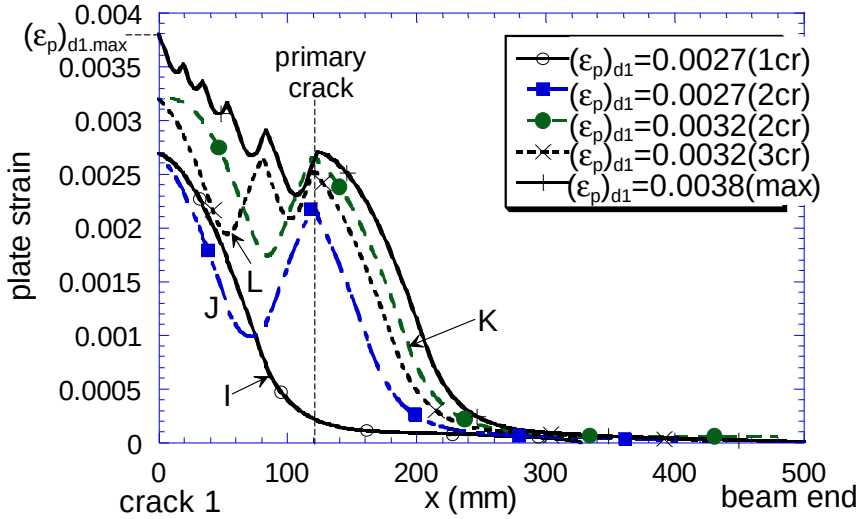

Fig. 21 Plate strain ε_p distribution for plated beam with 2Y12 bars [L=500mm]

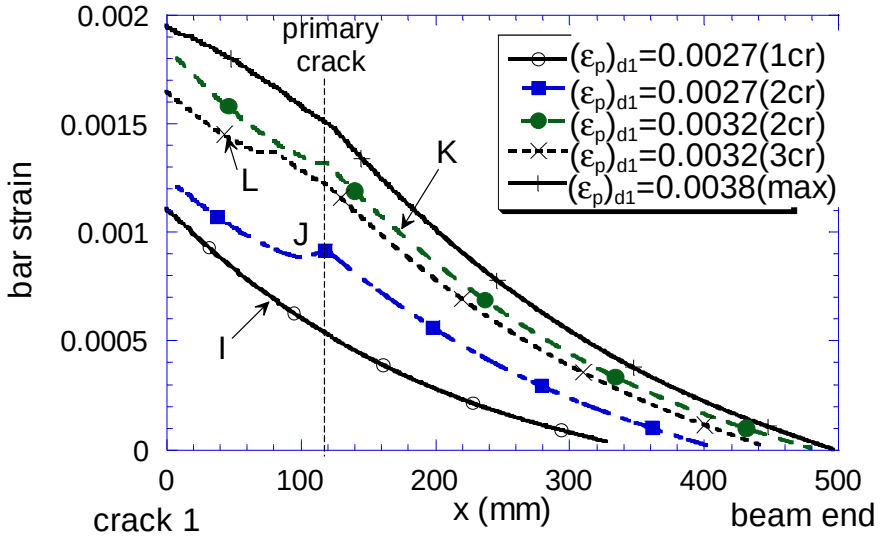

Fig. 22 Bar strain ε_b distribution for plated beam with 2Y12 bars [L=500mm]

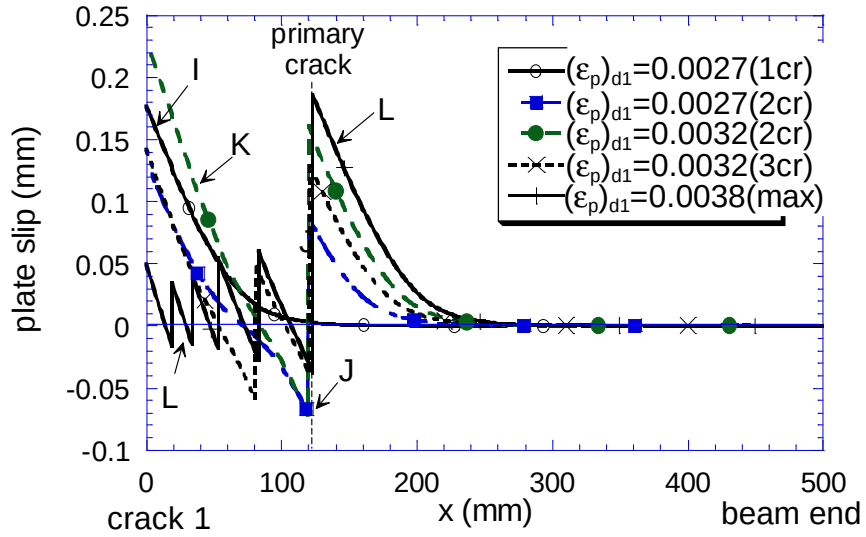

Fig. 23 Plate slip s_p distribution for plated beam with 2Y12 bars [L=500mm]

The occurrence of new cracks largely affects the behaviour along the beam. It is found that when primary cracks occur, that is cracks that form between the last crack and the end of the beam, the plate strain largely increases near this new crack as shown by lines I and J in Fig.21 which represents the behaviour immediately before and after the primary crack forms. This crack also causes the bar strain to increase not only near the crack, but along the entire beam as shown in Fig.22. When a secondary crack occurs i.e. cracks that form between primary cracks, the plate strain increases near the crack but decreases further along the beam, while the bar strain reduces along the entire beam, as illustrated by lines K and L for before and after crack formation respectively.

As secondary cracks form, both plate and bar slip will reduce along the beam except at the new crack. From Fig. 23, it can be seen that the plate slip is very small within the crack region between crack 1 and the next primary crack, and as there is a point of zero slip in between each crack, therefore little debonding occurred in that region and much of the applied force is taken by the plate. This is why the bar strain is significantly less than the plate strain as shown in Fig.24 for the beam at $(\varepsilon_p)_{d1}$ = 0.0035. Figure 25 shows the slip distribution along the beam at the bar/concrete and plate/concrete interface

at $(\varepsilon_p)_{d1}$ = 0.0035. It is interesting to see that the slip at the bar/concrete interface is actually greater than that at the plate/concrete interface and there is no point of zero slip between cracks for the bars, however as the bond of the bar is much stronger, debonding failure does not occur in the bar layer.

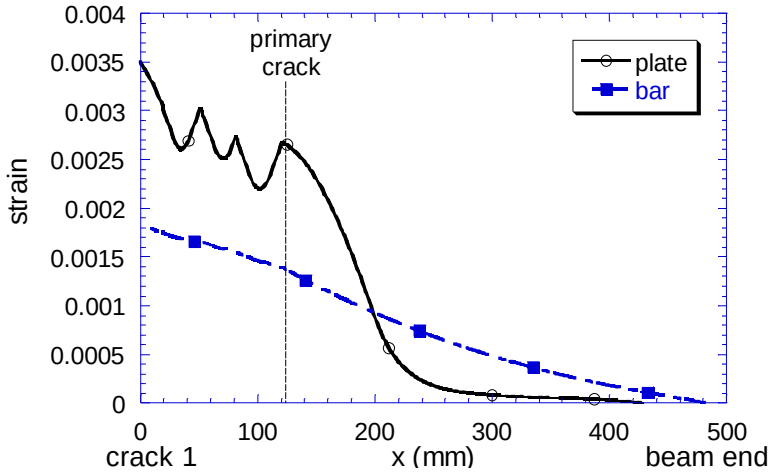

Fig. 24 Strain ε distribution for plated beam with 2Y12 bars at $(\varepsilon_p)_{d1}$=0.0035 [L=500mm]

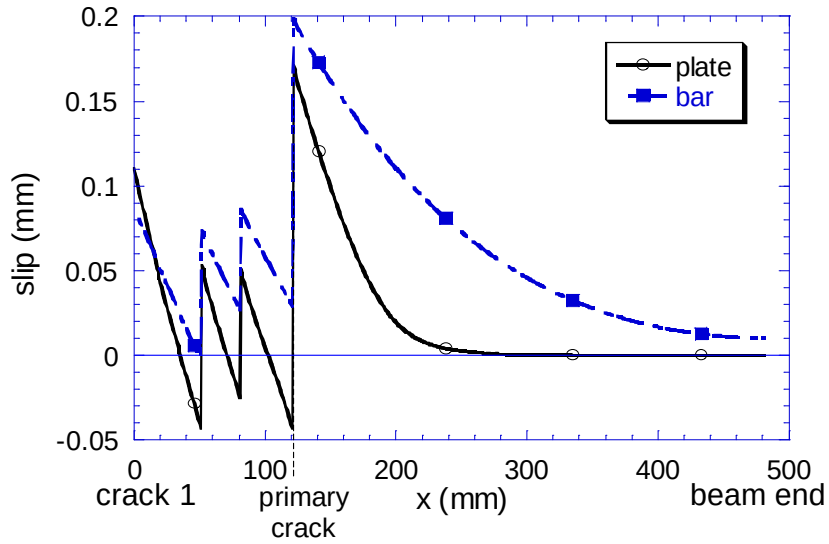

Fig. 25 Slip s distribution for plated beam with 2Y12 bars at $(\varepsilon_p)_{d1}$=0.0035 [L=500mm]

A higher plate strain of $(\varepsilon_p)_{d1}$ = 0.0038 is obtained in this beam compared to the beam with L=250mm due to more cracks being developed, which increased the bond at the plate/concrete interface and hence a greater force in the plate is achieved. However as debonding of the plate initiated from the last crack and propagated rapidly to the plate end, failure of the beam is very brittle.

6.2.2 Ductile Behaviour

An identical beam as above with a shear span L of 1000mm is analysed to study the ductile behaviour of plated RC beams. Figures 26-27 show the peak concrete tensile strain $\varepsilon_{ct,}$ and plate slip distribution along the beam for various $(\varepsilon_p)_{d1}$ considered. The concrete strain ε_{ct} increases away from the crack, which is often referred to as 'tension stiffening' effect. As more cracks form, the tensile strain becomes highest near crack 1 e.g. line M in Fig.26, and at $(\varepsilon_p)_{d1}$=0.00325, the disturbed region begins to extend further along the beam as shown by line N. As the disturbed region x_{dis} widens, the bond in this region

is lost, resulting in a large increase in slip at the plate/concrete and bar/concrete interface near this region (line N in Fig.27), which eventually causes some secondary cracks to close near this area.

It was found in the analysis that x_{dis} continued to extend up to 170mm as shown by line O in Fig.26. After that, due to the large slips developed in the disturbed region, debonding initiated propagating from crack 1. As the debonding cracks move along the beam which means that bond is lost at the plate/concrete interface, the uncracked concrete between the cracks slide towards to beam end causing cracks to close as the debonding cracks propagated. A maximum strain of 0.0043 was reached in the plates, after which, due to extensive debonding occurring, the bond at the plate/concrete interface between the cracks weakens hence causing reduction in plate strain, that is beam softening occurs. Eventually, failure is found to occur as debonding cracks propagated from crack 1 to the plate end. From the analysis it was found that bars yielded before debonding failure occurred. Once the bars yield, large increases in bar strain in the disturbed region was observed for small increase in plate strain, which eventually caused the bar strain to be greater than the plate strain at crack 1 as illustrated in Fig.30.

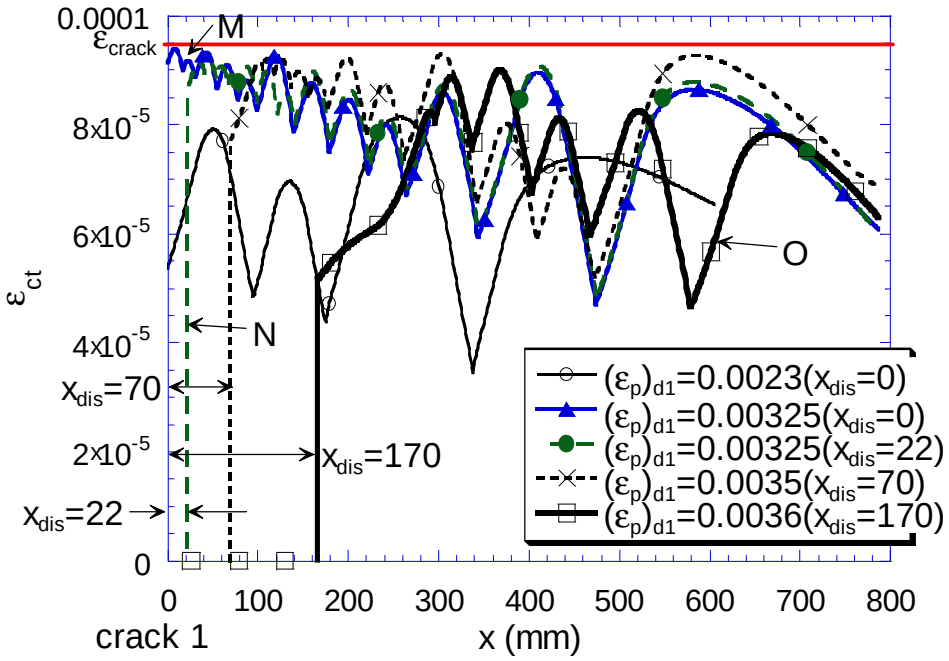

Fig. 26 Peak concrete tensile strain ε_{ct} distribution for plated beam with 2Y12 bars [L=1000mm]

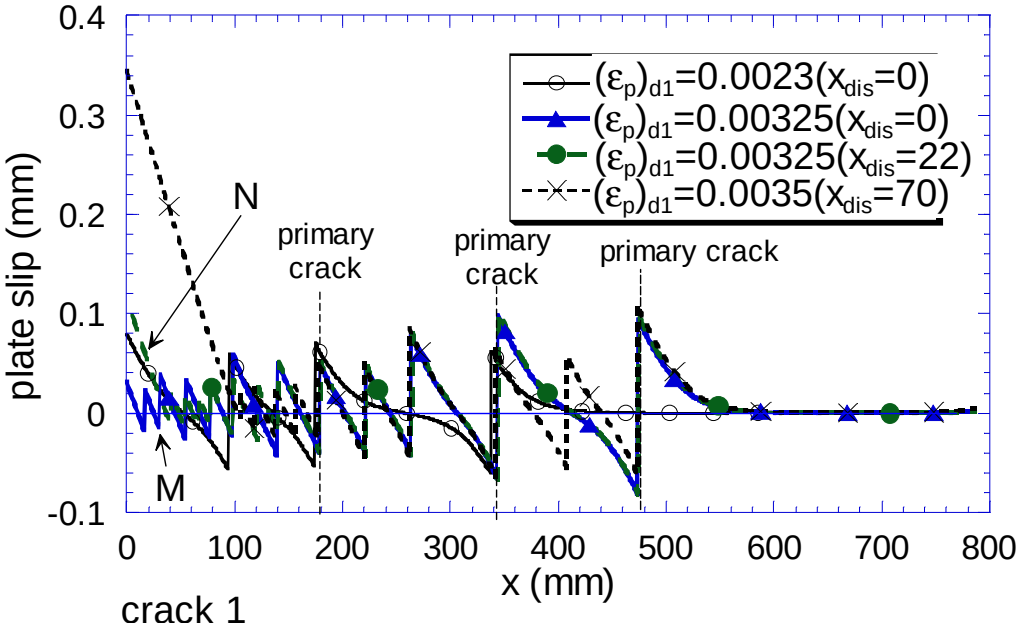

Fig. 27 Plate slip s_p distribution for plated beam with 2Y12 bars [L=1000mm]

Figures 28-29 show the plate strain, bar strain, and slip distribution at $(\varepsilon_p)_{d1}$=0.0035. Comparing with Figs.24-25 for the beam at the same $(\varepsilon_p)_{d1}$ but at a steeper rate of change of moment dM/dx, it can be seen that a much larger cracked region occurs in a beam with a shallow dM/dx. Note how in the beam with L=1000mm, the disturbed region has extended further along the beam causing the plate and bar strain to remain constant over that region. Unlike the beam with L=500mm, where dM/dx is large and plate debonding initiated from the last crack propagating very rapidly to the plate end. For beams with shallow dM/dx, slip is a maximum at a region of high moment, that is at midspan in this case, and so debonding cracks propagate gradually from midspan to the plate end, resulting in a much more ductile failure.

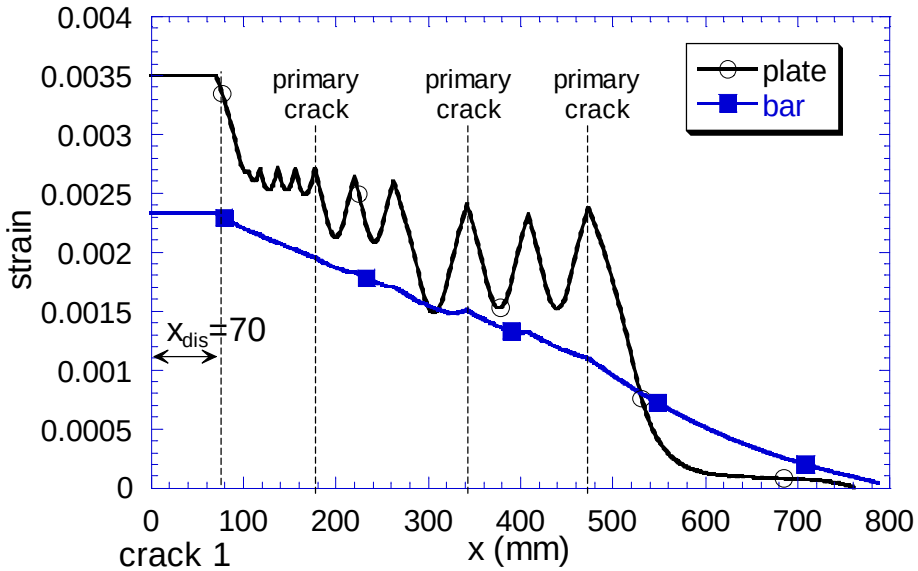

Fig. 28 Strain ε distribution for plated beam with 2Y12 bars at $(\varepsilon_p)_{d1}$=0.0035 [L=1000mm]

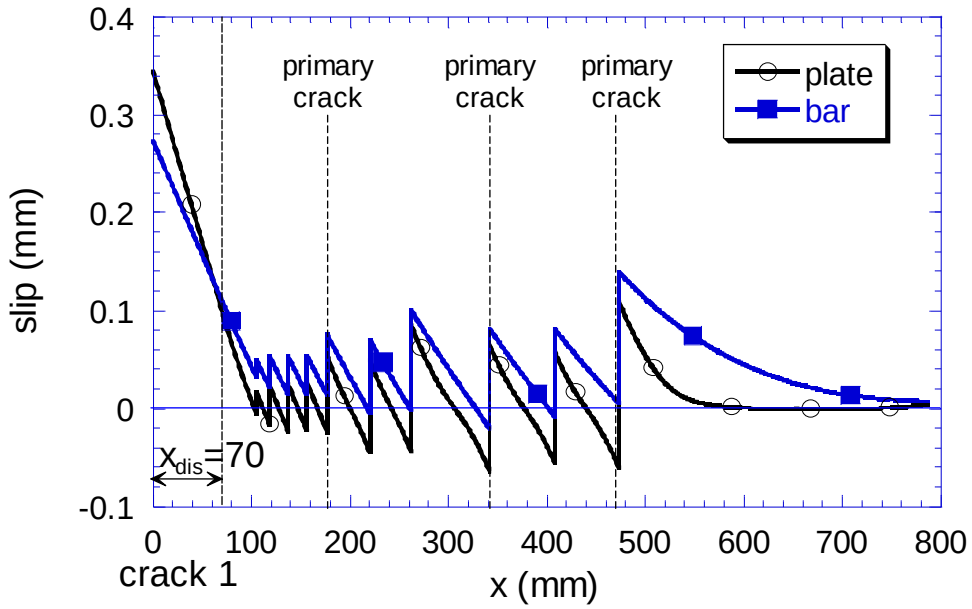

Fig. 29 Slip s distribution for plated beam with 2Y12 bars at $(\varepsilon_p)_{d1}$=0.0035 [L=1000mm]

Comparing Fig.24 with Fig. 28, it is found that for the same plate strain at crack 1, the maximum bar strain along the beam with a shallow moment gradient dM/dx is higher than that with a steep dM/dx. This means that more force is transferred to bars when cracks form in beams with small dM/dx, which is why it is different to beams with steep dM/dx; the formation of primary and secondary cracks in beams with shallow dM/dx result in an increase in both plate and bar strain along the beam. Figure 30 shows the plate and bar strain at midspan of the beam for the different shear spans considered, where it can be seen that a higher plate strain is required to achieve a desired moment for beam with steep dM/dx compared to that with shallow dM/dx. It is interesting to see how the bar strain tends to vary more or less linearly along the beam as opposed to the large variations observed in the plate strain (Figs. 20, 24 and 28).

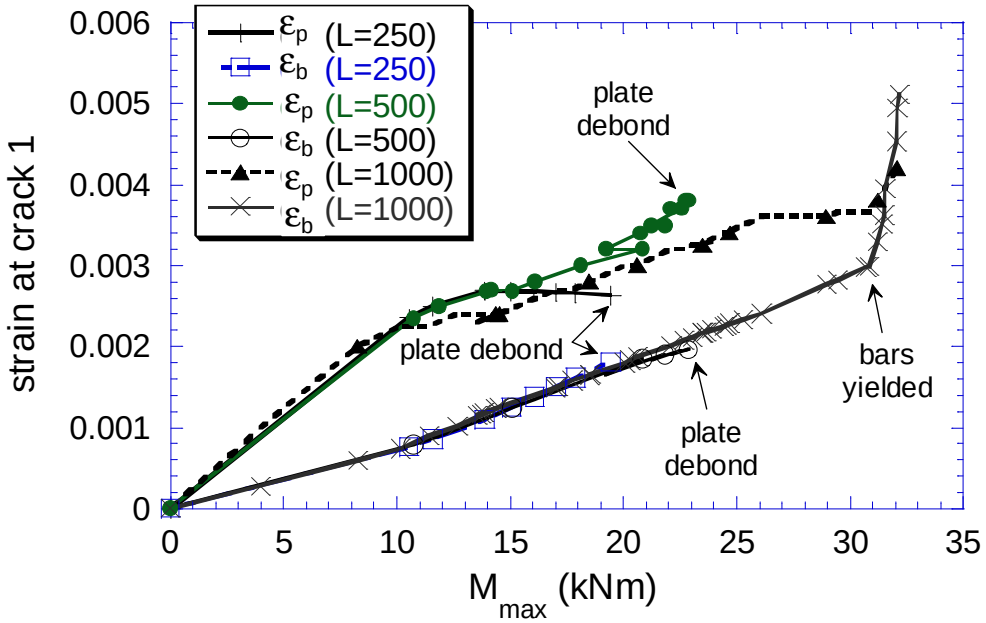

Fig. 30 Comparison between different L for plated beam without bars

In general the formation of new cracks affects the bar and concrete behaviour over a large region of beam and not just around the crack, especially for widely spaced cracks. This is because when crack forms, large plate strain develops to accommodate the crack, which will in turn cause an increase in slip around that crack. Due to the increased slip, bars will act to prevent sliding of the concrete towards the plate end, hence bar strain is increased along the beam as new cracks occur. This behaviour is different to that of reinforced concrete beams with 2 layers of bars[20], where it was found that when new cracks form there is only a very little increase in strain of the inner bar layer near the newly formed crack, and that the new crack only affects the behaviour of the uncracked concrete adjacent to it but not further along the beam.

7. CONCLUDING REMARKS

A numerical partial-interaction model has been developed that simulates the IC debonding behaviour of plated reinforced concrete beams taking into account slips at both bar/concrete and plate/concrete interfaces. The model is based on three boundary conditions: the slip-strain and slip tend to zero at the full-interaction boundary of the hinge; the boundary stress resultants at flexural cracks; and the rigid body rotation of the flexural crack faces of flexural cracks that induce a linear variation in crack width and slip difference. Through the use of these boundary conditions the model: can cope with plated beams with and without reinforcing bars; automatically predicts the occurrence of flexural cracks; distinguishes between disturbed and undisturbed regions; and allows for the interaction between all of the discrete uncracked blocks along the length of the beam. Numerical simulations have illustrated: the different debonding behaviours associated with the behaviours of ductile and brittle hinges; the sequence of the formation of primary and secondary flexural cracks as well as their closure; and the gradual widening of the disturbed regions.

8. REFERENCES

1. FIB. Externally bonded FRP reinforcement for RC structures/Task Group 9.3. Lausanne: International Federation for Structural Concrete, 2001
2. ACI 440.2R-02. Emerging Technology Series. Guide for the Design and Construction of Externally Bonded FRP Systems for Strengthening Concrete Structures. Reported by ACI Committee 440. American Concrete Institute, Farmington Hills, Michigan, USA, 2002
3. Teng, J. G., Chen, J.F., Smith, S.T. and Lam, L. FRP Strengthened RC Structures. England: John Wiley & Sons, 2002
4. Oehlers, D.J. and Seracino, R. Design of FRP and Steel Plated RC Structures: retrofitting beams and slabs for strength, stiffness and ductility. Oxford: Elsevier, 2004
5. Niu, H., and Wu, Z. Strengthening effects of RC flexural members with FRP sheets affected by adhesive layers. Journal of Applied mechanics, JSCE, 2002; 5: 887-897
6. Niu, H., and Wu, Z. Interfacial Debonding Mechanism Influenced by Flexural Cracks in FRP-strengthened Beams. Journal of Structural Engineering, 2001, 47A: 1277-1288.
7. Niu, H., and Wu, Z. Prediction of debonding failure load due to flexural cracks of concrete for FRP-strengthened structures. FRPRCS-5: Bond, 2001;361-370
8. Sebastian, W.M. Significance of midspan debonding failure in FRP-plated concrete beams. Journal of Structural engineering, ASCE, 2001; 127(7): 792-798
9. Aiello, M. A., and Ombres, L. Cracking and deformability analysis of reinforced concrete beams strengthened with externally bonded carbon fiber reinforced polymer sheet. Journal of Materials in Civil Engineering, 2004; 16(5): 392-399

10. Newmark, N.M., Siess, C.P. and Viest, I.M. Tests and analysis of composite beams with incomplete interaction. Proceedings Society for Experimental Stress Analysis, 1951; 9(1): 75-92.
11. Oehlers, D.J. and Bradford, M.A. Composite steel and concrete structural members: fundamental behaviour. Oxford: Pergamon press, 1995
12. Mattock, A.H. Rotational capacity of hinging regions in reinforced concrete beams. Flexural mechanics of reinforced concrete. Proceedings of the international symposium, Miami, Florida, Nov. 10-12, 1964.
13. Corley, W.G. Rotational capacity of reinforced concrete beams. Journal of the Structural Division, ASCE 1966; 92(ST5): 121-147
14. Barnard, P.R. and Johnson, R.P. Plastic behaviour of continuous composite beams, Proc. Instn Civ. Engrs, 1965; 32: 161-210
15. Barnard, P.R. The collapse of reinforced concrete beams. Flexural Mechanics of Reinforced Concrete, Proceedings of the International Symposium, Miami, Florida, 1964, Nov., 501-511.
16. Wood, R.H. Some controversial and curious developments in the plastic theory of structures. In: Heyman, J. and Leckie, F.A., editors. Engineering Plasticity: Cambridge University Press, 1968, 665-691.
17. Langer, P. Verdrehfahigkeit Plastizierter Tragwerksbereiche im Atahlbeton bau. Institu fur Werkstoffe im Bauwesen, Universitat Stuttgart, Report 1987/1
18. Fantilli, A.P., Ferretti, D., Iori, I., and Vallini, P., Flexural deformability of reinforced concrete beams. *Journal of Structural Engineering*, ASCE, 1998; 1041-1049.
19. Manfredi, G., and Pecce, M., A refined R.C. beam element including bond-slip relationship for the analysis of continuous beams. Computers & Structures, 1998; 69: 53-62.
20. Oehlers, D.J., Liu, I.S.T., and Seracino, R. The gradual formation of hinges throughout reinforced concrete beams. Submitted to Magazine of concrete research
21. Oehlers, D.J., Liu, I.S.T., Seracino, R. The gradual formation of hinges throughout reinforced concrete beams. Departmental report, School of Civil and Environmental Engineering, University of Adelaide, Australia
22. fib. Bond of reinforcement in concrete: state-of-art report /prepared by Task Group Bond Models (former CEB Task Group 2.5). Lausanne, Switzerland, International Federation for Structural Concrete, 2000

2.6.3 FURTHER DISCUSSIONS

In the following context, further discussions on the sectional analyses of the disturbed and undisturbed regions are presented in Sections 2.6.3.1 and 2.6.3.2 respectively. Additional information on the geometry and the material properties of the beams analysed in Sections 2.6.1 and 2.6.2 are included in Section 2.6.3.3.

2.6.3.1 DISTURBED REGION SECTIONAL ANALYSIS

Consider the plated RC beam illustrated in Figure 2.60, with a disturbed region x_{dis} around the crack, crack 1. As discussed in Sections 2.6.1 and 2.6.2, one method of modelling the disturbed region is to assume rectangular concrete stress blocks, where compressive stress is allowed to develop at the tip of the crack as illustrated in Figure 2.60b. To analyse the disturbed region, sectional analysis is firstly performed at the crack, with the crack height *h* estimated using elastic analysis of the flexural rigidity of a cracked cross-section. For a plate strain $(\varepsilon_p)_1$ considered at the crack, k_2 is guessed and the bar strain at the crack $(\varepsilon_b)_1$ is evaluated, where $(\varepsilon_p)_1=k_2(\varepsilon_b)_1$. The plate $(\sigma_p)_1$ and bar $(\sigma_b)_1$ stresses are then determined using the known stress-strain relationships such as that shown in Figure 1.1. As no external longitudinal forces is being applied, equilibrium requires that the total sum of the internal forces to be equal to zero i.e. $\sum F=0$. Therefore, the stress in the concrete at the crack $(\sigma_c)_1$ is iterated until horizontal equilibrium is achieved, where the depth of the stress block is equal to the depth of the neutral axis $(d_n)_1$. From the resultant distribution of forces shown in Figure 2.60c, the moment at the crack M_1 is obtained, and hence, the moment distribution, or the boundary moments, along the beam can be evaluated as illustrated in Figure 2.60a. It is assumed that within the disturbed region where large slip occurs, the bar and plate bond stresses are equal to zero. Therefore, the forces in the bar and the plate remain unchanged over the disturbed region, and the bar and plate forces of the next section within the disturbed region, i.e. section 2 in Figure 2.60d, is known.

To analyse a section within the disturbed region at distance *x* away from the crack, such as section 2 in Figure 2.60d, where the bar and plate forces are the same as that at the crack, the depth of the concrete stress block $(d_n)_2$ is iterated for a concrete stress $(\sigma_c)_2$ guessed until horizontal equilibrium is obtained. The moment of the section is then calculated based on the resultant force distribution along the section as shown in Figure 2.60e. If this moment is not equal to the boundary moment, M_2 in Figure 2.60a, then $(\sigma_c)_2$ guessed is changed and the section is reanalysed until rotational equilibrium is achieved. It is worth noting that as it is assumed that the concrete strain at the bar/concrete interface is negligible, the slip-strain is equal to the bar strain so that the change in slip can be

determined by integration of the bar strain. Same applies to the plate/concrete interface. Disturbed region sectional analysis is performed up to the boundary at $x=x_{dis}/2$; for $x>x_{dis}/2$, undisturbed region sectional analysis is carried out as discussed in the following Section.

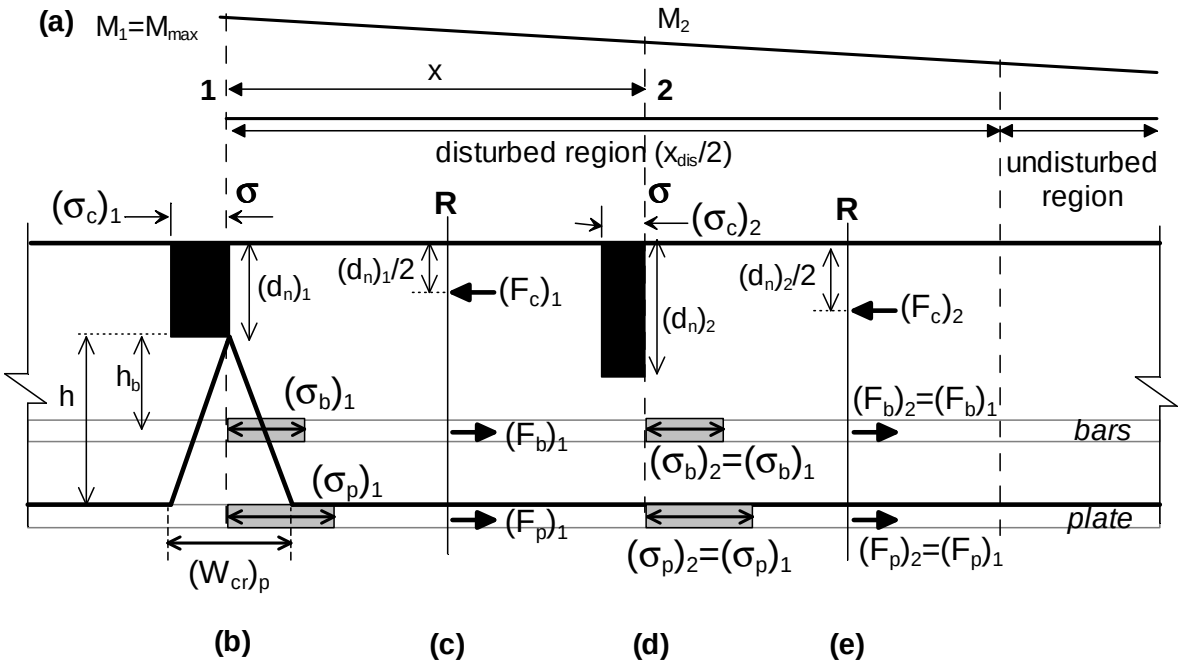

Figure 2.60 Sectional analyses of the disturbed region

2.6.3.2 UNDISTURBED REGION SECTIONAL ANALYSIS

Consider the plated reinforced concrete beam with a single layer of reinforcing bars illustrated in Figure 2.61, which is subjected to a point load *P*. When a crack occurs, this induces a slip at the plate/concrete s_p, and at the bar/concrete s_b interface as illustrated in Figure 2.61a. As a result, the strain at the bar ε_b and at the adjacent concrete ε_c is different and same applies to the plate/concrete interface. Therefore partial interaction applies, where the strain profile at section A-A is now given by Figure 2.61b, with a curvature in the concrete of χ_{PI}, and slip-strains at the bar/concrete ds/dx_b and bar/concrete ds/dx_p interfaces. Because the bond-slip characteristics at the two interfaces are different, the slips at each interface may differ i.e. $s_p \neq s_b$. With different slip, and hence, bond force at the interfaces, therefore the plate and bar strains will not be the same, resulting in different slip-strains i.e. $ds/dx_p \neq ds/dx_b$, as illustrated by Figure 2.61b.

To perform sectional analysis on a partial interaction strain profile ε_{PI} such as Figure 2.61b, for the plate ε_p and bar strains ε_b considered, the flexural stress profile σ_{PI} is firstly evaluated based on the known stress-strain relationships of the concrete, the plate and the bar. The flexural forces within the beam can hence be derived by integrating the stress over the cross-section. For example, the cross-

section can be divided into *n* layers with the mean stress within each layer determined from Figure 2.61c. It is assumed that the axial force of each layer acts at the mid-depth of the layer, and so the magnitude and distribution of the internal forces *F* is known, as illustrated in Figure 2.61d. As no external longitudinal forces is being applied, equilibrium requires that the total sum of the internal forces to be equal to zero i.e. $\sum F=0$. Therefore, for a curvature in the concrete χ_{PI} guessed, the neutral axis d_n in Figure 2.61b is iterated until horizontal equilibrium is achieved, and the internal moment M_{int} can hence be evaluated. If M_{int} is not equal to the external applied moment, χ_{PI} is then iterated until rotational equilibrium with the applied moment is achieved.

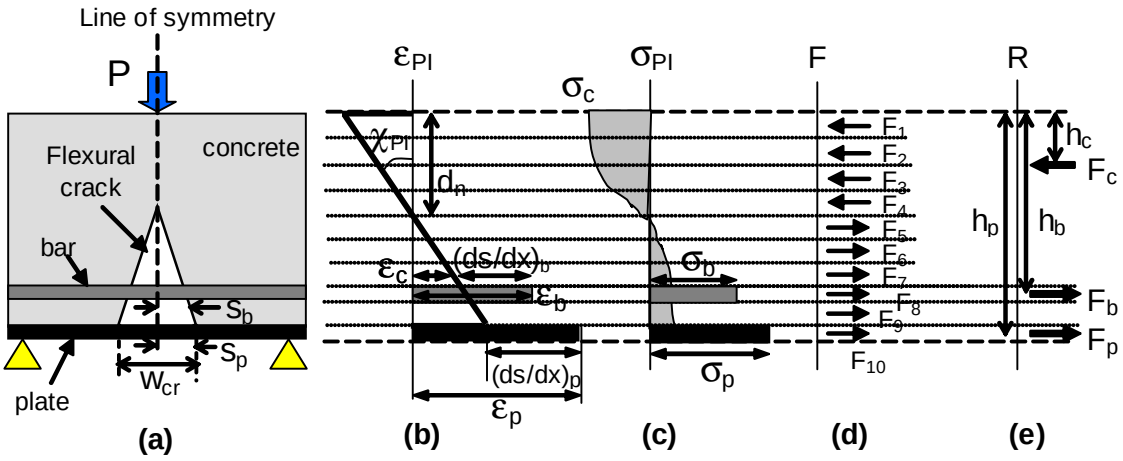

Figure 2.61 Sectional analyses of the undisturbed region

Alternatively, the resultant internal force distribution of the plated RC beam with a single layer of reinforcing bar can be expressed by Figure 2.61e, where F_c, F_p and F_b are the resultant forces in the concrete, plate and bar respectively, acting at depths h_c, h_p and h_b from the beam top. From the equilibrium of internal forces in the concrete element, F_b is equal to the total bond force at the bar/concrete interface $(F_{shear})_b$ over the shear span L_{sh}, and F_p is equal to the total bond force at the plate/concrete interface $(F_{shear})_p$ over L_{sh}. This indicates that the force in the reinforcement is dependent on the bond force at the reinforcement/concrete interface.

2.6.3.3 Properties of Beams Analysed in Sections 2.6.1 and 2.6.2

In the analyses examples presented in the journal papers in Section 2.6.1 and Section 2.6.2, the stress-strain relationships used for the different elements are illustrated in Figure 2.62.

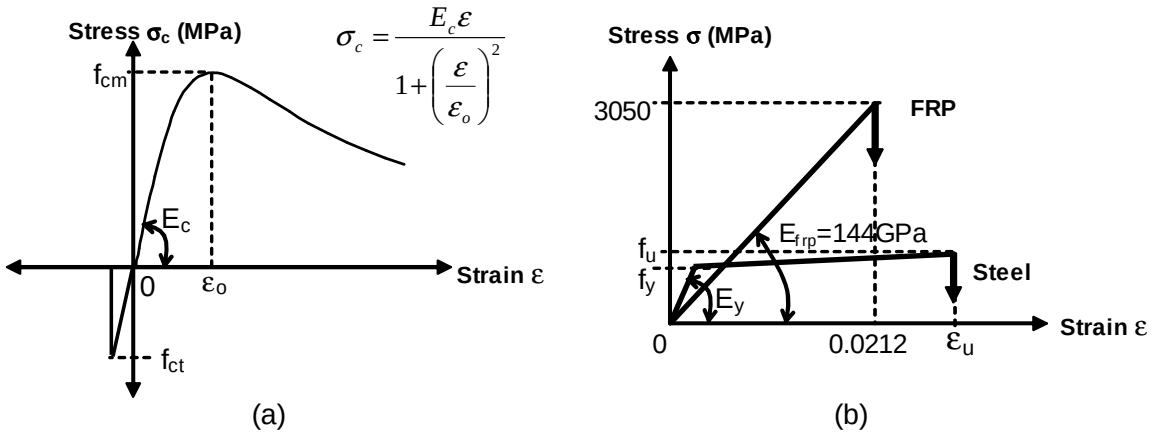

Figure 2.62 Stress-strain relationships for [a] concrete (Desayi and Krishnann 1964); [b] steel or FRP

All the beams analysed in Section 2.6.1 and Section 2.6.2 have the same concrete properties, with maximum compressive stress f_{cm}=33MPa at a strain ε_o=0.002; maximum tensile stress f_{ct}=3.46Mpa; and Young's Modulus E_c=36951MPa. The stress-strain relationship developed by Desayi and Krishnann (1964; cited in Warner et al. 1998), shown in Figure 2.62a, was used in the analyses.

For the RC beams analysed in Section 2.6.1, the steel bars have a bilinear stress-strain relationship as shown in Figure 2.62b, where yield strength f_y=558MPa, Young's modulus E_y=200GPa, ultimate strength f_u=646MPa and ultimate strain ε_u=0.05. For the beams with a single layer of 2Y12 bars, the bars are at 200mm from the top of the beam; and for beams with two layers of 2Y12 bars, the bars are located at 160mm and 200mm from the top of the beam. The bond-slip model used for the bar/concrete interface (Huang et al. 1996; cited in *fib* 2000) is shown in Figure 2.33, where the peak bondstress $\tau_{b.max}$ is dependent on the concrete compressive stress f_c; the slips s_1=1mm, s_2=3mm, s_3=4mm and an ultimate slip s_f of $3s_3$.

All the RC beams analysed in Section 2.6.2 are plated with 50mm wide by 1.2mm thick FRP plates over the tension face, where the stress-strain relationship of the FRP is shown in Figure 2.62b. For the beams with 2Y12 bars at 200mm from the top of the beam, the bars have a yield strength f_y=601MPa, Young's modulus E_y=200GPa, ultimate strength f_u=717MPa and ultimate strain ε_u=0.07. The stress-strain relationship of the steel bars is shown in Figure 2.62b.

2.7 SUMMARY

In this chapter, a literature review was carried out on existing rotation capacity models for unplated RC beams and it was found that the models based on discrete cracking are best suited for analysing the local deformation of cracked RC beams. However as most of these existing local deformation models can only account for a single layer of reinforcement, none of them can be applied to beams with an externally bonded plate, and so, a new model was developed. As intermediate crack debonding of plated beams is initiated by cracks intercepting the plate, discrete cracking was also used to develop a model for plated members. Through the literature review, it was found that the behaviour of plated, unplated and composite beams are similar in that they exhibit partial interaction. Therefore the partial interaction theory originally developed for composite beams, has been applied to unplated and plated RC members.

The partial interaction model was first developed for tensile specimens with without bars, where the boundary conditions of: zero slip and slip-strain at the boundaries of the partial interaction region; cracks having constant crack widths; and zero concrete tensile strain at a crack applies. The "shooting technique" was used to obtain a solution using non-linear analysis. In additional to the non-linear approach, a mathematical model was developed for tensile specimens with single reinforcing layer, which was based on the mixed approach for composite beams, where it is assumed that the bond force is constant.

Partial interaction model was first proposed to simulate the local deformation behaviour of plated members and unplated RC beams. However this model suffers a shortfall in that the disturbed region around a crack is ignored in the analysis. This led to the development of the modified partial interaction model, which allows for the disturbed regions within the partial interaction region, where it is assumed that there is zero curvature in the compressive concrete above the crack and the height of the crack is predefined. In the areas away from a crack, undisturbed region analysis applies where the concrete strain is assumed to vary linearly along a section. The modified partial interaction model is presented in the journal papers attached in Sections 2.6.1 and 2.6.2 for unplated and plated RC beams respectively.

The most important part in the development of the partial interaction model was to determine the boundary conditions. The proposed modified partial interaction model is based on three boundary conditions: the slip-strain and slip tend to zero at the full-interaction boundary of the hinge; the boundary stress resultants at flexural cracks; and the rigid body rotation of the crack faces of flexural cracks that induce a linear variation in crack width and slip difference. Through the use of these

boundary conditions the model: can cope with any number of reinforcing layers; automatically predicts the occurrence of flexural cracks; distinguishes between disturbed and undisturbed regions; and allows for the interaction between all of the discrete blocks along the length of the beam.

Numerical simulations have been carried out on plated and unplated RC beams using the proposed model in this chapter to study the local deformation behaviour of these structures. The results have demonstrated:

- the different debonding behaviours associated with the behaviours of ductile and brittle hinges;
- sequence of the formation of primary and secondary flexural cracks as well as their closure; and the gradual widening of the disturbed regions;
- sliding of the reinforcement through the concrete blocks as well as the movement of the zero slip position;
- how the curvature in the concrete block is not at its greatest at a flexural crack;
- the large slip-strains at flexural cracks; and
- the gradual spread of the partial-interaction hinge.

2.8 REFERENCES

Aiello, M. A., Ombres, L. (2004). "Cracking and deformability analysis of reinforced concrete beams strengthened with externally bonded carbon fiber reinforced polymer sheet." *Journal of Materials in Civil Engineering*, 16(5), 392-399

Alca, N., Alexander, S.D.B., MacGregor, J.G. (1997). "Effect of size on flexural behaviour of high-strength concrete beams" *ACI Structural Journal*, 94(1), 59-67

Bachmann, H. (1967). *Zur plastizit:atstheoretischen Berechnung statisch unbestimmter Stahlbetonbalken*. PhD Thesis, ETH Zürich

Baker, A.L.L. (1961). Note for discussion at Monaco, CEB Bulletin d'Information No. 30, Comité Euro-International du Béton, Lausanne

Bizindavyi, L., and Neale, K.W. (1999). "Transfer lengths and bond strengths for composites bonded to concrete." *Journal of Composites for Construction*, ASCE, 3(4), 153-160

CEB-FIP (1998). *Ductility of Reinforced Concrete Structures – synthesis report of CEB task group 2.2*. Bulletin d'Information no. 242, Comité Euro-International du Béton, Lausanne, Switzerland.

Chaallal, O., Nollet, M.J., and Perraton, D. (1998) "Strengthening of reinforced concrete beams with externally bonded fibre-reinforced-plastic plates: design guidelines for shear and flexure", *Canadian Journal of Civil Engineering*, 25(4), 692-704

Chajes, M.J., Finch, W.W.Jr., Januszka, T.F., and Thompson, J.A.Jr (1996). "Bond and force transfer of composite material plates bonded to concrete". *ACI Structural Journal*, 93(2), 296-303

Chajes, M.J., Januszka, T.F., Mertz, D.R., Thompson, J.A.Jr., and Finch, W.W.Jr. (1995). "Shear strengthening of reinforced concrete beams using externally applied composite fabrics". *ACI Structural Journal*, 92(3), 295-303

Chen, J.F., and Teng, J.G. (2001). "Anchorage Strength Models for FRP and Steel Plates Bonded to Concrete". *Journal of Structural Engineering*, 127(7), 784-791

Chen, J.F., Yang, Z.J., and Holt, G.D. (2001). "FRP or steel plate-to-concrete bonded joints: effect of test methods on experimental bond strength", *Steel and Composite Structures – An International Journal,* 1(2), 231-244

Concrete Society Committee (2000). *Design guidance for strengthening concrete structures using fibre composite materials*. Concrete Society Technical Report no. 55, Concrete Society, UK

Cosenza, E., Greco, C., and Pecce, M. (1991). "Nonlinear design of reinforced concrete continuous beams." *Structural Engineering International*, 1(1), 19-27

Eligehausen, R., Popov, E.P., Bertero, V.V. (1983). *Local Bond Stress-Slip Relationships of Deformed Bars Under Generalized Excitations: experimental results and analytical model*. University of California, California

Fantilli, A.P., Ferretti, D., Iori, I., and Vallini, P. (1998). "Flexural deformability of reinforced concrete beams." *ASCE Journal of the structural division*, 124(9), 1041-1049

Ferretti, D., and Savoia, M. (2003). "Non-linear model for R/C tensile members strengthened by FRP-plates." *Engineering Fracture Mechanics*, 70, 1069-1083

fib (2000). *Bond of reinforcement in concrete: state-of-art report /prepared by Task Group Bond Models (former CEB Task Group 2.5)*. Bulletin 10, International Federation for Structural Concrete, Lausanne, Switzerland.

Graubner, C.A. (1987). *Schnittgrößenverteilung in statisch unbestimmten Stahlbetonbalken unter Berücksichtigung wirklichkeitsnaher Stoffgesetze – Baustofftechnologie Abweichungen von elastizitätstheoretischen und plastizitätstheoretischen Lösungen (in German).* Technische Universität München, Munich, Germany.

Graubner, C.A. (1997). *Redistribution capacity of reinforced and prestressed concrete structures*. CEB Bulletin No. 239, CEB, 69-95

Gravina, R.J. (2002). *Non-linear Overload Behaviour and Ductility of Reinforced Concrete Flexural Members Containing 500MPa Grade Steel Reinforcement*. PhD thesis, University of Adelaide, Adelaide

Hiroyuki, Y., and Wu, Z. (1997) "Analysis of debonding fracture properties of CFS strengthened member subject to tension", *Non-Metallic (FRP) Reinforcement for Concrete Structures, Proceedings of the 3rd International Symposium,* Sapporo, Japan, 287-294

Holzenkämpfer, O. (1994). *Ingenieurmodelle des Verbundes geklebter Bewehrung für Betonbauteile,* Dissertation, TU Braunschweig

Huang, Z., Engström, B., and Magnusson, J. (1996). "Experimental analytical studies of the bond behaviour of deformed bars in high strength concrete". *4th International Symposium on Utilization of High-Strength/High-Performance Concrete*, Paris, France

Johnson, R. P. (1994). *Composite Structures of Steel and Concrete.* Blackwell Scientific Publications, England

Khalifa, A., Gold, W.J., Nanni, A., and Aziz, A. (1998) "Contributions of externally bonded FRP to shear capacity of RC flexural members." *Journal of Composites for Construction ASCE*, 2(4), 195-203

Kodur, V.K. (1992). *Redistribution of moment and the influence of secondary moment in continuous prestressed concrete beams*. PhD thesis, Queen's University, Kingston, Ontario, Canada

Kreller, H. (1989). Zum nichtilinearen Trag- und Verformungsverhalten von Stahlbetonstabtragwerken unter Last- und Zwangeinwirkung. PhD Thesis, Universität Stuttgart, Stuttgart, Germany

Kwak, H.G., and Song, J.Y. (2002). "Cracking analysis of RC members using polynomial strain distribution function." *Engineering Structures*, 24, 455-468

Langer, P. (1987), *Verdrehfähigkeit plastizier Tragwerksbereiche im Stahlbetonbau,* phD thesis, University of Stuttgart

Leung, C.K.Y. (2001) "Delamination failure in concrete beams retrofitted with a bonded plate" *Journal of Materials in Civil Engineering*, 13(2), 106-113

Liu, I.S.T., Oehlers, D.J., and Seracino, R. (2005). "Partial interaction numerical simulation of hinges in FRP plated reinforced concrete beams." *Computers and Structures*, submitted

Maeda, T., Asano, Y., Sato, Y., Ueda, T. , Kakuta, Y. (1997) "A study on bond mechanism of carbon fibre sheet." *Non-Metallic (FRP) Reinforcement for Concrete Structures, Proceedings of the 3rd International Symposium,* Sapporo, Japan, 279-285

Manfredi, G., and Pecce, M. (1998). "A refined R.C. beam element including bond-slip relationship for the analysis of continuous beams." *Computers & Structures*, 69, 53-62

Matthys, S. (2000). *Structural behaviour and design of concrete members strengthened with externally bonded FRP reinforcement*, Doctoral thesis, Ghent University

Neubauer, U., and Rostásy, F.S. (1997). "Design aspects of concrete structures strengthened with externally bonded CFRP plates", *Proceedings of the 7th international Conference on Structural Faults and Repairs,* edited by M.C. Forde, Engineering Technics Press, Edinburgh, UK, 109-118

Newmark, N.M., Siess, C.P., and Viest, I.M. (1951). "Tests and analysis of composite beams with incomplete interaction." *Proceedings Society for Experimental Stress Analysis,* 9(1), 75-92

Niedermeier, R. (1996). "Stellungnahme zur Richtlinie für das Verkleben von Beton-bauteilen durch Ankleben von Stahllaschen – Entwurf März 1996." *Schreiben Nr 1390 vom 30.10.1996 des Lehrstuhls für Massivbau*, TU München.

Niedermeier, R. (2000). *Zugkraftdeckung bei klebearmierten bauteilen (Envelope line of tensile forces while using externally bonded reinforcement)*, Doctoral Diessertation, TU München

Niu, H., and Wu, Z.S. (2001a). "Interfacial debonding mechanism influenced by flexural cracks in FRP-strengthened beams." *Journal of Structural Engineering*, 47A, 1277-1288

Niu, H., and Wu, Z.S. (2001b). "Prediction of debonding failure load due to flexural cracks of concrete for FRP-strengthened structures." *FRPRCS-5: Bond*, 361-370

Oehlers, D.J. and Seracino, R. (2004). *Design of FRP and Steel Plated RC Structures: retrofitting beams and slabs for strength, stiffness and ductility.* Elsevier, Oxford

Oehlers, D.J.(2000) "The choice of plating techniques for retrofitting of reinforced concrete bridge beams and slabs" *Austroads 4th Bridge Conference, Bridges for the new millennium*, Australia

Oehlers, D.J., and Bradford, M.A. (1995). *Composite Steel And Concrete Structural Members: Fundamental Behaviour*. Elsevier Science Ltd., UK

Oehlers, D.J., and Sved, G. (1995) "Composite beams with limited-slip-capacity shear connectors". *Journal of Structural Engineering ASCE*, 121(6), 932-938

Oehlers, D.J., Liu, I.S.T., and Seracino, R. (2005). "The gradual formation of hinges throughout reinforced concrete beams." *Mechanics Based Design of Structures and Machines*, accepted for publications

Pecce, M. (1997). "Experimental evaluation of rotation capacity of HPC beams." CEB Bulletin d'Information no. 242 Ductility – reinforcement: synthesis report, Comité Euro-International du Béton, Lausanne, Switzerland.

Rebentrost, M. (2003). *Deformation capacity and moment redistribution of partially prestressed concrete beams.* PhD Thesis, University of Adelaide, Adelaide, Australia

Rebentrost, M., and Warner, R.F. (2002) "Post-cracking deformations and ductility of prestressed concrete beams." *Proceedings of 17th Australiasian Conference on the Advances in Mechanics of Structures and Materials*, ACMSM17, Queensland, Australia

Sebastian, W.M. (2001). "Significance of midspan debonding failure in FRP-plated concrete beams." *Journal of Structural engineering ASCE*, 127(7), 792-798

Täljsten, B. (1994). *Plate Bonding Strengthening of Existing Concrete Structures with Epoxy Bonded Plates of Steel or Fibre Reinforced Plastics*, Doctoral Thesis, Luleå, University of Technology

Täljsten, B. (1997). "Defining anchor lengths of steel and CFRP plates bonded to concrete." *International Journal of Adhesion and Adehesives,* 17(4), 319-327

Tanaka, T. (1996). *Shear resisting mechanism of reinforced concrete beams with CFS as shear reinforcement*, Graduation Thesis, Hokkido University

Teng, J.G., Chen, J.F., Smith, S.T., and Lam, L. (2002). *FRP Strengthened RC Structures*. John Wiley & Sons, England

van Gemert, D. (1980). "Force transfer in epoxy-bonded steel-concrete joints", *International Journal of Adhesion and Adhesives*, 1, 67-72

Warner, R. F., Rangan, B.V., Hall, A.S. & Faulkes, K.A. (1998). *Concrete Structures*. Addison Wesley Longman, Australia

Wong, K.W., and Warner, R.F. (1998). *Collapse load analysis of prestressed concrete structures.* Research report no. R162, The University of Adelaide

Wong, K.W., and Warner, R.F. (1999). "Collapse load analysis of prestressed concrete structures." Australian Journal of Structural Engineering, 2(1), 11-18

Wu, Z.S., Niu, H. (2000). "Study on debonding failure load of RC beams strengthened with FRP sheets." *Journal of Structural Engineering*, 46A, 1431-1441

Yuan, H., and Wu, Z. (1999) "Interfacial fracture theory in structures strengthened with composite of continuous fibre" *Proceedings of Symposium of China and Japan*, Science and Technology of 21st Century, Tokyo, Japan, pp142-155

Yuan, H., Teng, J.G., Seracino, R., Wu, Z.S., and Yao, J. (2003). "Full-range behaviour of FRP-to-concrete bonded joints:A closed-form analytical solution." *Engineering Structures*, submitted

Yuan, H., Wu, Z.S., and Yoshizawa, H. (2001) "Theorectical solutions on interfacial stress transfer of externally bonded steel/composite laminates.", *Journal of Structural Mechanics and Earthquake Engineering JSCE*, 675/1-55, 27-39

Zilch, K., Niedermeier, R., and Blaschko, M. (1998). *Bericht über versuche zum verstärken von betonbauteilen mit CFK (Test report on retrofitting concrete members with CFRP*, Versuchsbericht Nr. 1310, Technische Universität München, Lehrstuhl für Massivbau

2.9 NOTATIONS

The following symbols are used in this chapter:

$(P_b)_b$	bond force at bar/concrete interface
$(P_b)_p$	bond force at plate/concrete interface
$(P_{sh})_x$	bond force over segment x
$(s_L)_b$	left crack face slip at bar/concrete interface
$(s_L)_p$	left crack face slip at plate/concrete interface
$(s_R)_b$	right crack face slip at bar/concrete interface
$(s_R)_p$	right crack face slip at plate/concrete interface
$(w_{cr})_b$	crack width at bar level
$(w_{cr})_p$	crack width at plate level
A_c	cross-sectional area of concrete

A_f	cross-sectional area of FRP plate
A_p	cross-sectional area of plate
A_s	cross-sectional area of bars
b	beam width
b_2	FRP plate width
b_a	width of adhesive
b_c	width of concrete block
b_p	plate width
c_f	constant
d_n	neutral axis depth
ds/dx	slip-strain
ds/dx_b	slip-strain at bar/concrete interface
ds/dx_p	slip-strain at plate/concrete interface
e	segment size in partial interaction segmental analysis
E_2	young's modulus of FRP
E_a	young's modulus of adhesive
E_c	young's modulus of concrete
E_{frp}	young's modulus of FRP
E_p	young's modulus of plate
E_s	young's modulus of steel
E_y	young's modulus of steel
F	force
F_b	bond force; resultant axial force in bars
$F_{b.shear}$	total bond force at bar/concrete interface
$f_{b.y}$	yield stress of bars
f_c	concrete cylinder compressive strength
F_c	resultant axial force in concrete element
f_c'	concrete cylinder compressive strength
f_{cm}	maximum concrete compressive stress
F_{conc}	resultant axial force in concrete element
f_{ct}	tensile strength of concrete
$f_{ct.max}$	maximum concrete tensile stress
f_{frac}	fracture stress of FRP
F_p	resultant axial force in plate
$F_{p.shear}$	total bond force at plate/concrete interface
$f_{p.y}$	yield stress of steel plate
F_R	resultant axial force in reinforcement
F_s	resultant axial force in bars
F_{shear}	total bond force over the shear span
F_{steel}	resultant axial force in steel element
f_u	ulitmate strength
f_y	yield stress of steel
G_f	fracture energy
h	depth of beam
h_b	distance from beam top to F_b
h_c	distance from beam top to F_c
h_c	distance from F_{conc} to steel/concrete interface in composite beams
h_p	distance from beam top to F_p
h_s	distance from F_{steel} to steel/concrete interface in composite beams
I_a	lever arm
I_{cs}	second moment of area of strengthened concrete equivalent cracked section
I_p	second moment of area of plate
k	coefficient
L	bond length; length; shear span
l_b	anchorage length

L_b	development or bond length
L_e	effective bond length
L_{sh}	shear span
M	moment
M_{conc}	internal moment of concrete element
M_{int}	internal moment
M_{steel}	internal moment of steel element
n	number of layers in sectional analysis
N_f	tensile forces of external plate
N_s	tensile forces of reinforcing bars
P	applied load
P_b	bond strength
P_b	ultimate bond strength
P_{max}	maximum transferable load in a simple shear test
P_u	ultimate bond strength
q_{sh}	bond force per unit length
R	resultant force distribution
s	slip
s_b	slip at bar/concrete interface
s_f	ultimate slip
s_{IC}	slip at the intermediate crack
s_L	left crack face slip
s_{max}	slip at peak bondstress; maximum slip
s_p	slip at plate/concrete interface
s_R	right crack face slip
s_{rm}	crack spacing
T	axial load
t_2	FRP plate thickness
t_a	adhesive thickness
t_c	concrete thickness
t_{frp}	FRP plate thickness
t_p	plate thickness
u	deformation
u_c	deformation of concrete at reinforcement/concrete interface
u_p	deformation of plate at plate/concrete interface
u_r	deformation of reinforcement at reinforcement/concrete interface
u_s	deformation of steel at steel/concrete interface
V	ultimate shear force; vertical shear force
w_{cr}	crack width
x	depth of neutral axis of strengthened section; distance away from crack 1
x_{crack}	distance of between adjacent cracks
x_{dis}	length of disturbed region
x_{max}	distance of crack 1 to position of $\varepsilon_{ct.max}$
x_{min}	distance from crack 1 to point of full interaction
α	coefficient
α_f	short-term modular ratio of FRP to concrete
β_L	bond length coefficient
β_p	width coefficient
χ	curvature
χ_{FI}	curvature in full interaction analysis
χ_{PI}	curvature in partial interaction analysis
ε	strain
ε_b	bar strain
ε_c	concrete strain
ε_{crack}	concrete cracking strain

ε_{ct}	concrete tensile strain
$\varepsilon_{ct.max}$	maximum concrete tensile strain
ε_{FI}	full interaction strain profile
ε_o	concrete strain at f_{cm}
ε_p	plate strain
ε_{PI}	partial interaction strain profile
$\varepsilon_{R,}\ \varepsilon_r$	reinforcement strain
ε_s	bar strain
ε_u	ultimate strain
θ	rotation
θ_{el}	elastic rotation
θ_{pl}	plastic rotation
σ	stress
σ_b	bar stress
σ_c	concrete stress
σ_{fd}	maximum possible increases in tensile stress within the plate
σ_{IC}	plate stress at the intermediate crack; IC debonding stress
σ_p	plate stress
σ_{PI}	partial interaction stress profile
τ	shear stress
τ_b	bondstress
$\tau_{b.\ max}$	peak bondstress
τ_f	ultimate bondstress
τ_u	average bondstress at failure

The following subscripts are commonly used in this chapter:

b	bar
c	concrete
cr	crack
FI	full interaction
i	section i
max	maximum
p	plate
PI	partial interaction
s	steel
x	section x

The following acronyms are used in this chapter:

CFRP	carbon fibre reinforced polymer
EB	externally bonded
FRP	fibre reinforced polymer
IC	intermediate crack
LHS	left hand side
PI	partial interaction
RC	reinforced concrete
RHS	right hand side
UDL	uniformly distributed loading